ACS Partner Journal

CHEMICAL & BIOMEDICAL IMAGING

Editors' Choice

Open Access

pubs.acs.org/ChemBioImaging

Review

Advances in Tracing Techniques: Mapping the Trajectory of Mesenchymal Stem-Cell-Derived Extracellular Vesicles

Jingqi Li, Zhaoyu Wang, Yongchun Wei, Wenshuai Li, Mingzhu He, Jingjing Kang, Jia Xu, and Dingbin Liu*

Cite This: *Chem. Biomed. Imaging* 2025, 3, 137−168

Read Online

ACCESS | Metrics & More | Article Recommendations

ABSTRACT: Mesenchymal stem-cell-derived extracellular vesicles (MSC-EVs) are nanoscale lipid bilayer vesicles secreted by mesenchymal stem cells. They inherit the parent cell's attributes, facilitating tissue repair and regeneration, promoting angiogenesis, and modulating the immune response, while offering advantages like reduced immunogenicity, straightforward administration, and enhanced stability for long-term storage. These characteristics elevate MSC-EVs as highly promising in cell-free therapy with notable clinical potential. It is critical to delve into their pharmacokinetics and thoroughly elucidate their intracellular and *in vivo* trajectories. A detailed summary and evaluation of existing tracing strategies are needed to establish standardized protocols. Here, we have summarized and anticipated the research progress of MSC-EVs in various biomedical imaging techniques, including fluorescence imaging, bioluminescence imaging, nuclear imaging (PET, SPECT), tomographic imaging (CT, MRI), and photoacoustic imaging. The challenges and prospects of MSC-EV tracing strategies, with particular emphasis on clinical translation, have been analyzed, with promising solutions proposed.

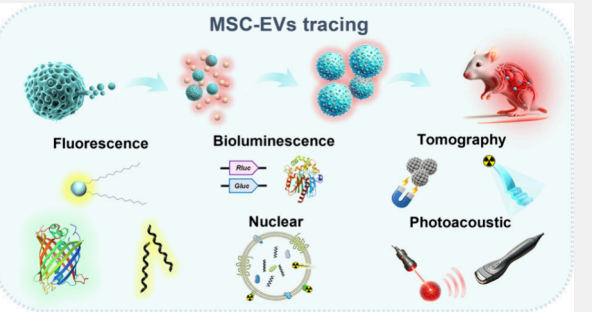

KEYWORDS: *Extracellular vesicles, Optical imaging, Magnetic resonance imaging, Computed tomography, In vivo, Stem cells, Theranostics*

1. INTRODUCTION

Mesenchymal stem cells (MSCs) are adult stem cells derived from diverse tissues, including bone marrow, adipose tissue, and umbilical cord.[1] The notable self-renewal capacity and multipotent differentiation potential have positioned them as a promising candidate for clinical translational research.[2] However, empirical evidence gleaned from clinical trials has consistently fallen short of anticipated outcomes.[3,4] MSC-based therapies are limited by several factors, including low postinjection survival rates, immune rejection risks, the potential to promote tumor progression, functional instability due to heterogeneity, and difficulties in large-scale manufacturing. Additionally, regulatory and ethical considerations present significant barriers to their clinical translation.[5] Therefore, to overcome these problems, researchers have scrutinized the mechanisms by which MSCs function through paracrine actions. Gradually, the focus has shifted to cell-free therapies dominated by extracellular vesicles (EVs) derived from MSCs.[6−8] These nanoscale lipid bilayer vesicles, referred to as MSC-EVs, serve as conveyors of bioactive factors (including genetic material, lipids, growth factors, and regulatory proteins) from the parent cell, thereby mediating intercellular communication in physiological and pathological settings.[9,10] The "off-the-shelf" utility of MSC-EVs positions them as potent disease interventions. Simultaneously, the inherent advantages of MSC-EVs, including low immunogenicity (no pathological reaction develops into tumors), efficient delivery, and long-term storage stability, circumvent the risks of whole-cell injections described above.[11,12]

Due to their strong regenerative and modulatory capabilities, MSC-EVs have emerged as the most promising EV-based therapeutics for clinical application. MSC-EVs modulate the microenvironment of injured tissues via the active molecules they carry, such as proteins and miRNAs, thereby enhancing the efficacy of bone and tissue repair.[13,14] In immunomodulation, MSC-EVs reduce inflammatory responses by inhibiting T cell activation and modulating macrophage polarization, making them suitable for treating conditions such as rheumatoid arthritis.[15,16] Moreover, MSC-EVs act as drug delivery vehicles, leveraging their intrinsic targeting capabilities to deliver chemotherapeutic agents or gene therapy molecules

Received: November 3, 2024
Revised: December 30, 2024
Accepted: January 3, 2025
Published: February 2, 2025

https://doi.org/10.1021/cbmi.4c00085
Chem. Biomed. Imaging 2025, 3, 137−168

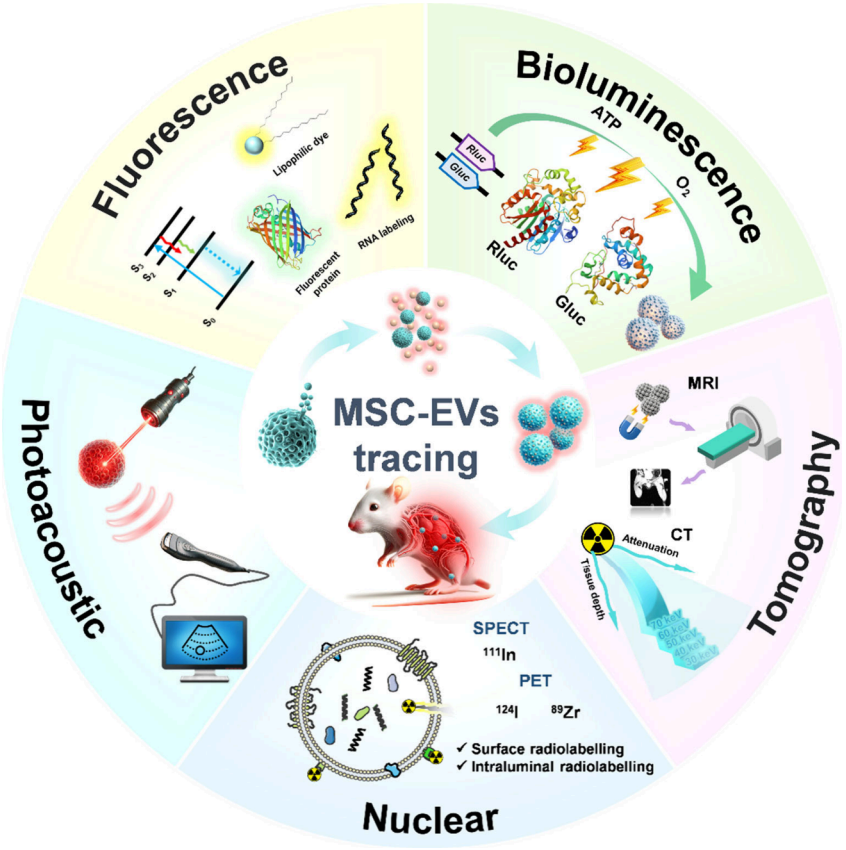

Figure 1. Schematic illustration of the tracing strategies of MSC-EVs.

to tumor sites, demonstrating advantages in cancer treatment.[17] In neurological disorders, MSC-EVs have exhibited promising effects in models of Alzheimer's disease and spinal cord injury (SCI) by protecting neuronal cells and promoting neural regeneration.[18,19]

Despite the considerable therapeutic potential of MSC-EVs, their *in vivo* distribution, metabolism, and targeting mechanisms remain incompletely understood, posing challenges to their clinical translation. Therefore, the development of advanced tracing techniques to elucidate their pharmacological properties and fate within cells and organisms is of paramount importance. This includes evaluating cellular uptake, biodistribution, pharmacokinetics, biodegradation, *in vivo* stability, and circulation. These techniques are essential for verifying therapeutic reliability (e.g., minimizing off-target effects), optimizing administration routes and dosages, and enhancing treatment safety. Furthermore, tracing methods facilitate studies on interactions between MSC-EVs and target cells, thereby deepening our understanding of their underlying mechanisms of action. In recent years, tracer strategies for EVs *in vitro* and *in vivo* have been extensively investigated, primarily categorized by imaging modalities such as fluorescence imaging (FLI), bioluminescence imaging (BLI), nuclear imaging, and tomography.[20−24] Labeling strategies for EV tracking are broadly categorized into direct labeling, involving the labeling of EVs postisolation with a suitable reagent, and indirect labeling, wherein parent cells are modified with exogenous agents that are subsequently incorporated into secreted EVs. Each of these strategies boasts unique advantages and disadvantages concerning biocompatibility, depth of penetration, spatial and temporal resolution, half-life time, and clearance rate.[25]

To date, numerous articles have summarized the tracing techniques and imaging strategies for EVs.[20,24,26,27] However, a comprehensive and systematic review specifically focusing on MSC-EVs has yet to be compiled by researchers. Given the emerging role of MSC-EVs as a potent cell-free therapy, standing out among various types of EVs with the greatest potential for application, it is imperative to comprehensively summarize the tracing strategies and outcomes to facilitate their clinical translation. To this end, we systematically review the tracing strategies for MSC-EVs, categorizing them based on different biomedical imaging modalities (Figure 1). Initially, we summarize the real-time evaluation of the fluorescently labeled MSC-EVs targeting distinct components, such as lipids, proteins, and RNA. We then provide an overview of the research progress and prospects in BLI, nuclear imaging, tomography imaging, photoacoustic imaging (PAI), and multimodal imaging of MSC-EVs. Lastly, we discuss the current challenges and future directions for MSC-EV tracking, offering promising solutions to the hurdles faced in their clinical translation.

2. FLI

FLI currently reigns as the predominant methodology employed for tracing EVs within the scientific community.[28−30] This tracing technique entails integrating fluorescent tags or nanomaterials, which emit fluorescence upon excitation, captured by specialized low-light cameras equipped with appropriate filters.[31] In light of the biological functions exhibited by MSC-EVs and their immense therapeutic

https://doi.org/10.1021/cbmi.4c00085
Chem. Biomed. Imaging 2025, 3, 137−168

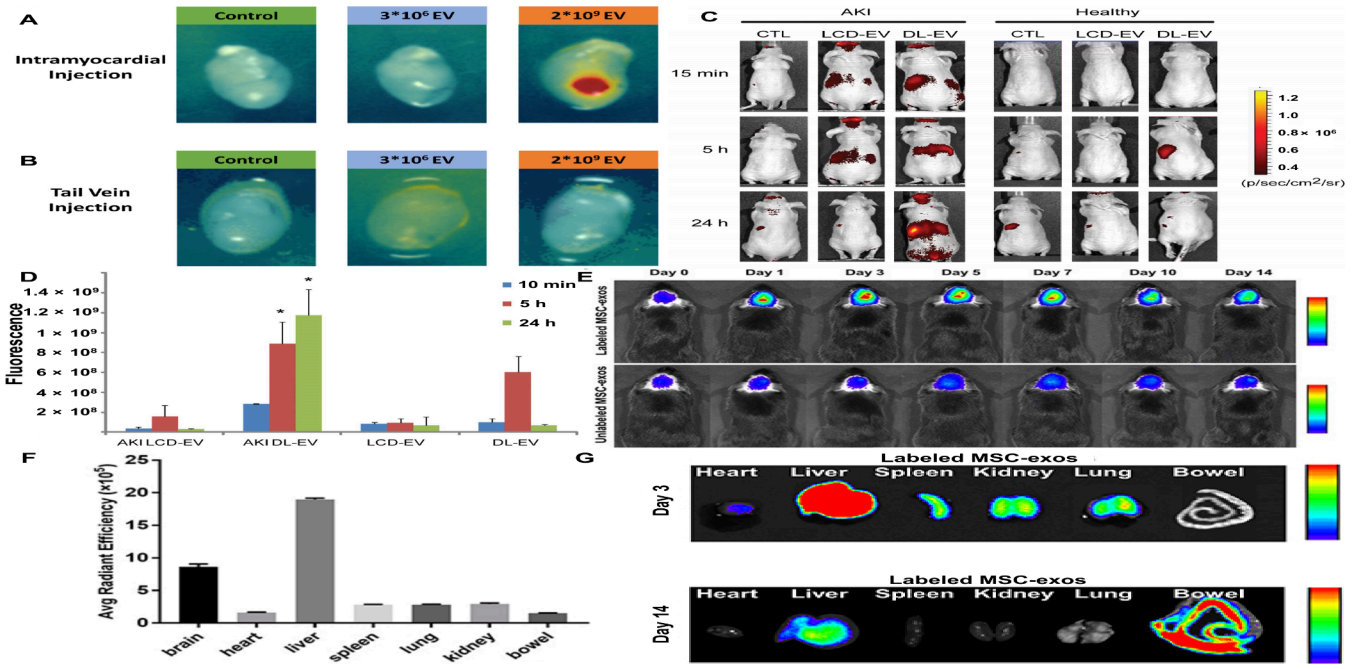

Figure 2. MSC-EVs tracing by carbocyanine dyes. (A,B) Fluorescence molecular tomography of the heart after intramyocardial injection or tail vein injection of either a negative DiD-saline control or DiD-labeled human bone marrow mesenchymal stem cell-derived extracellular vesicles (BMSC-EV). (A) Uptake of MSC-EV was only detected after intramyocardial (upper panels) injection of 2×10^9 particles. (B) No fluorescence was detected in the heart after tail vein (lower panels) injection of either 3×10^6 or 2×10^9 particles MSC-EV. Reproduced from ref 46. Available under a CC BY 4.0 license. Copyright 2023 Xu, C. M.; et al. (C,D) *In vivo* cell-derived extracellular vesicle (EV) biodistribution in kidney region by optical imaging (OI). (C) Representative OI images, acquired in the posterior position following the induction of acute kidney injury (AKI) in mice and healthy mice treated intravenously with 200 μg of LCD-EVs or DL-EVs or with an equal volume of phosphate-buffered saline (PBS; CTL). (D) Quantification of fluorescence intensity in regions-of-interest (ROI) draw a free hand in the region of kidneys, expressed as the average radiance ± standard deviation (SD). Sixteen AKI mice were treated with LCD-EVs. 11 AKI mice were treated with DL-EVs, and healthy mice received the same amount of LCD- and DL-EVs (n = 12 for LCD-EVs and n = 6 for DL-EVs). ANOVA with the Newman-Keuls multicomparison test was performed. *P < 0.01 AKI DL-EV vs all the other groups. LCD-EV, labeled EVs produced by donor cells; DL-EV, directly labeled EVs. Reproduced from ref 53. Available under a CC BY-NC 3.0 license. Copyright 2014 Grange, C.; et al. (E−G) DiR-labeled MSC-EVs homed to ischemic foci after stroke. (E) Representative NIRF images of ischemic stroke brains from the DiR-labeled group MSC-EV-treated and unlabeled MSC-EV-treated group. (F) The average radiant efficiency based on NIRF images of isolated organs from the DiR-labeled MSC-EV-treated group on day 3. (G) Representative NIRF image of tissues from the DiR-labeled MSC-EV-treated group on days 3 and 14. Reproduced from ref 66. Available under a CC BY-NC 3.0 license. *Int. J. Nanomed.* **2020**, *15*, 9011−9023. Originally published by and used with permission from Dove Medical Press Ltd.

potential in various diseases, the simplicity and user-friendly nature of FLI (e.g., color and brightness adjustments) have facilitated its extensive adoption in MSC-EV studies. The efficacy of FLI primarily depends on the efficiency of fluorescent labeling strategies adopted. Thus, the review delineates the various labeling strategies employed in FLI of MSC-EVs, encompassing membrane lipid labeling, protein labeling, and RNA labeling approaches.

2.1. Membrane Lipid Labeling

The commercialization and widespread utilization of lipophilic dyes have undoubtedly contributed to the ease and reliability of achieving FLI of MSC-EVs.[32,33] Consequently, studies pertaining to this subject have reached a certain level of maturity, establishing a standardized protocol for dye labeling and subsequent evaluation. Among the frequently utilized dyes, carbocyanine dyes, PKH dyes, and cyanine dyes stand out as the most prevalent choices.

2.1.1. Carbocyanine Dyes. The suite of long-chain dialkyl carbocyanine dyes, including DiO (λ_{ex} = 487 nm/λ_{em} = 502 nm; green), DiI (λ_{ex} = 549 nm/λ_{em} = 565 nm; red), DiD (λ_{ex} = 644 nm/ λ_{em} = 665 nm; NIR), and DiR (λ_{ex} = 748 nm/λ_{em} = 780 nm; NIR), represents a class of dyes noted for the distinctive molecular structure and pronounced hydrophobicity. This inherent hydrophobic nature enables them to integrate into the membrane of MSC-EVs through non-covalent interactions effortlessly. In turn, diffusion achieves efficient FLI across the entire EV profile.

2.1.1.1. DiO. Due to the limited imaging penetration of short-wavelength fluorescence, DiO green fluorescent dyes are commonly employed to evaluate the cellular uptake of MSC-EVs.[34,35] This is a critical step in assessing their efficacy or predicting underlying mechanisms. Typically, a coincubation period of approximately 6 h is employed, during which DiO-labeled MSC-EVs are allowed to interact with the target cells. Following this incubation, phosphate-buffered saline (PBS) washing is performed. EV uptake is assessed by subjecting the cells to fixation in 4% paraformaldehyde, followed by fluorescence visualization subsequent to DAPI staining for 15 min. Furthermore, DiO-labeled imaging of superficial tissues can also be achieved. Lin et al. evaluated the ability of 3D-printed scaffolds in subcutaneous tissues to retain MSC-EVs by DiO labeling.[36] In turn, enhanced demonstration of the efficacy of MSC-EVs bioink biology in regenerating cartilage defects was achieved.

2.1.1.2. DiI. DiI, a widely investigated fluorescent dye, has been more extensively studied to assess cellular uptake capacity

https://doi.org/10.1021/cbmi.4c00085
Chem. Biomed. Imaging 2025, 3, 137−168

than DiO.[37−42] The established approach similar to DiO has, in turn, shaped the prevailing paradigm in MSC-EV research. Moreover, the red fluorescence emission characteristics of DiI dye have facilitated explorations into the behavior of MSC-EVs within isolated tissues.[43,44] Illustratively, Yang et al. harnessed DiI labeling on MSC-EVs in brain tissue sections, demonstrating that miR-124, specifically delivered to the injured region by RVG (rabies virus glycoprotein)-modified MSC-EVs, achieved notable localization.[45] In contrast, mice injected with unmodified EVs displayed minimal DiI fluorescence in the core of the injured region, highlighting the efficacy of RVG in crossing the blood-brain barrier (BBB). Furthermore, robust fluorescent signals were observed exclusively within the ischemic region of mice administered RVG-EVs, with comparably weak signals observed in the normal brain. DiI is able to demonstrate the capability of MSC-EVs to target pathological areas in *in vitro* tissue studies. The investigation of *in vivo* distribution still necessitates the development of fluorescent probes with longer wavelengths.

2.1.1.3. DiD. The progressive red shift in the fluorescence of carbocyanine dyes, attributable to elongation in the conjugated structure of the probe molecule, has facilitated the development of near-infrared (NIR) fluorescent probes, specifically DiD and DiR. DiD provides a visual approach for evaluating the influence of pretreatment procedures on the therapeutic efficacy of MSC-EVs. Abid et al. conducted an examination of MSC-EV biodistribution through different injection methods in myocardial injury, utilizing DiD imaging (Figure 2A and B).[46] They confirmed that intracardiac injection stands as the most efficacious means of MSC-EV delivery. Moreover, they successfully demonstrated the retention of MSC-EVs in lesioned areas through DiD labeling under diverse conditions, including hindlimb ischemia, radiation-induced hematopoietic damage in the spleen and bone marrow, and other pertinent scenarios.[47−49] Capitalizing on the deep tissue penetration capabilities, the *in vivo* imaging of MSC-EVs has been advanced. The different labeling methods for MSC-EVs lead to varying imaging outcomes. Within this context, the noteworthy work of Camussi et al. deserves attention. Their previous studies have demonstrated the ability of MSC-EVs to expedite recovery from acute kidney injury (AKI), prompting a subsequent investigation on EV biodistribution and renal localization in AKI models while concurrently assessing different labeling methods.[50−52] Two distinct labeling methods for MSC-EVs were employed: (i) LCD-EVs, generated from MSCs preincubated with DiD and subsequently collected from the cell supernatants, and (ii) DL-EVs, wherein EVs were directly labeled with DiD during ultracentrifugation for purification.[53] Optical imaging revealed a specific accumulation of MSC-EVs in the kidneys of AKI mice, as depicted in Figure 2C. Notably, the direct labeling approach exhibited a higher, brighter, and more persistent fluorescence signal, albeit accompanied by a relatively higher background signal (Figure 2D). Deep learning approaches, including convolutional neural networks and autoencoders, for processing fluorescent images significantly improve the signal-to-noise ratio.

2.1.1.4. DiR. DiR, another more penetrating NIR fluorophore, is the most widely used carbocyanine dye for *in vivo* tracing of MSC-EVs.[54−65] To assess the targeting ability of MSC-EVs in therapy, Ju et al. undertook an investigation into the migration of MSC-EVs into the ischemic brain and their potential protective effects against ischemic stroke.[66] MSC-EVs were labeled with DiR dye followed by the removal of unlabeled EVs via ultracentrifugation. The labeled EVs were then intravenously administered to mice with induced ischemic stroke, with their migration monitored using NIR fluorescence imaging techniques. The results indicated a marked increase in fluorescence within the ischemic brain area, peaking 3 days postinjection (Figure 2E). Interestingly, fluorescence accumulation was also noted in the liver. By day 14, enhanced signals were observable in the intestine, suggesting that MSC-EVs are predominantly excreted through hepatic pathways and ultimately expelled via the gastrointestinal tract. (Figure 2F and G).

Similar to DiD, DiR has also been used in the assessment of the mode of administration of MSC-EVs. To elucidate the pharmacokinetics of DiR-labeled MSC-EVs, Collino et al. conducted an investigation employing three different injection methods: intravenous (IV), intratracheal (IT), and intranasal (IN).[67] The researchers utilized FLI to monitor the distribution of MSC-EVs at 3 and 24 h postinjection. The findings unveiled a distinct organ-selective pattern upon local administration of MSC-EVs, thereby minimizing the off-target effects on nontarget organs. Significantly, MSC-EVs administered intranasally demonstrated the capacity to cross the BBB and the choroid plexus epithelium, accumulating within the brain. It is essential to acknowledge that the lower signal uptake observed in this group may be attributed to inherent challenges associated with nasal uptake, including factors such as limited intrinsic permeability (e.g., lipophilic-hydrophilic balance), rapid mucociliary clearance, and active enzymatic degradation.[68] The conquest of these hurdles holds promise as an imperative approach in future therapeutic strategies targeting neurodegenerative diseases. Similar findings were corroborated through DiR labeling in murine models harboring 4T1 tumors.[69] Intratumoral administration of drug-loaded MSC-EVs exhibited enhanced antitumor efficacy compared to the conventional intravenous injection route.

2.1.2. PKH Dyes. PKH dyes have gained considerable popularity as a widely employed lipophilic dye in the field. Distinguishing them from carbocyanine dyes, which typically diffuse throughout the membrane, PKH dyes incorporate long aliphatic tails that embed the membrane of MSC-EVs. Consequently, the fluorophore becomes exposed on the outer surface of the lipid bilayer, enabling effective labeling mechanisms.[70] Two PKH dyes have garnered substantial attention for their utility in research: PKH26, characterized by its red fluorescence (λ_{ex} = 551 nm/λ_{em} = 567 nm), and PKH67, boasting green fluorescence (λ_{ex} = 490 nm/λ_{em} = 502 nm).

PKH26, a red fluorescent dye, has emerged as a tool for both *in vitro* labeling and long-term *in vivo* tracking of MSC-EVs, owing to the extended lifetime.[71−87] For instance, Tabata et al. used PKH26 to label EVs, simultaneously validating the cellular uptake *in vitro* and the efficacy in targeted drug delivery *in vivo*.[88] A challenge encountered in the therapeutic use of MSC-EVs lies in the suboptimal tissue targeting in tissue damage, such as liver injury, attributable primarily to phagocytic and immunological functions of the macrophages.[89,90] To tackle this predicament, researchers have developed surface modifications of EVs by leveraging cationized pullulan polysaccharides, capable of targeting hepatocyte desialylate glycoprotein receptors. Consequently, the utilization of PKH26 labeling assumes significance in validating the effectiveness of the modifications. On the one hand, it facilitates the assessment of enhanced internalization

https://doi.org/10.1021/cbmi.4c00085
Chem. Biomed. Imaging 2025, 3, 137−168

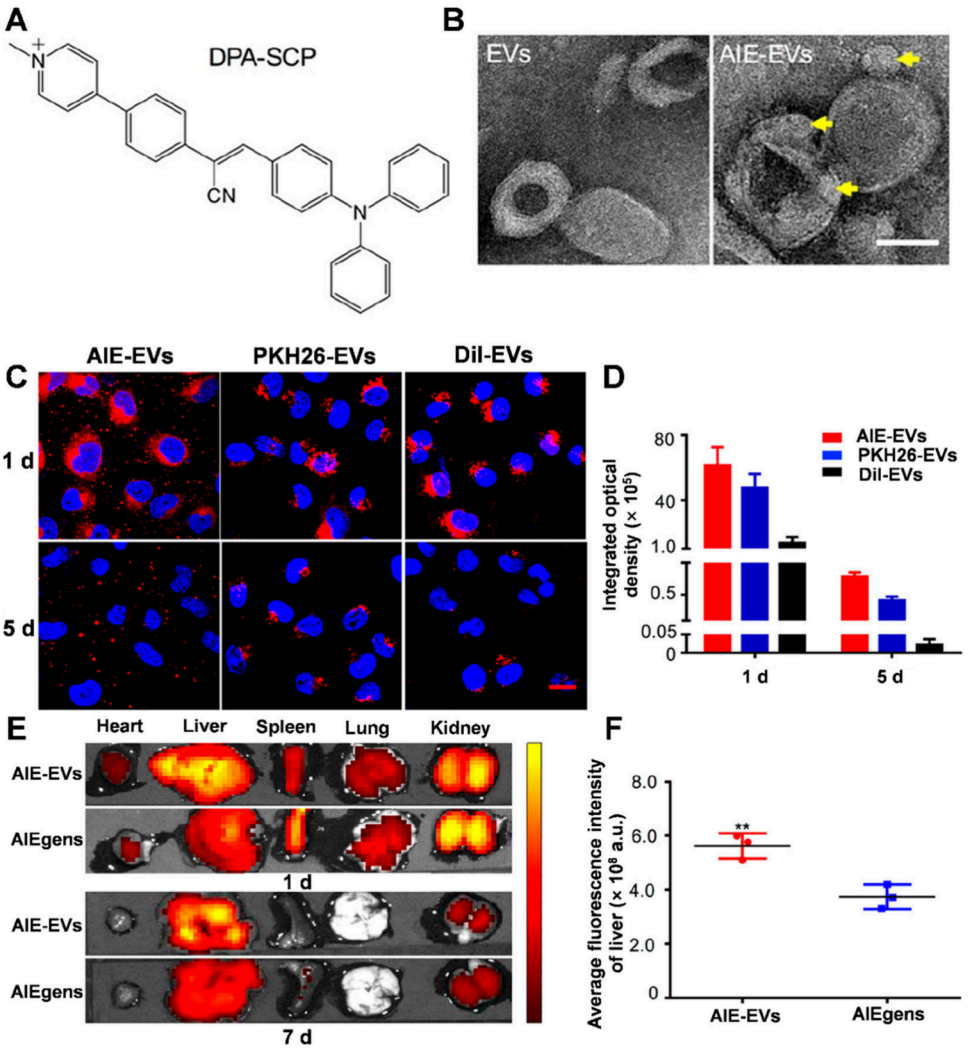

Figure 3. MSC-tracing by AIEgens. (A) Chemical structure of DPA-SCP. (B) TEM images of EVs and AIE-EVs. (C) CLSM images of EVs labeled with DPA-SCP, PKH26, or DiI for 1 and 5 days. Red: AIE-EVs. Blue: DAPI. Scale bar, 20 μm. (D) Quantitative analysis of the integrated optical density in CLSM images. Data are represented as the mean ± SD. Each experiment was performed in triplicate. (E) Ex vivo imaging of major organs dissected after sacrificing the mice on days 1 and 7. (F) Time-dependent fluorescence intensity changes in the liver on day 7 (n = 5; $^{**}P$ < 0.01 versus AIEgens). Data are represented as mean ± SD. Each experiment was performed in triplicate. Reproduced from ref 114. Copyright 2019 American Chemical Society.

of MSC-EVs by HepG2 cells. On the other hand, the *in vivo* tracing effect gauges the potential of EVs to selectively target liver-injured tissues, shedding light on their therapeutic efficacy. Hence, the straightforward yet powerful labeling strategy enables an evaluation of MSC-EVs, furnishing valuable insights for advancing and validating their engineered functionalities.

Despite the growing acceptance of PKH dyes as prominent tools in MSC-EV tracing, challenges pertaining to their labeling mechanism persist as significant obstacles. An in-depth examination utilizing nanoparticle tracking analysis (NTA) has demonstrated that PKH labeling leads to a notable increase in EV size and significant alterations in zeta potential.[91] These outcomes hold substantial implications for the cellular uptake, biodistribution, and pharmacokinetics of MSC-EVs, potentially compromising their intended biological effects. Consequently, it becomes imperative to address these concerns by devising suitable modifications to the structure of PKH dyes. For instance, incorporating negatively charged moieties, such as glutamate, into the two-armed cyanine scaffold, could optimize tailoring PKH-based probes to the intricate membrane architecture of MSC-EVs.[32]

2.1.3. Cyanine Dyes. Cyanine dyes are fluorescent, rigid, and planar compounds, including Cy3 (λ_{ex} = 550 nm/λ_{em} = 570 nm), Cy5 (λ_{ex} = 649 nm/λ_{em} = 670 nm), and Cy7 (λ_{ex} = 710 nm/λ_{em} = 767 nm).[92] These dyes exhibit a unique structural composition, comprising a conjugated chain that is formed by an odd number of electron-deficient methane moieties, linking heterocycles at both termini, as well as aromatic rings and cyclic olefinic compounds, establishing an extensive π-conjugated system.[93] This highly adjustable push–pull electronic configuration underpins their fluorescence emission, conferring a high molar extinction coefficient upon them.[94] Consequently, the dyes offer immense potential for achieving heightened signal intensities and sensitivities in the context of tracer imaging of MSC-EVs.

Given the excellent fluorescence of Cyanine dyes in the NIR region, tracing MSC-EVs in isolated organs and *in vivo* has shown promising applications.[95] To demonstrate the role played by EVs derived from human placenta choriodecidual

https://doi.org/10.1021/cbmi.4c00085
Chem. Biomed. Imaging 2025, 3, 137−168

membrane-derived MSCs (PC-MSC-EVs) in combating obesity-induced sepsis, researchers conjugate the EVs with Cy7 mono NHS ester.[96] Subsequently, by imaging the isolated organ to better eliminate background signals, the biodistribution was imaged, enabling an in-depth analysis that firmly validated their promise for therapeutic use. Similarly, Cy7 labeling was employed to investigate the interactions and mechanisms linking human umbilical cord-derived MSC-EVs (UC-MSC-EVs) with hepatic glucose/lipid metabolism and autophagy.[97] Following the tail vein injection of Cy7-labeled and PBS-treated UC-MSC-EVs, an advanced *in vivo* imaging system (IVIS) was utilized for post-24-h analysis. The results unveiled a wide distribution throughout the body.

Cy5.5 distinguishes itself from counterparts like Cy5 and Cy7 by incorporating benzoindole as its chromophore rather than indolenine. It incorporates an additional benzene ring into its molecular structure, facilitating a red-shift in absorption and emission peaks, broadening its fluorescence spectrum.[98] This inherent property confers a significant advantage for tracing MSC-EVs, unlocking new possibilities for investigation. An illustrative example lies in the application of Cy5.5 *N*-hydroxysuccinimide (Cy5.5-NHS) monoester for the labeling of MSC-EVs, facilitating targeted tracing at wound sites.[99] Notably, the results revealed a spatial confinement of the fluorescent signal, with Cy5.5 exclusively detected in the vicinity of the treated wounds. Even upon maximizing the radiation efficiency, no signal emanated from the healthy control areas. However, further investigations are imperative to comprehensively assess the acute and chronic toxicity, as well as the potential immunogenicity associated with Cy5.5 labeling. In addition, MSC-EVs hold promise for the treatment of osteoporosis (OP).[100] However, the assessment and enhancement of the skeletal targeting ability remain a challenge. To tackle this obstacle, Liu et al. modified the Cy5.5 molecule with azide (N_3) and the membrane surface of MSC-EVs with a commercially available jointed alkyne group (DBCO).[101] Subsequently, these two components were coupled by the click chemistry, enabling the evaluation of the EVs' skeletal targeting ability. This provides a new idea for the labeling of fluorescent dyes.

While Cyanine dyes have proven valuable as tracing markers for MSC-EVs, their utility is compromised by several limitations. The primary concern is their low fluorescence quantum efficiency combined with a propensity for aggregation, leading to false positive signals reminiscent of EVs. Mitigating this challenge often necessitates additional purification steps, such as ultracentrifugation or size exclusion chromatography, to eliminate the aggregation products. However, it typically comes at the cost of reduced EV recovery.[102] To tackle the issues, researchers have been developing modifications to enhance the hydrophilicity of the molecular framework of anthocyanine dyes. The development of analogous MemBright and Mem-family dyes has shown the potential to reduce aggregation and improve performance.[32,103] Another avenue worth exploring involves fluorescent probes based on lipid bilayer mimetic structures of amphiphilic molecular frameworks, such as COE, which can also be considered for the exploration and application of the functions of MSC-EVs.[104]

2.1.4. AIEgen. The aforementioned issue of false-positive signals due to dye aggregates and micelles formation, a consequence of the highly hydrophobic nature of fluorescent dyes, has long posed challenges. However, a revolutionary breakthrough emerged in 2001 with the discovery of luminescent materials possessing aggregation-induced emission properties (AIEgen) by Tang et al.[105] In stark contrast to conventional aggregation-caused quenching (ACQ) fluoresceins, AIEgens exhibit a distinct behavior: they remain nonemissive in the solution but turn highly emissive when aggregated, due to the restriction of molecular motions.[106,107] This endows AIEgens with the capability to minimize background noise during imaging while concurrently exhibiting brightness stability, resistance to photobleaching, and biocompatibility.[108−110] Amidst the urgent demand for mechanistic exploration and clinical translation of therapies concerning MSC-EVs, researchers are increasingly focusing on validating the reliability of this innovative tracer.

The surface of EVs is a rich array of proteoglycans, sialic acids, and lipids, imparting an overall negative charge to their membrane structure.[111,112] Recognizing the significance of membrane modification, Wang et al. developed a lipophilic, positively charged AIEgen, DPA-SCP (Figure 3A), strategically tailored for enhancing human placenta-derived mesenchymal stem cell-derived EVs (hP-MSC-EVs) through precise imaging and tracking during Acute Liver Injury (ALI) and Liver Regeneration Therapy (Figure 3B).[113] In the *in vitro* experiments, the researchers demonstrated the efficiency and tracking prowess of DPA-SCP, surpassing the performance of well-established commercially available EV dyes, PKH26, and DiI (Figure 3C and D). In subsequent *in vivo* investigations using a mouse model of ALI, they observed that DPA-SCP achieved precise and quantitative tracking of EVs for 7 days without compromising the targeting efficiency toward the liver injury site (Figure 3E and F). Expanding their exploration horizon beyond labeling, the group applied the same AIEgen to establish real-time *in vivo* imaging of MSC-EVs in an acute kidney injury (AKI) model of ischemia-reperfusion (I/R).[114] The results highlighted the specific accumulation of MSC-EVs within the injured kidney, predominantly taken up by the renal proximal tubular epithelial cells (TECs). The spatial and temporal resolution and tracking capabilities of DPA-SCP are superior to the conventional PKH26, setting the stage for further exploration of the associated pathway with interacting cells.

The AIEgens engrosses researchers with the promise of groundbreaking advancements. To maximize the potential of AIEgens for MSC-EVs tracking, smart designs are imperative. Strategically integrating specific and sensitive biomarker response units, for instance, can enhance imaging specificity and sensitivity at the target locations.[115] Moreover, AIEgens possess programmability. Incorporating strong electron donor/acceptor chromophores into the molecular designs can result in enhanced extinction coefficients and extended emission wavelengths.[116] The enhancement significantly improves tissue penetration and fluorescence intensity for imaging, presenting a promising direction for researchers.

2.2. Protein Labeling

2.2.1. Fluorescent Protein Labeling (GFP and RFP). Typically introduced into parental cells via transfection, fluorescent protein reporters are fused with the membrane proteins of EVs, acting as genetically encoded fluorophores.[117−119] In comparison with the dyes mentioned above, this approach ensures unhindered cellular secretion of EVs, facilitating labeling and continuous tracking of EVs in a more natural manner. Visiting the therapeutic potential of

https://doi.org/10.1021/cbmi.4c00085
Chem. Biomed. Imaging 2025, 3, 137−168

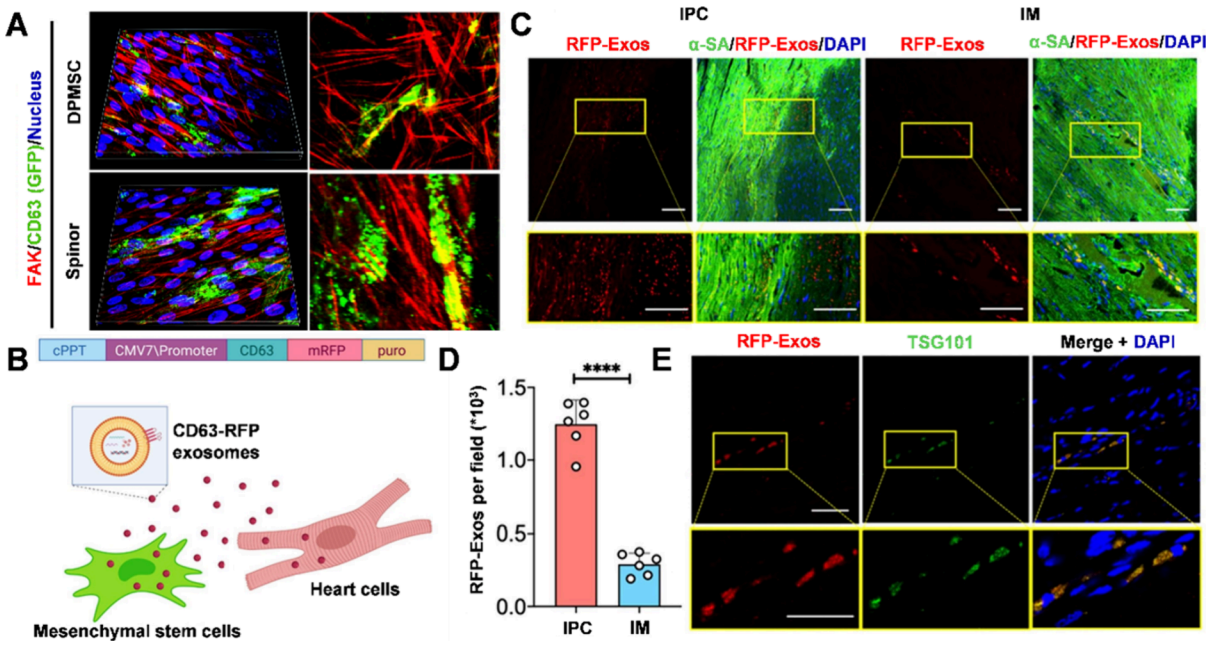

Figure 4. MSC-EV tracing by fluorescent protein. (A) EV images in MSC and Spinor taken by confocal laser scanning microscopy. EVs were labeled by (GFP)-fused CD63, and the cytoskeleton as well as cell nucleus were dyed in red (FAK) and blue (DAPI), respectively. Fluorescent intensity results are shown as 3D views of surface remodeling presented as angled views (400X). Reproduced from ref 124. Available under a CC BY-NC-ND 4.0 license. Copyright 2022 Yang, J.; et al. (B) Schematic showing the genetic modification of MSCs leads to RFP labeling of EVs. (C) Representative fluorescence images showing the RFP-EVs (red) uptake in heart cells including cardiomyocytes (green) in mouse MI hearts injected with ER-MSCs by the IPC route or IM route. Scale bar, 100 μm. (D) Quantitation of RFP+ cells based on F. for the IPC group and IM group. (n = 6, biological replicates). (E) Representative fluorescence images showing colocalization of RFP-EVs (red) and EV-specific markers TSG101(green). Reproduced from ref 127. Available under a CC BY-NC-ND 4.0 license. Copyright 2022 Li, J.; et al.

MSC-EVs, the spontaneous membrane protein labeling method through plasmid transfection can facilitate functional validation and real-time spatial and temporal monitoring during the entire therapeutic process.

The MSC-EVs have demonstrated potential in enhancing neural regeneration and functional recovery in animal models of central nervous system (CNS) diseases and injuries.[120,121] However, the exploration of the mechanisms pauses at immune regulatory signaling molecules, with the direct or indirect modes of interaction requiring further investigation.[122] To this end, Chopp et al. sought to monitor the behavior of MSC-EVs during treatment in models of inflammatory demyelination and toxic demyelination.[123] They transfected CD63-GFP plasmids into MSCs through electroporation. They first transfected CD63-GFP plasmids into MSCs by electroporation. Subsequently, the isolated CD63-GFP-carrying MSC-EVs were injected into mice via the tail vein. The green signal within the CNS affirmed the traversing prowess of MSC-EVs through the BBB, finding internalization within the parenchymal cells. Furthermore, the colocalization results from double immunofluorescence staining showcased the direct targeting of MSC-EVs with oligodendrocyte precursor cells, shedding light on potential therapeutic avenues for other neurological injury diseases. For example, in cell-free therapy for SCI, a developmental engineering strategy was employed to create a bionic spinal repair device, named "Spinor," based on pulp-derived MSCs (DPMSCs).[124] It mimics the geometric structure of spinal tissues and autonomously releases EVs to induce in situ neuroplasticity within the spinal cord, facilitating the process of injury repair. Employing a stable transfection strategy akin to the above-mentioned method, they traced EVs through confocal laser scanning microscopy (CLSM). The Spinor group radiated with significantly enhanced green EV signals while maintaining similar cytoskeleton expression, surpassing the DPMSCs control group (Figure 4A). This indirect labeling approach circumvents interference with MSC-EVs biogenesis, proffering a reliable solution for assessing metrics necessary for the clinical translation of MSC-EVs.

Similar to GFP, RFP serves as another fluorescent protein reporter molecule, facilitating the tracking of MSC-EVs.[125,126] Leveraging multichannel fluorescence enables a more comprehensive understanding of mechanical probes, such as investigating the mode of injection and the paracrine mechanisms of MSCs during cellular therapeutic procedures.[127] The labeling process for RFP involves genetic modifications through lentiviral transduction (Figure 4B). The red fluorescent signal specifically binds to the CD63 protein on the surface of MSC-EVs, allowing for straightforward visualization under optical microscopy. Researchers used different delivery methods, such as intramyocardial (IM) injection and intrapericardial cavity (IPC) injection, to administer hydrogels containing MSCs. Notably, the results revealed that IPC injection extends the paracrine range of EVs (Figure 4C and D), enhancing cardiac repair by exerting more beneficial effects on cardiac cells following myocardial infarction. The colocalization imaging with EVs-specific proteins further provides new evidence for their identification (Figure 4E).

Furthermore, in the growing demand for *in vivo* imaging, the development and application of NIR fluorescent proteins (e.g., NIR FAP and Janelia fluorogens) hold significant value in this field.[128] Specifically, the development of corresponding far-red fluorescent proteins with enhanced emission penetration has proven instrumental in investigating the communication and

https://doi.org/10.1021/cbmi.4c00085
Chem. Biomed. Imaging 2025, 3, 137−168

transport mechanisms of MSC-EVs within the extracellular matrix (ECM). In this context, the Katushka2S (K2S) sequence, a far-red fluorescent protein, was integrated into a lentiviral construct containing CD63.[129] Following transfection into MSCs, the transport dynamics of MSC-EVs were visualized using multiphoton second-harmonic imaging. Notably, the excitation and emission spectra of this far-infrared probe exhibit minimal overlap with common green and red fluorescent probes, ideally suited for multiple fluorescence staining experiments. Moreover, it facilitates noninvasive *in vivo* imaging of MSC-EVs within deep tissues and throughout the body, potentially accelerating the clinical translation.[130]

While fluorescent protein reporters offer a natural tracking method for MSC-EVs, they possess limitations, such as a tendency to oligomerize, reliance on molecular oxygen, and delayed expression of fluorescent motifs.[131] Designs incorporating anaerobic fluorescent proteins, including FbFPs and UnaGs, can circumvent these dependencies, making them more suitable for MSC-EVs tracking.[132,133] Given extensive applications of MSC-EVs in tissue damage repair, it would be ingenious to exploit the limitations to enable simultaneous monitoring of damage conditions. For instance, engineering the protein reporter through circular rearrangement or segmentation allows for concurrent sensing of pH, oxygen content, calcium ion concentration, apoptosis, or protein interactions in the microenvironment, which could greatly benefit the further monitoring of the therapeutic process of MSC-EVs.[134]

2.2.2. Internal Protein Labeling. The therapeutic potential of MSC-EVs is attributed to the ability to transfer internal proteins, nucleic acids, and other biomolecules to recipient cells, inducing new behaviors through cell-to-cell communication.[135] Therefore, it becomes crucial to label the internal proteins not only to achieve a high abundance signal of the EV tracking but also for the simultaneous monitoring of protein-dependent communication. To address this need, researchers have developed Exo-Green stains for tracking internal proteins in MSC-EVs.[136−140] Leveraging the membrane permeability of carboxyfluorescein succinimidyl diacetate ester (CFSE), which undergoes hydrolysis by corresponding esterases to remove the diacetate moiety upon entering EV membranes, Exo-Green allows access to amino terminals of the proteins. Consequently, CFSE emits green fluorescence, enabling the simultaneous monitoring of protein behavior and EVs. However, this esterase-responsive labeling mechanism presents certain limitations and is prone to producing false-positive signals in samples.

2.3. RNA Labeling

As essential transporters within MSC-EVs, RNAs offer potential as tracers. Oligonucleotides, including miRNAs and siRNAs, have been extensively investigated for their role in MSC-EVs communication. Their involvement in gene expression regulation, RNA interference, and gene silencing processes in target cells bestows them with significant biological functions.[141−143] To establish the functional profile of EVs, it is imperative to trace and label the RNAs, akin to the protein labeling discussed earlier.

RNA labeling of MSC-EVs is commonly achieved using the Exo-Red dye, which possesses an acridine orange framework with high cell permeability.[144−146] Through intercalation and electrostatic attraction, respectively, it can interact with DNA and RNA, leading to distinct fluorescence signals at different excitation and emission wavelengths (DNA: λ_{ex} = 502 nm/λ_{em} = 525 nm; RNA: λ_{ex} = 460 nm/λ_{em} = 650 nm). Employing the typical RFP filter set can achieve the effective RNA-mediated tracing of MSC-EVs. The endocytic labeling approach exhibits a low off-target rate, making it an ideal method to investigate the uptake capability of MSC-EVs by recipient cells and assess the associated functions.[147]

Another investigation of RNA labeling in MSC-EVs is the cyc3 dye, which allows for internalized RNA labeling with cyc3-labeled pre-miRNA control oligos (cyc3-oligo) that are transfected into MSCs.[148] The pre-miRNAs in this context refer to the unsheared and unmatured miRNAs, which are the precursors of miRNAs.[149] To achieve this, cyc3 is covalently linked to oligonucleotides through NHS ester chemistry. In a study exploring the mechanism of miRNA delivery using engineered MSCs (miR-let7c-MSCs) for kidney injury treatment, researchers transfected the cyc3 dye into MSCs. Following a 72-h coculture with NRK52E cells (mature rat renal tubular epithelial cells), immunofluorescence micrographs revealed significant cyc3 staining in the cytoplasm of the target cells. In contrast, NRK52E cells treated with the EVs inhibitor GW4869 exhibited an absence of fluorescence, indicating that miRNAs from MSCs can enter renal epithelial cells through EVs-mediated intercellular delivery. Moreover, this study provides evidence supporting the antifibrotic effect of miR-let7c in MSC-EVs on NRK52E cells, further validating the therapeutic potential of miRNA delivery via MSC-EVs.

The RNA labeling methods mentioned above exhibit high labeling efficiency for MSC-EVs, and the imaging operations are easily implementable. However, direct RNA labeling strategies might interfere with the intrinsic communication pattern of MSC-EVs. To address this concern and enable real-time monitoring, developing metabolic labeling-based RNA tracer strategies holds promise.[150] It involves converting modified nucleotides into nucleoside triphosphates (NTPs) and incorporating them into different types of RNA during transcription or catalyzing the process using adenosine phosphorothioate sulfate (PAPS). It allows for fluorescent labeling via click chemistry.[151] Nonetheless, further exploration is needed to ensure the specificity. Moreover, there is potential for its use in conjunction with Next-Generation Sequencing (NGS) to study transcription kinetics and potential modification kinetics of MSCs, thereby facilitating the in-depth exploration of the mechanisms associated with MSC-EVs.

2.4. Internal Labeling

In addition to the labeling of MSC-EV-specific structures, internal labeling by fluorescent organic dyes or materials has been widely investigated. Calcein-AM is a commonly used internal tracer dye for MSC-EVs.[152−154] Similar to CFSE, Calcein-AM is hydrolyzed by intracellular esterases, removing the acetoxymethyl group (-AM) and converting it into fluorescently active green Calcein. However, Calcein-AM does not label intracellular proteins, resulting in a more uniform fluorescence signal and improved tracing sensitivity. Despite these benefits, the stability of Calcein-AM labeling remains a significant challenge, limiting its application to short-term imaging studies. Additionally, organic photosensitizers such as verteporfin (VER) have also been studied for tracing and synergistic treatment with MSC-EVs.[155] Researchers have developed a classical indirect labeling method to overcome the limitations of traditional dyes related to stability and

https://doi.org/10.1021/cbmi.4c00085
Chem. Biomed. Imaging 2025, 3, 137−168

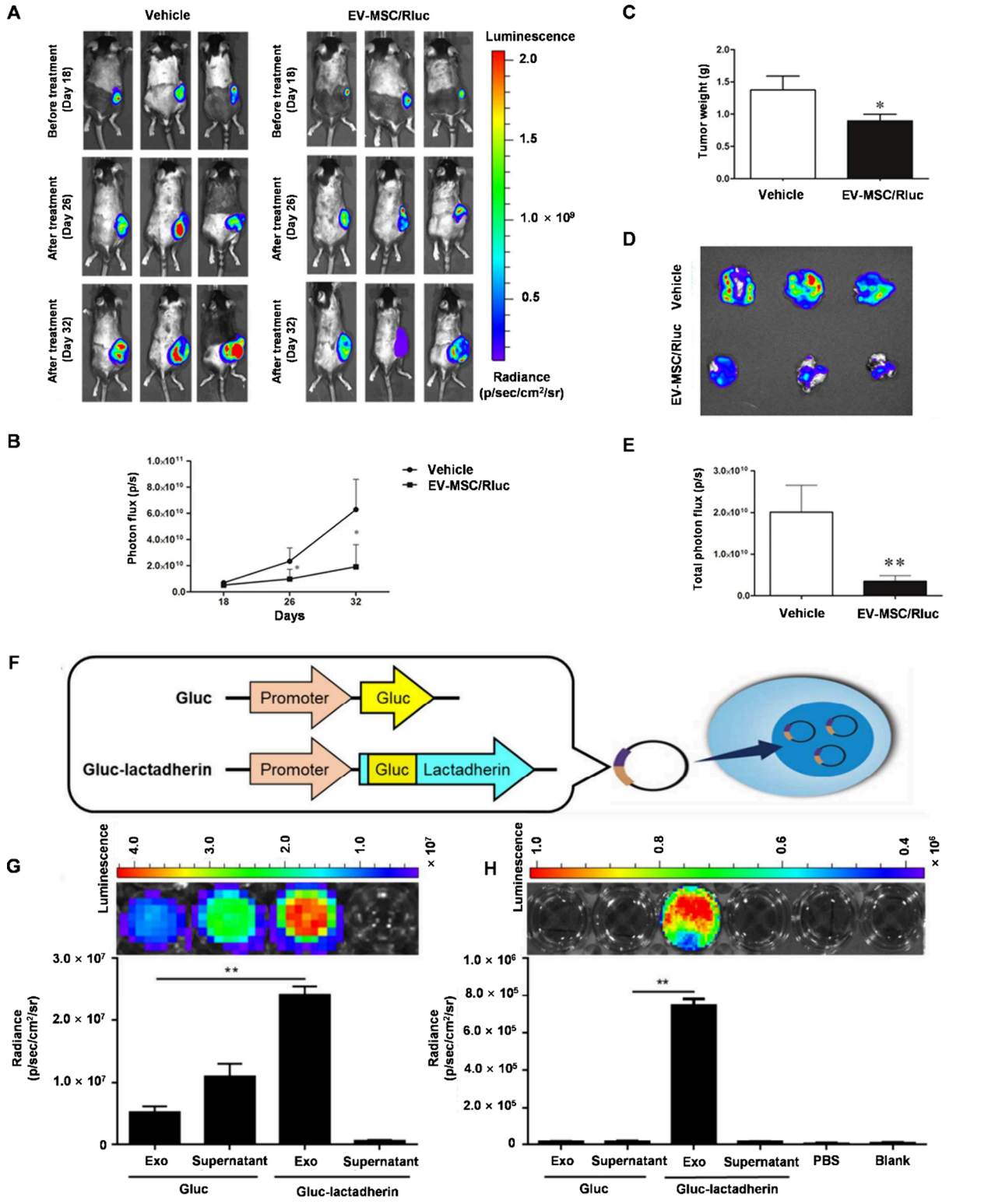

Figure 5. MSC-EVs tracing by BLI. (A) BLI of tumor LLC-effluc activity in mice subcutaneously injected with 1×10^6 LLC-effluc cells and treated with vehicle or EV-MSC/Rluc (50 μg) twice. (B) Quantitative BLI of LLC-effluc activity. (C) Tumor weight. (D) BLI imaging of LLC-effluc activity from *ex vivo* tumors. (E) *Ex vivo* quantitative BLI of LLC-effluc activity. Values are expressed as the mean ± standard deviation (SD), $^*P < 0.05$, $^{**}P < 0.01$ (by Student's *t* test). Reproduced from ref 164. Available under a CC BY 4.0 license. Copyright 2016 Kalimuthu, S.; et al. (F–H) Identification of EVs labeled with Gluc-lactadherin fusion proteins. (F) Schematic representation of pLV-Gluc and pLV-Gluc-lactadherin plasmids. (G) BLI images of EVs and EV-free proteins isolated from hP-MSCs transfected with pLV-Gluc or pLV-Gluc-lactadherin plasmid. (H) Internalization of EV and EV-free proteins detected by Gluc signals. Data were expressed as the mean ± SEM. All experiments were performed in three independent experiments in triplicate and are shown as the mean ± SEM ($n = 3$; $^{**}P < 0.01$). Reproduced from ref 165. Copyright 2018 American Chemical Society.

https://doi.org/10.1021/cbmi.4c00085
Chem. Biomed. Imaging 2025, 3, 137–168

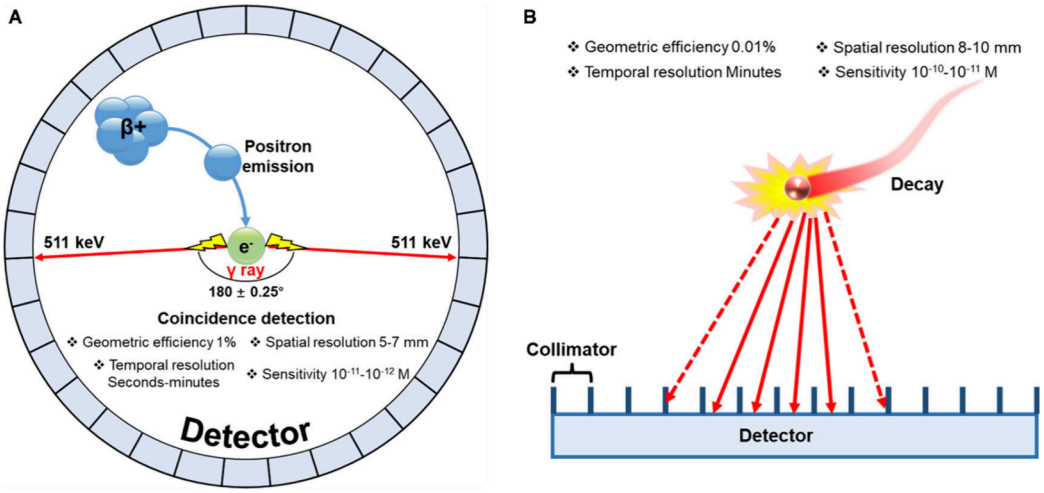

Figure 6. Schematic illustration of the principle of SPECT (A) and PET (B).

quantification, demonstrating effective uptake by BMSCs and targeted accumulation in inflamed lung regions both *in vitro* and *in vivo*. The fluorescent properties of nanomaterials, such as metal nanoclusters and quantum dots, also facilitate MSC-EV tracking.[156,157] Although numerous nanomaterials have been reported to hybridize with MSC-EVs, their potential for fluorescence tracing remains largely unexplored,[158] representing a promising direction for future research.

3. BLI

Given the significant therapeutic efficacy exhibited by MSC-EVs within biological tissues, the quest for tracers boasting high signal-to-noise ratios has emerged as a key research focus. Although GFP expression tracing without the need for excitation light has partially fulfilled this objective, its low sensitivity and propensity for intracellular accumulation limit its suitability for real-time monitoring.[159,160] Consequently, researchers have increasingly focused on BLI. Analogous to GFP, BLI circumvents the requirement for excitation light, relying instead on luciferases, such as Gaussia princeps luciferase (Gluc), firefly luciferase (Fluc), and Renilla luciferase (Rluc), in conjunction with the corresponding substrates (e.g., coelenterazine, CTZ) that react with ATP and Mg^{2+} or oxygen alone, resulting in the emission of luminescent signals through the luciferase-substrate reaction.[161−163] Typically, the protein reporter gene encoding the detection signal is transduced into MSCs, enabling protein expression within EVs or on cellular membranes, thereby facilitating the tracking of MSC-EVs with high sensitivity and optimal signal-to-noise ratio.

Ahn et al. employed Rluc as a luciferase to develop the first BLI strategy for MSC-EVs.[164] They commenced with the stable transduction of the Rluc gene into murine bone marrow-derived MSCs by lentiviral particles engineered for Rluc expression. Following culture, EVs were isolated, thereby yielding MSC-EVs/Rluc, which were subsequently injected intratumorally for visualization within a mouse model of lung cancer (LLC-efffuc). The optical signal also enabled the simultaneous monitoring of tumors and the assessment of therapeutic efficacy. The results marked reductions in LLC-effuc activity, tumor weight, and *in vitro* effluc activity in the MSC-EVs/Rluc treated group (Figure 5A-E), establishing an ideal system for visualizing both therapeutics and targets within the same model. Building upon this, Li et al. expanded the repertoire of luciferases employed for MSC-EV tracing by incorporating Gluc.[165] In addition, they integrated lactadherin, an EV-associated membrane protein, into the labeling system to optimize the anchoring of Gluc to the EV membrane, as demonstrated in Figure 5F. The results indicated the improved labeling efficiency exhibited by the fusion protein GlucDlactadherin (GlucD) (Figure 5G and H). More notably, they concurrently achieved the visualization of tissue damage treatment by BLI. They engineered the expression of Fluc downstream of the vascular endothelial growth factor receptor 2 (VEGFR2) promoter, thereby integrating angiogenic responses with the tracing of MSC-EVs into a cohesive work.

Despite BLI has contributed to the specific and reliable in *in vivo* imaging of MSC-EVs in murine models, the transition to clinical practice remains limited. This is primarily attributed to the challenges in the inadequate signal intensity and tissue penetration capabilities.[166,167] Moreover, the requirement for repeated CTZ injections complicates experimental protocols. Compounded by the exceedingly short half-life (up to 5 min), the limitations restrict the possibility of long-term real-time imaging. Each imaging session necessitates prior injections, underscoring the need for rapid and accurate imaging systems.[168] A notable example is the work of Klose and Paragas, who devised a body-friendly animal shuttle alongside a statistical mouse atlas integrated with multispectral BL tomography.[169] It enables the expeditious quantification of distributed bioluminescent reporter genes within living organisms automatically. Moreover, ensuring efficient and interference-free gene transduction also remains a challenge within the field. Incorporating bioluminescent nanoparticles or CRISPR/Cas knock-in methodologies may offer promising solutions.[170−173]

4. NUCLEAR IMAGING

Nuclear imaging, a ubiquitous noninvasive technique in clinical diagnostics, is celebrated for its high sensitivity and tissue-penetrating capabilities, rendering it indispensable. For the tracing of MSC-EVs, radioisotopic labeling via coincubation is commonly employed. Subsequently, specialized imaging apparatus, such as gamma cameras or PET/CT systems, are used to detect radiation signals from the isotopic decay. These systems generate detailed three-dimensional images through single photon emission computed tomography (SPECT) or

https://doi.org/10.1021/cbmi.4c00085
Chem. Biomed. Imaging 2025, 3, 137−168

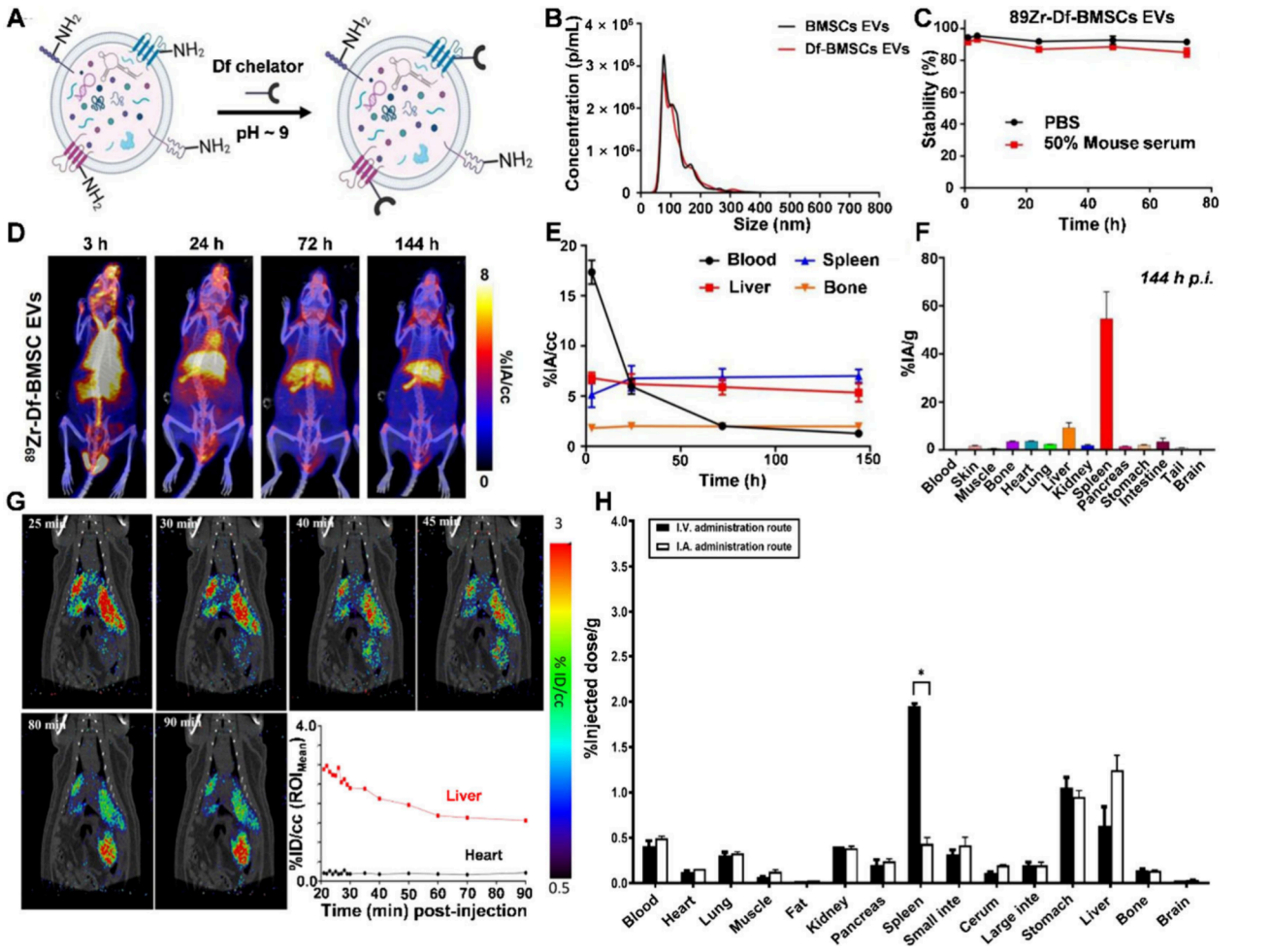

Figure 7. MSC-EVs tracing by PET. (A) Schematic showing the conjugation of the chelator (Df) to the surface of EVs. (B) Nanoparticle tracking analysis showed no differences in the size distribution of BMSC EVs and Df-BMSC EVs after conjugation. (C) Stability studies of ^{89}Zr-Df-BMSC EVs showing that radiolabeling was stable in PBS and 50% mouse serum up to 72 h following incubation (n = 3). (D) Serial maximum intensity projection PET/CT images of healthy NSG mice intravenously injected ^{89}Zr-Df-BMSC EVs. (E) Volume of interest quantification of ^{89}Zr-Df-BMSC EVs at various time points postinjection (×3). (F) *Ex vivo* biodistribution studies of ^{89}Zr-Df-BMSC EVs following the final imaging time point at 144 h postinjection (n = 3). Marked liver and spleen uptake were observed in these mice. Incongruences in spleen uptake between imaging and *in vitro* results are likely attributed to partial volume effects. Reproduced from ref 180. Copyright 2024 American Chemical Society. (G) MicroPET imaging of I.V. administered [^{124}I]I-UC-MSC-EVs in male rats. The representative MRP PET/CT serial images are shown (top and left bottom) at 0.5, 1, 1.5, 2, 4, 5, 10, 30, 50, and 90 min postinjection. MicroPET imaging provided clear visualizations of [^{124}I]I-UC-MSC-EVs accumulation and clearance in the organs from 0 to 90 min. Tissue time−activity curves of the liver and heart are also shown (right bottom). (H) Comparative biodistribution of [^{124}I]I-UC-MSC-EVs for the I.V. group vs the I.A. group after PET-CT scanning (96−98 min postinjection). Rats were injected with ∼8 MBq of [^{124}I]I-UC-MSC-EVs, and tissue biodistribution analyses were performed. *P < 0.01. Reproduced from ref 189. Available under a CC BY 4.0 license. Copyright 2022 Li, J.; et al.

positron emission tomography (PET).[174] Distinctive dissimilarities between the two lie in the selection of radioisotopes and the methods for signal detection and conversion into 3D images. For a detailed explanation of these principles, along with an analysis of their merits and demerits, refer to Figure 6. Additionally, tomographic imaging modalities like computed tomography (CT) and magnetic resonance imaging (MRI) are frequently integrated with nuclear imaging to enhance understanding of the metabolic profiles and biodistribution patterns of MSC-EVs, thus providing a more thorough assessment of their clinical implications.

4.1. PET

In MSC-EVs, the employment of radionuclide labels unveils an opportunity for PET tracing, wherein detecting γ rays indirectly emitted from the radioactive carrier. Positrons travel in an energy-dependent trajectory spanning submillimeters to a few millimeters before the annihilation by electrons. This process generates a pair of γ rays, each with an energy of 511 keV, emanating in opposite directions simultaneously. Through a ring detector, these γ rays can be captured and accurately mapped at a 180° angle, thus achieving coincident detection (Figure 6A).[175−177] The advantages conferred by PET, including its heightened geometric efficiency (a ratio of detected to emitted γ rays), refined temporal resolution, and reduced concentration of radiotracer requirements, have propelled its clinical prevalence, exceeding the practicalities of SPECT.[178,179]

To enhance the spatial localization of EVs, the integration of PET with CT imaging technique, known as PET/CT, is commonly employed. In a pioneering study, Hernandez et al. utilized Zr-89 ($t_{1/2}$ = 78.4 h), a highly efficient and stable radionuclide, for labeling MSC-EVs and subsequently tracking

https://doi.org/10.1021/cbmi.4c00085
Chem. Biomed. Imaging 2025, 3, 137−168

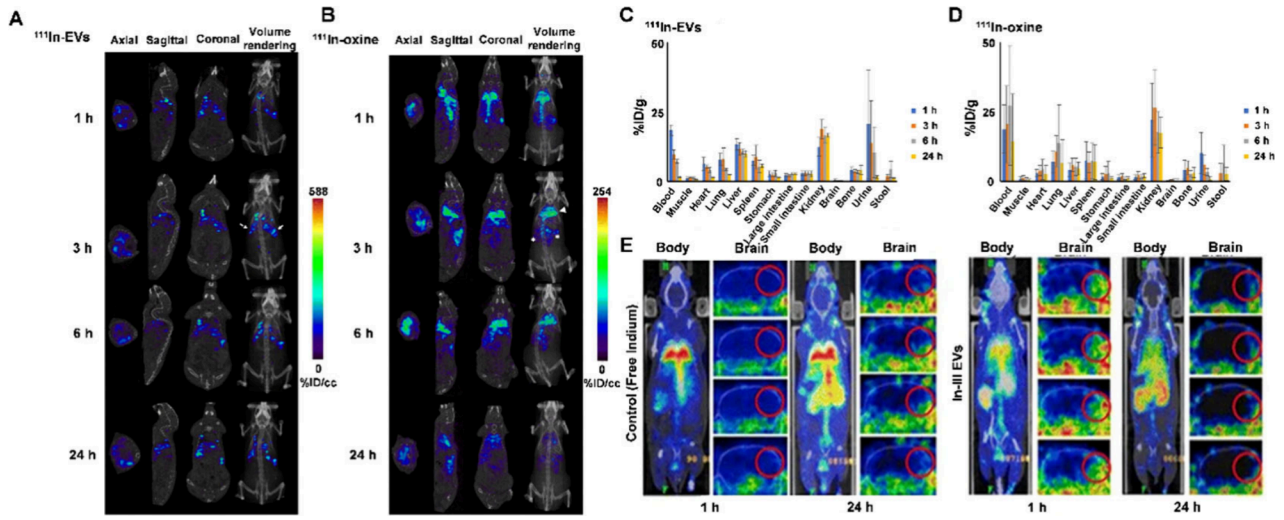

Figure 8. MSC-EVs tracing by SPECT. (A, B) *In vivo* μSPECT/CT imaging of ^{111}In-EVs. (A) After intravenous injection of ^{111}In-EVs; μSPECT/CT image was acquired at 1, 3, 6, and 24 h in C57BL/6 mice. (B) Micro-SPECT/CT image of ^{111}In-oxine-administered groups. White arrow, spleen; dotted white arrow, liver; white arrow, head, lung; white asterisk, kidney. (C, D) *Ex vivo* biodistribution of ^{111}In-EVs. ^{111}In-EVs or ^{111}In-oxine were intravenously injected into mice sacrificed at 1, 3, 6, and 24 h after injection to assess *ex vivo* radioactivity of organs. Reproduced from ref 198. Available under a CC BY-NC-ND 4.0 license. Copyright 2020 Lu, C. H.; et al. (E) One hour after stroke induction either free In-111 or labeled EVs (left and right, respectively) were administered into mice via tail vein injection and analyzed by SPECT. EVs were present in the infarct region 1 h after injection (red circles, left brain panels) but were largely cleared by 24 h (red circles, right brain panels). Systemic presence in the lungs, liver, and spleen is in agreement with other EV biodistribution studies (body panels). Reproduced from ref 203. Available under a CC BY 4.0 license. Copyright 2017 Webb, R. L.; et al.

them *in vivo* using PET imaging modality.[180] The labeling process involved the conjugation of desferrioxamine, acting as a chelator, to BMSC-EVs via isothiocyanate chemistry, followed by isotopic labeling with Zr-89 (Figure 7A). This membrane-based labeling approach had minimal impact on EV size (Figure 7B). The stability of labeled EVs was preserved at a rate of approximately 85% even after 72 h in mouse serum (Figure 7C). To evaluate the biodistribution and targeting efficacy of BMSC-EVs, the researchers established immunodeficiency and melanoma mouse models in NSG mice, utilizing PET imaging and Volume-of-Interest (VOI) analysis. The outcomes revealed a significant increase in splenic uptake of BMSC-EVs, comparable to that observed with human monoclonal antibodies (Figure 7D-F).[181] Following intravenous administration, the tumor uptake efficiency of BMSC-EVs also exhibited an increase, which is closely related to the glycosylation of the EV surface. Therefore, the impact of the labeling method on the biological characteristics of EVs warrants further investigation.[182,183] Intriguingly, such imaging results suggest the potential of BMSC-EVs as therapeutic vectors in both diseases, setting the stage for defining the targeting behavior of other MSC-EVs to optimize their therapeutic deployment. For instance, an in-depth analysis of different administration routes for Umbilical Cord MSC-derived EVs (UC-MSC-EVs) in treating diabetes has been undertaken.[184−186] Previous investigations have indicated the efficacy of intra-arterial injection (I.A.) in precisely targeting the pancreas. However, concerns have been raised regarding the potential risks of occlusion or embolism. On the other hand, the less invasive intravenous (I.V.) administration route presents the challenge of off-target effects, whereby uptake in organs such as the spleen and lungs may occur.[187,188]

To address this issue, Kandeel et al. undertook the radioiodination of human UC-MSC-EVs using the direct IODOGEN method, employing the radioisotope ^{124}I−NaI.[189] With the extended half-life of up to 4.18 days, [^{124}I] is among the optimal radionuclides for evaluating therapeutic efficacy and targeting. *In vivo* PET-CT imaging and *ex vivo* biodistribution analysis demonstrated that the pancreatic uptake levels (%ID/gram) of both administration methods were comparable (0.20 ± 0.06 for I.V. and 0.24 ± 0.03 for I.A.) (Figure 7G and H). Notably, the I.V. route exhibited higher spleen uptake, thereby presenting potential implications for expanding the immunomodulatory applications of UC-MSC-EVs. Nonetheless, the challenge lies in the low stability of the carbon−iodine bond in [^{124}I], potentially leading to the accumulation of radioactive deiodination in the thyroid and stomach, thus introducing signal interference. Hence, exploring more robust and dependable labeling techniques remains an ongoing pursuit, demanding groundbreaking advancements in probe research.

PET tracking of MSC-EVs, utilizing straightforward modification techniques, enables whole-body imaging and precise quantification of signals. Complementary CT imaging provides a reliable technological upgrade for further exploring the biodistribution and metabolic pathways, propelling its potential for clinical translation. Nonetheless, the necessity for complex and costly cyclotrons, while the rapid decay of radionuclides poses limitations. To ensure optimal imaging outcomes, the timely transportation of radiotracers from production to imaging sites becomes imperative, necessitating collaborative efforts from instrumentation and radiological sciences experts.

4.2. SPECT

In contrast to PET, SPECT utilizes a collimator to detect the decay of gamma photons emitted by a radioisotope.[190,191] This process involves the detection of γ radiation from multiple gamma cameras positioned at various specific angles (known as views), subsequently amplifying the signal and reconstructing the image (Figure 6B).[192] It is worth noting that the gamma

https://doi.org/10.1021/cbmi.4c00085
Chem. Biomed. Imaging 2025, 3, 137−168

photons emitted by the particular nuclides possess specific energy levels. For instance, ^{99m}Tc ($t_{1/2}$ = 6 h), the most frequently employed radioisotope in nuclear medicine, emits gamma photons at an energy value of 140 keV.[193,194] As previously mentioned, despite the notable advantages of PET in terms of performance, when combined for assessing clinical translational capabilities, SPECT offers cost-effective radiographic contrast and gamma scanning equipment compared to PET. Moreover, SPECT enables the utilization of radionuclides emitting γ rays with varying energy levels, enabling multiradionuclide imaging. Additionally, SPECT radiographic agents generally exhibit longer decay times in comparison to PET agents, which aligns with the requirement for a prolonged window for tracking MSC-EVs.

A strategy for labeling EVs in SPECT imaging was initially introduced in 2015, as reported by Zhang et al.[195] The researchers successfully radiolabeled B16-BL6 sEVs containing streptavidin using biotin-conjugated ^{125}I, specifically [^{125}I]I-IBB. Unfortunately, this is not a straightforward method of labeling. Despite attempts to enhance the labeling methods for ^{111}In and ^{64}Cu by incorporating diethylenetriaminepentaacetic acid (DTPA) and PEGylation, respectively, the current techniques still struggle to fully meet the requirements for clinical translation of MSC-EVs.[196,197] To address the issues encountered during the labeling process, Liu et al. proposed an alternative strategy by a ^{111}In-Oxine-based method for MSC-EVs labeling ($t_{1/2}$ = 2.8 d).[198] The commercial availability of ^{111}In-Oxine proves to be advantageous for clinical applications.[199−202] It possesses lipophilic properties, allowing it to traverse the phospholipid bilayer of EVs. Subsequently, ^{111}In is released from the oxyquinoline complex and decays to ^{111}Cd via isomeric transition and electron capture, thereby emitting γ photons to facilitate SPECT/CT imaging. Notably, they compared the injection of ^{111}In-MSC-EVs with ^{111}In-Oxine as a control (Figure 8A and B). Quantitative analyses of the percentage of injected dose per cubic centimeter (%ID/cc) were performed on the volume of interests (VOIs) obtained from various organs at 1 and 3 h postinjection. Results demonstrated differential accumulation of ^{111}In-MSC-EVs, with higher levels of uptake in the liver and spleen and lower levels in the lung, kidney, and heart (Figure 8C and D). This pattern diverged markedly from the results obtained in the ^{111}In-Oxine group, indicating minimal off-target effects associated with this specific labeling approach.

Building upon the labeling strategy mentioned above, Stice et al. conducted an in-depth investigation on the biodistribution and metabolism of MSC-EVs in a mouse model subjected to thromboembolic (TE) stroke.[203] The study demonstrated a preferential accumulation of EVs in the penumbra region surrounding the injury site, followed by significant clearance from the infarct region within 24 h. Nevertheless, traces of EVs remained detectable in other organs (Figure 8E). These results lay the groundwork for optimizing the dosage, injection frequency, and interval between MSC-EV administrations within corresponding treatment protocols. Furthermore, they provide valuable insights for subsequent analyses, including neurological deficit scoring (NDS) and adhesive tape testing (ATT).

The ^{111}In-Oxine-based labeling approach has been validated for its high stability and has also demonstrated the value of MSC-EVs in disease models. However, the labeling efficiency of this strategy remains limited to just 5%. An urgent need is to develop more efficient labeling methods while ensuring rapidity and simplicity. In addition, SPECT imaging labeling based on other metal isotopes should also gain further practice in MSC-EVs. Given the wide range of applications of MSC-EVs, the physical properties of a specific radioactive metal should match the biokinetics of disease-specific target molecules.[204] For instance, a high degree of labeling stability is essential for oncological targeting, whereas perfusion studies may benefit from more dynamic, adaptable labeling properties for the observation of the flow and diffusion of drugs or substances. Achieving this balance necessitates further research into chemical coordination and structural optimization.

PET and SPECT rely on the radiolabeling of MSC-EVs, a process encompassing two distinct strategies: surface radiolabeling and intraluminal radiolabeling. Undeniably, the investigations mentioned above have yielded substantial advancements in follow-up imaging applied to MSC-EVs. Moreover, the integration of anatomical imaging modalities like CT and magnetic resonance imaging (MRI) has conferred the advantage of precise localization of MSC-EVs within deeper tissues. However, several challenges persist. The inherent instability of MSC-EVs often introduces confounding signals, disrupting the accurate interpretation of results.[205] The rapid clearance and lysis of the EVs may lead to nonspecific binding of the radiolabeled marker to proteins, vesicles, and other lytic byproducts, thereby generating hot spots beyond EVs. Furthermore, instability in radiolabeling during serum verification introduces complexities. In instant thin-layer chromatography (ITLC), unstable radionuclides tend to migrate, while stably labeled EVs remain at the origin (R_f = 0). Proteins tend to precipitate in the presence of organic solvents, and radioactive signals chelated with serum proteins and other impurities do not migrate either, making it challenging to discern whether the radioactivity is associated with EVs or serum proteins. Addressing the concerns necessitates further strategy refinement, including the direct membrane coupling of bifunctional radionuclide complexes and intraluminal labeling using ion carriers like oxine.

5. TOMOGRAPHIC IMAGING

Tomographic scanning represents a technique for the efficient and noninvasive imaging of EVs, boasting potential for clinical translation. This modality is well-suited for longitudinal imaging of targets. To perform tomographic scans, EVs must be labeled with nanoparticles as tracers. Commonly employed tomographic imaging devices include CT and MRI.

5.1. CT

In clinical medicine, CT imaging has emerged as a cost-effective and efficient technique, primarily due to its high temporal and spatial resolution.[206−209] Based on the Beer−Lambert Law, this imaging technique utilizes X-ray attenuation coefficient imaging, where the Radon transform is used to reconstruct 3D images to diagnose relevant diseases.[210−213] The advent of nanotechnology has heightened interest in the X-ray attenuation properties of nanoparticles,[214,215] leading to a proliferation of studies integrating these particles with target cells for CT-based tracing.[216−217220] Consequently, utilizing similar strategies for tracing MSC-EVs appears highly feasible and has already been successfully validated. It is noteworthy that the group led by Rachela Popovtzer has made a significant contribution in this area, and their findings are expected to facilitate the clinical translation of related research.

https://doi.org/10.1021/cbmi.4c00085
Chem. Biomed. Imaging 2025, 3, 137−168

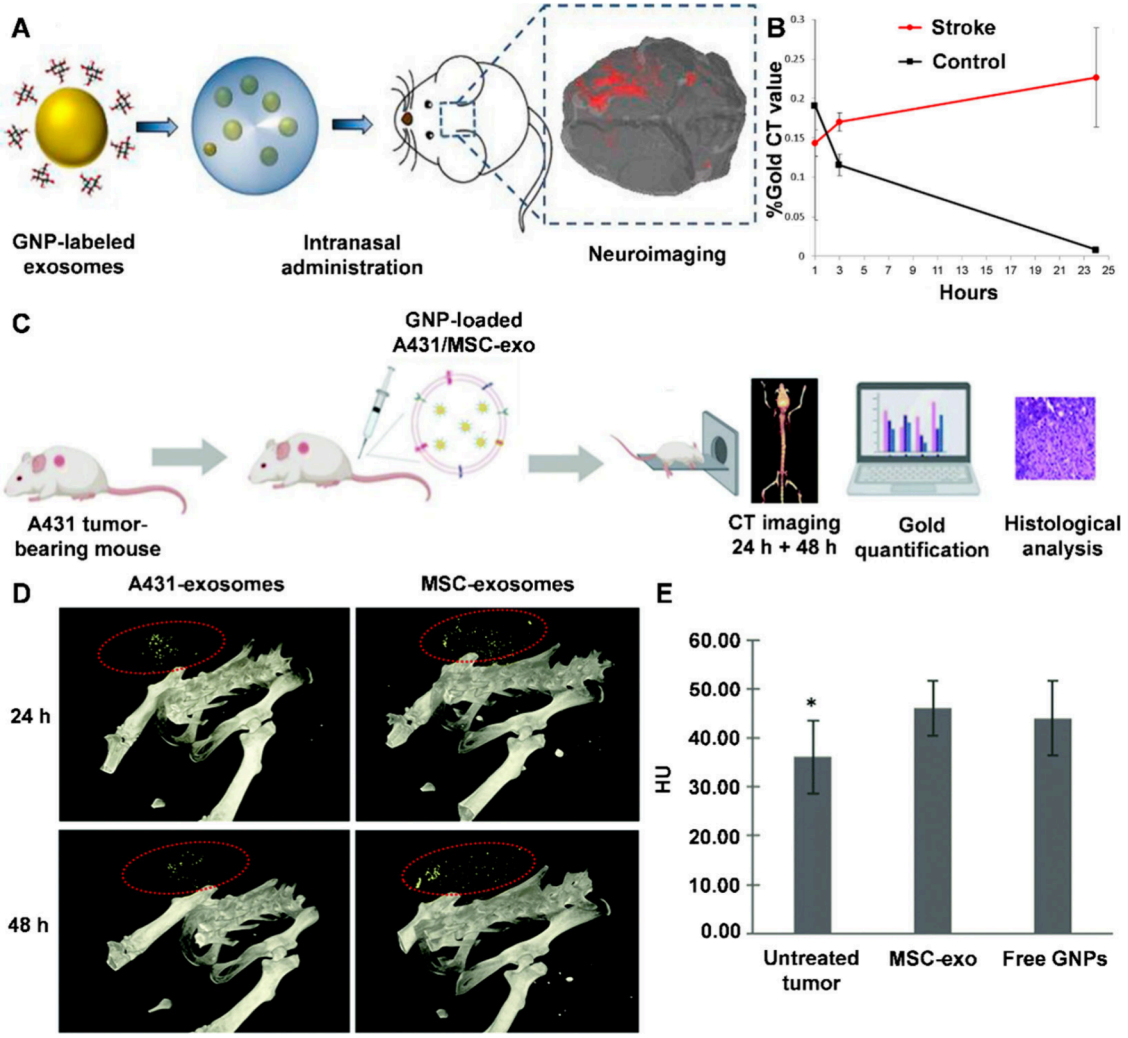

Figure 9. MSC-EVs tracing by CT. (A) Schematic illustration for in vivo neuroimaging strategy of EVs using GNPs. (B) Measurements of contrast enhancement in whole brain and in the ischemic striatum over time. A gradual increase in CT signal was observed in the ischemic area over 24 h, while the signal decreased over time in control mice. Reproduced from ref 228. Copyright 2017 American Chemical Society. (C) Schematic illustration of the study design. A431-exo or MSC-exo were loaded with GNPs and IV injected into an A341 tumor-bearing mouse. Mice were then imaged with CT at 24 and 48 h after injection. Mice were sacrificed after the last scan, and gold was quantified within major organs and the tumor, using ICP-OES. Histological analysis was performed on tumor sections. (D) *In vivo* CT tracking of EV accumulation within an HNSCC tumor in mice. 3D volume rendered images focusing on the tumor region (demarcated in red) in the back flank of a representative mouse, 24 and 48 h after injection. GNP-labeled EVs of both types (seen as yellow dots) are observed in the tumor, at both time points. (E) CT number (expressed in Hounsfield units, HU) of tumor density at 24 h post administration (left column), of GNP-loaded EVs (middle) and free GNPs (right). *$P < 0.05$ for the different treatments vs the untreated tumor. $n = 5$ per group. Reproduced from ref 249. Available under a CC BY-NC-ND 4.0 license. Copyright 2021 Cohen, O.; et al.

The unique ability of EVs to traverse the BBB positions them as promising candidates for cell-free therapies targeting brain disorders.[221−223] MSC-EVs, in particular, demonstrate parallel therapeutic efficacy to MSC-based treatments while avoiding the risks associated with MSC transplantation.[224,225] Nonetheless, further elucidation of their biodistribution and pharmacokinetics through tracer markers could advance their therapeutic use.[90] While fluorescence and optical imaging modalities have limitations in imaging and tracer EVs within deep brain structures, CT tracing strategies have been developed using gold nanoparticles (GNP) as contrast agents for *in vivo* CT imaging and cell tracking.[226,227] Direct labeling of MSC-EVs with GNP for *in vivo* neuroimaging and tracing has also shown great potential, overcoming the inefficiency of indirect labeling methods based on mother cell culture and difficulties posed by the size of EVs and the skull barriers.[228,229] Researchers have developed an energy-dependent active labeling mechanism for EVs mediated by the glucose transporter GLUT-1 and endocytosis proteins, wrapping GNPs with a glucose coating (Figure 9A). As shown in Figure 9B, CT imaging clearly revealed the accumulation of MSC-EVs in stroke-affected regions of the brain, with distinct contrast observed against nonaffected regions within 24 h of intranasal administration. This GNP-based labeling method represents the first universal CT detection platform for MSC-EV tracking, advancing the study and application of MSC-EV-based therapies for various brain disorders.

Therefore, further research has focused on elucidating the specific migration and homing mechanisms of EVs in various brain disorders, including neurovascular (such as ischemic stroke), neurodegenerative (including Parkinson's and Alzheimer's), and neuropsychiatric (such as autism) diseases.[230]

https://doi.org/10.1021/cbmi.4c00085
Chem. Biomed. Imaging 2025, 3, 137−168

Using the previously mentioned platform, researchers have discovered that MSC-EVs exhibit 96-h specific accumulation in pathological brain regions of murine models. In contrast, they show diffuse migration in healthy controls and are cleared within 24 h. This selectivity is attributed to the neuroinflammatory signals associated with these diseases, which correlate highly with the homing accumulation of MSC-EVs.[231−233] Notably, MSC-EVs bypassed glial cells and were selectively internalized by neurons in the affected regions, highlighting the potential of this approach for diagnosing brain disorders. Previous studies have shown that MSC-EVs can reduce neuroinflammation and promote neurogenesis and angiogenesis in models of epilepsy.[234] They can also break down spatial learning deficits and improve functional recovery in models of traumatic brain injury.[235] With the aid of this tracer platform, it may be possible to monitor treatments, substantially advancing the path toward clinical translation.

Interestingly, their subsequent research focused on the treatment of SCI,[236] a debilitating condition that poses a hurdle to successful treatment.[237−242] In the postinjury microenvironment, SCI is characterized by limited axonal regrowth and a diminished capacity for intrinsic neuronal regeneration. This deficiency is primarily attributed to the expression of phosphatase and tensin homologue (PTEN) in neurons and regenerating axons, which inhibits mammalian target of rapamycin (mTOR) activity, thereby restricting axonal growth.[243−246] To address this issue, the intranasal administration of PTEN-siRNA-loaded MSC-EVs has been demonstrated to be a rapid, cell-free, lesion-specific, and effective therapeutic strategy for SCI. Employing GNP-based labeling method, researchers utilized microcomputed tomography (micro-CT) and inductively coupled plasma (ICP) detection to demonstrate the selective accumulation of MSC-EVs in injured spinal cord regions for over 24 h, a pattern distinct from the diffuse accumulation observed in the brains of healthy mice. In addition, flame atomic absorption spectroscopy (FAAS) was employed to quantify GNP levels in major organs (i.e., liver, lungs, heart, kidneys, and spleen) within 24-h postadministration. The results revealed elevated GNP concentrations in the liver and kidneys of healthy rats compared to those in the SCI group, suggesting that the reticuloendothelial system facilitates more rapid excretion of MSC-EVs in healthy rats than in injured counterparts. Beyond serving as contrast agents for EV tracing, GNPs provide critical information for monitoring SCI treatment. Thus, elucidating the inorganic information and correlating it with other biological changes will undoubtedly facilitate the development of EV-mediated cell-free therapies.

Further expanding the application of MSC-EVs in the treatment of neurological diseases remains a focus of future research. Among these challenges, head and neck tumors present substantial obstacles, as the cranial barrier exacerbates the limitations of optical imaging that are not easily quantifiable.[247] Additionally, the high metabolic rate of tumors decreases the resolution of nuclear imaging.[248] Hence, the use of CT imaging is becoming more pronounced. MSC-EVs can potentially be a promising carrier for treating head and neck squamous cell carcinoma (HNSCC). The tumor-targeting properties of MSC-EVs were confirmed through CT imaging validation.[249] In A431 tumor-bearing mice, MSC-EVs and A431 squamous carcinoma cell-derived EVs (A431-EVs) were longitudinally and quantitatively tracked (Figure 9C). As shown in Figure 9D, the *in vitro* analysis and CT imaging over 48 h exhibited a higher tumor-homing effect of MSC-EVs. Furthermore, MSC-EVs could penetrate and disperse within the tumor, while free GNPs localized primarily around the tumor periphery (Figure 9E). This study marks the first direct evaluation of the therapeutic potential of EVs from distinct sources as candidate carriers, emphasizing tumor-targeting and penetration capabilities. It pioneers the use of CT-based assessments for evaluating EV efficacy in tumor models. Furthermore, it was found that A431-EVs exhibited a greater GNP loading capacity, suggesting that GNP loading efficiency should be considered as an evaluation criterion in future research.

The "Golden" EVs have been shown to have substantial benefits in numerous studies, including investigations of brain disease mechanisms, therapeutic monitoring, and CT imaging of MSC-EVs with excellent resolution and penetration capabilities. However, as with any technique, some limitations need to be addressed. One such drawback of direct labeling of GNPs loaded in EVs is that they can be freely released during circulation, resulting in inaccurate readings of EV trajectories. Consequently, the development of more reliable labeling materials and modification strategies is essential to mitigate these challenges. Additionally, the inherent issue of ionizing radiation associated with CT imaging necessitates the development of effective solutions to enhance safety.

5.2. MRI

MRI is among the most widely utilized imaging modalities in clinical practice. Compared to CT, MRI offers superior spatial resolution and superior soft tissue contrast, particularly for deep anatomical structures.[250−253] Furthermore, the absence of ionizing radiation makes MRI a better option for safety. Given the significant involvement of MSC-EVs in the paracrine signaling mechanisms of MSCs, elucidating the biodistribution and tracking assumes crucial significance in understanding tissue repair and other related biological processes.[254−256] Consequently, the utilization of MRI, with its unique merits, has garnered considerable attention for investigating the tracing of MSC-EVs.

MRI tracing of MSC-EVs is commonly achieved by utilizing superparamagnetic iron oxide nanoparticles (USPIO) as a contrast agent, with iron content measurement serving as a means to validate labeling efficiency.[257] The most straightforward method involves the electroporation of USPIO into EVs for labeling. Despite achieving high labeling efficiency, the electrical pulses can transiently disrupt the membranes, potentially altering the composition of the membrane and internal cargo, which could compromise their functional integrity.[258] To address this concern, a more common strategy involves labeling MSCs with USPIO and subsequently isolating the labeled EVs from these cells after cultivation. It originated from research aimed at investigating nonspecific MRI signals in cell transplantation. Silva et al. were the first to coincubate USPIO with MSCs, leveraging the internalization mechanisms of the cells for labeling, followed by the induction of starvation stress.[259] Notably, they discovered that EVs released by the labeled cells carried the MRI signal and were subsequently internalized by naïve cells, thus illuminating the paracrine mechanisms of MSCs. In a subsequent study utilizing a similar coincubation strategy, researchers investigated ASCs.[260] They observed that labeling was dose- and time-dependent, as assessed by metrics including cell viability, labeling efficiency, iron content, and MRI contrast. It is worth

https://doi.org/10.1021/cbmi.4c00085
Chem. Biomed. Imaging 2025, 3, 137−168

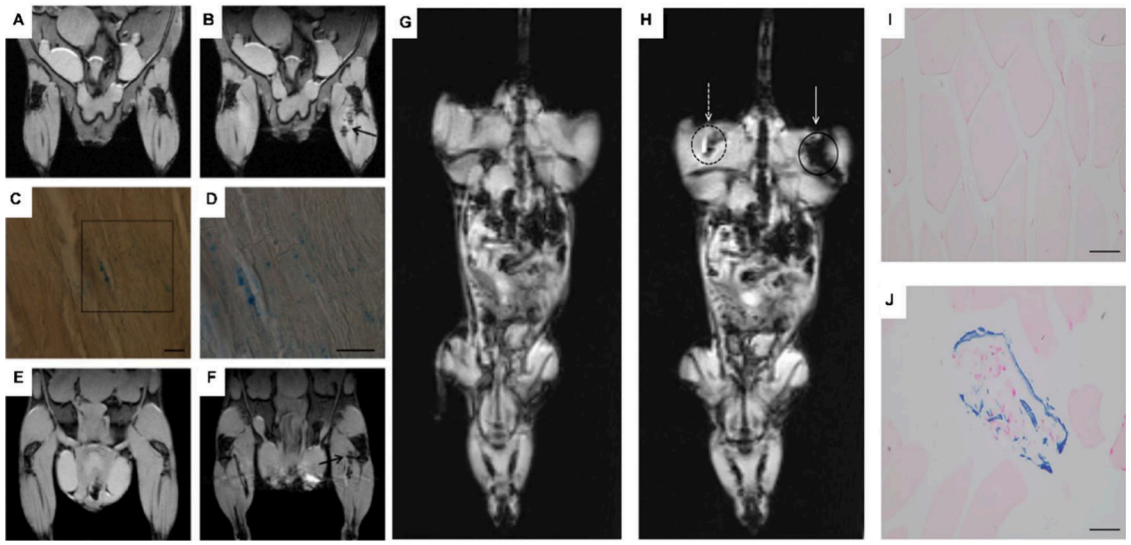

Figure 10. MSC-EVs tracing by MRI. (A−F) *In vivo* MR images acquired preintramuscular (A) and postintramuscular (B) injections of EVs-USPIO (arrow). Prussian blue histological examination of extracted muscle tissue: blue spots inside the muscle confirmed the presence of iron nanoparticles (C; magnification ×20). Scale bar, 50 μm. D shows a higher magnification (×40) of the boxed area shown in C. Scale bar, 50 μm. *In vivo* MR images acquired preintramuscular (E) and postintramuscular (F) injections of plain USPIO (arrow) containing the same amount of iron of labeled EVs; the signal is comparable with that detected in EVs-USPIO (B). Reproduced from ref 260. Available under a CC BY-NC 3.0 license. *Int. J. Nanomed.* **2016**, *11*, 2481−2490. Originally published by and used with permission from Dove Medical Press Ltd. (G−J) *In vivo* MRI of EV−MSC/FTH1 versus EV−MSCs. *In vivo* MR images acquired preintramuscular (G) and postintramuscular (H) injections of EV−MSC/FTH1 (circle and arrow) and EV−MSCs (dotted circle and arrow). Prussian blue histological examination of the extracted muscle tissue from EV−MSCs (I) and EV−MSC/FTH1 (J) from the injected hind limbs: blue spots inside the muscle confirmed the presence of FTH1 (J; magnification ×40). Scale bar, 50 μm. Reproduced from ref 262. Available under a CC BY-NC-ND 4.0 license. Copyright 2020 Liu, T.; et al.

noting that the isolated EVs exhibited discernible MRI signals. For in *vivo* validation, MSC-EVs were injected intramuscularly into mice, while a control group received an equivalent USPIO dosage. The comparative analysis demonstrated similar MRI signals between the two groups, thereby confirming the high sensitivity of MRI in tracking (Figure 10A-F). Considering the extensive range of MSC-EVs' applicability, forthcoming investigations should explore additional related mechanisms, including the homing effects and nuanced roles under diverse physiological and pathological conditions.

USPIO nanoparticles exhibit versatile properties, providing a basis for multimodal imaging applications. Molday ION, a product developed by BioPAL (Worcester, MA, USA), combines USPIO with rhodamine B and offers a novel approach to investigate the homing mechanism of human bone marrow MSC-derived EVs (hBM-MSC-EVs).[261] The technique circumvents the challenges associated with post-mortem identification inherent in electron microscopy, presenting the potential for real-time, *in vivo* monitoring of MSC-EVs. Importantly, Molday ION demonstrated a homogeneous distribution within EVs, contrasting with the aggregation phenomena commonly reported in previous studies involving direct USPIO labeling. Furthermore, USPIO labeling did not hinder the endocytosis of hBM-MSC-EVs or the diffusion within the cytoplasmic microenvironment. However, the potential release of free iron ions poses concerns regarding their impact on cellular processes and overall cell physiology. Therefore, further investigations are warranted to determine the therapeutic equivalence of labeled EVs compared to unlabeled EVs.

Despite extensive reporting of the aforementioned methods, they suffer from relatively low efficiency. The challenge lies in the decreasing average amount of USPIOs when labeling parent cells as cell populations expand, which leads to a dilution effect on the MRI signal. This poses difficulties for large-scale labeling and long-term *in vivo* tracking. To overcome the limitations, Xin et al. deviated from traditional USPIOs and drew inspiration from chemiluminescent reporter proteins studies previously discussed.[262] They introduced MRI reporter proteins capable of inducing contrast changes directly within MSCs, selecting ferritin heavy chain 1 (FTH1) and lactadherin, which were delivered via lentiviral transfection. FTH1, a candidate regulator of ferritin activity, is widely utilized as a functional and reproducible MRI reporter gene in molecular imaging studies.[263,264] As depicted in Figure 10G and H, the MRI images demonstrated a pronounced contrast enhancement in the hind limb injected with EV-MSC/FTH1. Histological analysis of the injected tissue further confirmed the presence of FTH1 (Figure 10I and J). The persistent expression of this gene during cell proliferation offers a viable approach for long-term MRI tracking of EVs. Nonetheless, the low abundance and sensitivity of FTH1 can potentially impact the efficacy of this strategy. Moreover, FTH1 expression may negatively impact MSC proliferation, necessitating further research to address these challenges.

In conclusion, MRI holds considerable potential for tracking MSC-EVs. Nevertheless, the drawback of low sensitivity demands relatively high contrast concentrations. Moreover, the lost retention of USPIOs within the original EVs complicates the interpretation of imaging data, leading to potential false-positive signals—an ongoing challenge in this field. Thus, developing more robust methods for conjugating contrast agents to EVs is imperative. Promising approaches may involve concentrating exogenously administered contrast agents within MSC-EVs via receptor-mediated reporter gene

https://doi.org/10.1021/cbmi.4c00085
Chem. Biomed. Imaging 2025, 3, 137−168

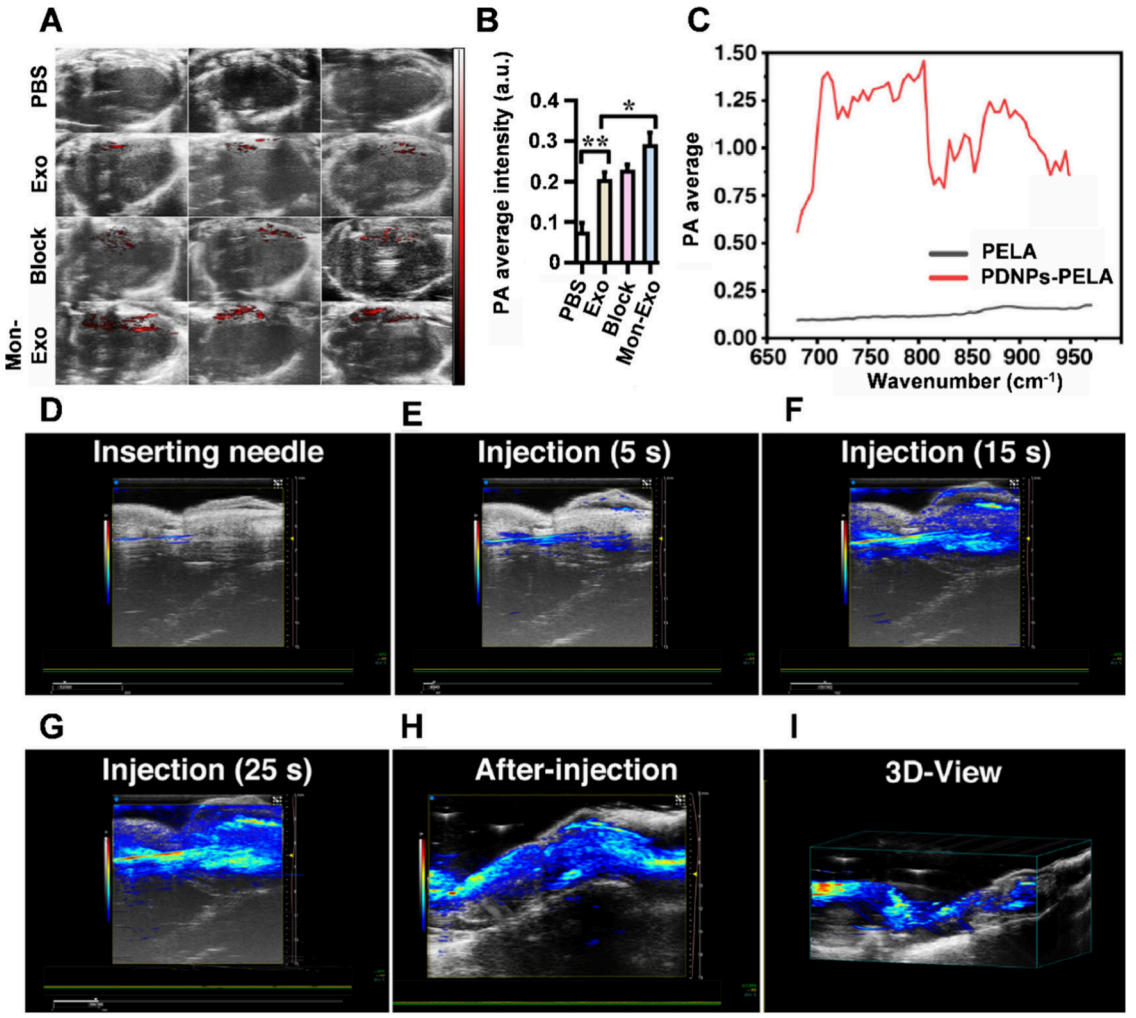

Figure 11. MSC-EVs tracing by PAI. *In vivo* targeting of Mon-Exo: PA images (A) and quantitation (B) of Exos and Mon-Exos distributed in the LVAW after intravenous (IV) injection in mouse MI/RI model (n = 3). Reproduced from ref 287. Available under a CC BY-NC-ND 4.0 license. Copyright 2020 Zhang, N.; et al. (C) Photoacoustic signals under wavelength scanning of PDNPs-PELA. *In vivo* PAI-guided intratunical injection: (D) The needle was punctured into tunica albuginea under the guidance of photoacoustic images. (E−G) EXO@PDNPs-PELA was injected and evenly distributed in the tunica albuginea. (H) EXO@PDNPs-PELA formed a gel after 3 min injection. (I) A representative 3D reconstructed image of (H). Reproduced from ref 291. Available under a CC BY-NC-ND 4.0 license. Copyright 2021 Liang, L.; et al.

expression, or amplifying imaging signals through interactions with activatable MRI contrast agents.[265−267]

Compared to nuclear imaging, tomographic imaging offers inherent advantages for tracing MSC-EVs, including faster scanning speeds and improved radiation safety (e.g., X-rays for CT and no radiation for MRI).[268−270] Furthermore, tomographic imaging yields high-resolution anatomical images that precisely delineate lesion morphology and localization, thereby enabling concurrent imaging and monitoring of MSC-EVs in therapeutic process. However, several challenges remain. For instance, due to the small size of MSC-EVs, their signals may be difficult to distinguish from imaging artifacts and background noise, particularly in large animal studies.[271,272] The integration of deep learning techniques, such as convolutional neural networks (CNNs) and generative adversarial networks (GANs), shows promise in enhancing image reconstruction, synthesis, and modality conversion—such as generating high-quality images from low-dose CT scans—thereby improving image quality while reducing radiation exposure. Moreover, the development of contrast agents specifically for tomographic imaging of MSC-EVs remains limited. Considering the challenges associated with achieving atomic-level precision in metals, the development of organic contrast agents that integrate functional modifications while ensuring high biocompatibility represents a promising direction.[273,274]

6. PAI

PAI represents a noninvasive biomedical imaging technique that integrates the superior contrast capabilities of traditional optical imaging with deep tissue penetration and high spatiotemporal resolution characteristic of ultrasound imaging.[275−278] This technique operates on the principle of the photoacoustic effect, wherein contrast agents absorb pulsed laser energy and undergo rapid thermoelastic expansion. This expansion generates broadband ultrasound waves, which are subsequently detected by ultrasound transducers and converted into electrical signals to produce PA images after appropriate processing.[279] To accomplish effective MSC-EV tracing, it is imperative that the contrast agents are efficiently incorporated into the EVs to enable precise image-guided therapeutic interventions.

https://doi.org/10.1021/cbmi.4c00085
Chem. Biomed. Imaging 2025, 3, 137−168

Table 1. Comparison of Advantages and Disadvantages of MSC-EV Tracing Methods

imaging technique	tracing agent	advantages	disadvantages	scopes
FLI	organic dyes	strong and long-lasting fluorescence signal withmultiple color options and chemical versatility	nonspecific binding with other lipid components and generating false-positive signals	*in vitro* and*in vivo*
	genetically encoded fluorescent proteins	bidirectional or multidirectional transport of EVs between cells	degradation or inactivation of fluorescent proteins	*in vitro* and *in vivo*
		no risk of dye diffusion or detachment	complex and time-consuming experimental process	
		highly specific labeling		
	fluorescent nanomaterials	outstanding optical characteristics and customizable functionalization	complex and time-consuming synthesis process	-
		cost-effective and scalable	potential cytotoxicity and biodegradability concerns	
BLI	luciferase	distinguishes between intact and nonintact (internalized) EVs *in vivo*	unlikely FDA approval for administering xenogenes and substrates to patients	*in vitro*
		produces localized "hot spot" signals without imaging artifacts	limited quantitative capability and imaging time	
		the small size of the label minimizing the likelihood of significant effects on EV structure or function	genetic modification of parental cells	
		low background signal and no need of excitation source	substrate migration to luciferase-labeled EVs essential for signal generation	
CT	GNPs	long shelf life of imaging agents and high spatial and temporal resolution	X-ray radiation exposure	*in vivo*
			poor soft-tissue resolution	
			toxicity of contrast agents	
MRI	USPIO, MRI reporter proteins	high soft tissue contrast, enabling detailed anatomical imaging	relies on the indirect detection of protons in proximity to the contrast agents	*in vivo*
		free from radiation exposure	image artifacts introduced by iron (e.g., blood) and patient movement	
		an extended shelf life of imaging agents	the requirement for a strong magnetic field means MRI necessitating nonmagnetic surgical and medical tools	
			unsuitable for patients with metal implants	
			the large size of USPIO particles altering the properties of EVs	
			gadolinium-based chelates associated with nephrogenic systemic fibrosis	
			limited ability to quantify imaging agents	
nuclear (PET and SPECT)	^{111}In, ^{124}I, ^{89}Zr	radionuclides directly detected with minimal imaging artifacts	requires combination with MRI or CT to provide anatomical context	*in vivo*
		the small size of the labels minimizing the likelihood of significant effects on EV structure or function	the administration of radioactive tracers to patients	
		signals allow for absolute quantification of EVs	short half-life due to radiodecay	
PAI	strong light-absorbing dyes or materials	deep tissue imaging capabilities	limited signal sensitivity	*in vivo*
		high spatial and temporal resolution with label-free endogenous contrast	tissue scattering and absorption effects; difficult to quantify in real time	
		low background noise	limitations of functional information	

The principles outlined above imply that an ideal contrast agent should possess specific photophysical properties, including low quantum yield, high molar extinction coefficient, and exceptional photostability. Additionally, it must exhibit low toxicity, minimal immunogenicity, high target affinity and specificity, as well as excellent biocompatibility.[280−282] DiR dye, a small molecule NIR-II PA contrast agent, meets these criteria.[283−286] It has been employed to track the homing effect of MSC-EVs, aiding in the treatment of acute myocardial ischemia/reperfusion injury (MI/RI) in murine models.[287] To enhance the targeting of this contrast agent, researchers employed a membrane fusion strategy to modify MSC-EV with monocyte mimics (Mon-Exos) to generate cardiac injury-specific adhesion molecules. To evaluate the enhanced targeting efficiency, Mon-Exo, Exo, and CD18-blocked Mon-Exo (Block) were labeled with DiR. Results indicated that the PA signal in the left ventricular anterior wall of the Mon-Exo group was significantly stronger than that of the Exo group (1.42-fold) at 2-h postadministration. Notably, even the Block group exhibited greater accumulation compared to the Exo group (1.14-fold) (Figure 11A and B). However, despite the ease of labeling small molecule dyes like DiR, they remain short-lived in circulation, susceptible to photobleaching, and poorly stable under prolonged laser light exposure. Thus, appropriate chemical modification has the potential to address the challenges.

The modification of polydopamine has emerged as a promising approach to enhance the photoacoustic (PA) effects of MSC-EVs.[288−290] In this context, Gu et al. have developed a thermosensitive hydrogel (PDNPs-PELA) composed of polydopamine nanoparticles (PDNPs) via *in situ* polymerization, which was employed for intrauterine injection of ADSC-EVs in the treatment of erectile dysfunction (ED).[291] The PA performance of the hydrogel was evaluated under near-infrared (NIR) laser excitation within the range of 680 to 980 nm. Compared to poly(ethylene glycol)-poly(ε-caprolactone-*co*-polymer) (PELA), the PDNPs-PELA hydrogel exhibited an increased ultrasound signal, with a peak signal intensity of 1.47 at 805 nm (Figure 11C). The gel was subsequently utilized for *in vivo* PAI-guided intratunical injection. The results indicated that the gel was clearly traced by PAI, facilitating precise needle positioning adjustment to improve the puncture accuracy (Figure 11D). The entire injection process is illustrated in detail in Figures 11E-G.

https://doi.org/10.1021/cbmi.4c00085
Chem. Biomed. Imaging 2025, 3, 137−168

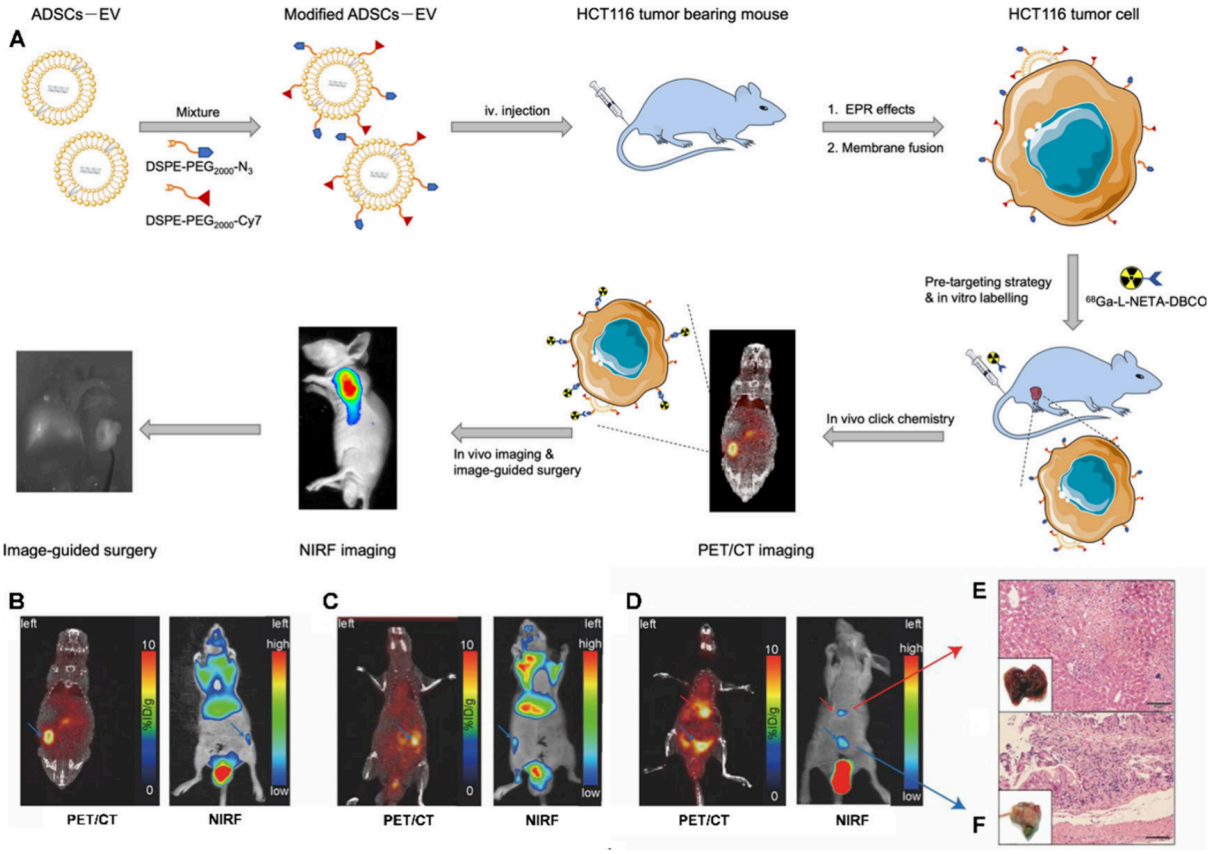

Figure 12. MSC-EV tracing by multimodal bioimaging. (A) The schematics of multimodal PET and NIRF imaging and real-time NIRF intraoperation based on EVs from ADSCs. (B, C) Multimodal PET/CT and NIRF images of the left and right orthotopic colon cancer model. The blue arrows denote colon tumors in situ. (D) Multimodal PET/CT and NIRF images of orthotopic colon cancer model (blue arrows) with liver metastasis (red arrows). (E, F) The visual observation of tumors and HE staining of pathological sections. Scale bar, 50 μm. Reproduced from ref 302. Available under a CC BY 4.0 license. Copyright 2021 Jing, B.; et al.

Between 5 and 25 s postinjection, the EXO@PDNPs-PELA suspension fully filled the corpus cavernosum. The thermosensitive sol−gel transition resulted in gel formation within 3 min (Figure 11H). A 3D PA scan conducted 24 h postinjection revealed band-shaped images indicative of gel formation within the lumen (Figure 11I). Additionally, the absence of significant differences in PA signal intensity suggested a uniform biodistribution of the EVs. This study represents the first successful instance of real-time fine tracing of MSC-EVs through PA imaging, pioneering their use in guiding therapeutic interventions. However, the mechanisms underlying in situ polymerization warrant further investigation to enable precise control over the polymerization process, including parameters such as particle size, morphology, thickness, and byproducts. Furthermore, the preservation of EV activity and functionality following release should be confirmed to ensure therapeutic efficacy.

In summary, PAI represents a promising technology for tracking MSC-EVs within deep tissues, thereby establishing a reliable foundation for expanding the therapeutic potential. Nevertheless, the limited penetration depth of current PAI systems remains a critical challenge.[292] Most available organic contrast agents lack absorption beyond 1064 nm, underscoring the need for advancements in NIR-II window technologies and the development of novel contrast agents.[293,294] In addition, the realization of PAI contrast agent encoding, simultaneous imaging of tissues on a tracer basis, and monitoring of therapeutic responses with high specificity would also fuel a PAI-directed breakthrough in treating MSC-EVs.[295] To achieve the ultimate goal of clinical translation, improvements in hardware are equally essential, including the development of more cost-effective excitation light sources (e.g., LEDs, laser diodes) and enhanced ultrasound transducers.[296−298]

7. MULTIMODAL BIOIMAGING

Multimodal bioimaging is a strategy that amalgamates various imaging techniques for tracking MSC-EVs. Each of the above-mentioned tracing strategies has its own advantages and disadvantages, as shown in Table 1. It combines the strengths of diverse imaging modalities to achieve mutual complementarity, thereby expanding the utility spectrum of the tracking system and augmenting imaging precision. The most classic is the bimodal tracking approach involving PET/CT and SPECT/CT, which has been discussed in nuclear imaging section. Furthermore, the attributes of NIR fluorescent dyes, characterized by the superior tissue penetration and robust MSC-EV labeling capabilities, render them ideal companions when juxtaposed with techniques like nuclear imaging and tomography imaging, ultimately affording an amplification of sensitivity within 3D imagery.

Fluorescent and magnetic dual-labeled superparamagnetic iron oxide (SPIO) nanoparticles were initially employed as a tracer tool for *in vitro* tracking of MSC-EVs, demonstrating the feasibility and utility.[261] Despite the effectiveness of this labeling strategy, concerns arise regarding the potential release

https://doi.org/10.1021/cbmi.4c00085
Chem. Biomed. Imaging 2025, 3, 137−168

of free iron ions, which could perturb cellular processes and compromise cellular physiology. To address these limitations, chelation is commonly employed to enhance the stability of contrast agents. Linear macromolecules like diethylenetriamine pentaacetic acid (DTPA) and cyclic macromolecules like 1,4,7,10-tetraazacyclododecane-1,4,7,10-tetraacetic acid (DOTA) are utilized to stabilize gadolinium (Gd), enabling the use of high-field MRI (14.1 T).[299] When coupled with NIR) dyes, this approach facilitates efficient and safe tracking of MSC-EVs.[300] Consequently, a high accumulation rate of MSC-EVs in osteosarcoma tissues is unveiled, underscoring its potential for metastasis detection.

Trimodal tracing of MSC-EVs, intertwining NIR dyes with PET/CT and SPECT/CT, has exhibited promising outcomes in tumor surveillance. The intrinsic tumor-targeting capabilities of MSC-EVs significantly enhance the efficacy of this imaging strategy.[301] While SPECT/CT facilitates comprehensive whole-body imaging with high tissue penetration, it is hindered by relatively long acquisition times, short imaging windows, and limited spatial resolution. In parallel, NIR fluorescence can provide real-time and high-resolution information on tissue structure. An et al. employed hydrazinonicotinamide as a chelator for ^{99m}Tc and labeled MSC-EVs with Cy7 through the DSPE membrane insertion technique.[302] This approach enabled precise delineation of tumor margins and effective assessment of MSC-EV biodistribution. However, signal accumulation was observed in the liver, spleen, and kidneys, which compromised tumor imaging quality. To address this limitation, a pretargeting strategy was employed, highlighting the distinct advantages of multimodal bioimaging.[303] Initially, MSC-EVs labeled with Cy7 and azide (N_3) were administered to visualize and pretarget tumor tissue, creating bio-orthogonal sites within the tumor region. Following a 20-h interval, ^{68}Ga-L-NETA-DBCO was introduced as the contrasting agent, orchestrating nuclear labeling through bioorthogonal reactions at the pretargeted site. The results demonstrated clear visualization of tumors at the primary lesion (right abdomen, Figure 12B and C), thereby aiding surgical guidance, as well as at metastatic sites in the liver (liver, Figure 12D). Histological examination with HE staining further validated the presence of colon cancer and liver metastasis (Figure 12E and F). This investigation harnessed the NIR molecule to determine the optimal pretargeting time frame, concurrently devising a strategy for drug delivery therapy that balances low toxicity with high efficiency.

In conclusion, amalgamating sensitive imaging modalities (PET, optical, etc.) with those endowed with spatial resolution (MRI, CT, etc.) is commonplace. Such combinations, however, typically necessitate multiple labeling procedures, wherein the intricacy of labeling directly affects MSC-EVs functionality. Ideally, a single labeling strategy that achieves multimodal imaging would be most advantageous—an idea uniquely enabled by nanoscale labeling of EVs, inspired by the metallization of EVs.[304] Gold nanomaterials, as an exemplar, amalgamate NIR fluorescence emission, X-ray absorption, and unique plasma absorption properties, thereby enabling concurrent fluorescence, tomography, and PAI.[305−307] The facile composability of nanomaterials further positions them as prospective probes for multimodal imaging.[308−311] Additionally, advances in imaging technologies and instrumentation are continuing to drive the development of multimodal imaging for MSC-EVs. This encompasses integrating diverse imaging devices into a unified apparatus or the advancement of multiplexed holography for the simultaneous measurement of multiple physical parameters, including polarization, fluorescence, and spectroscopy.[312,313] Given the therapeutic potential of MSC-EVs, leveraging the advantages of multimodal bioimaging to simultaneously visualize the functional molecules within MSC-EVs and the vesicles themselves can be a strategy offering heightened reliability in tracking and interaction information.

8. CONCLUSION AND PERSPECTIVES

MSC-EVs, which are currently the most promising type of EVs for clinical translation, have been the focus of an exponential surge in research publications.[314] To provide researchers with a comprehensive guide to visualizing their fate, this article delves into conventional biomedical imaging techniques (including FLI, BLI, SPECT, PET, CT, MRI, etc.) alongside an exploration of labeling methodologies (including direct and indirect), systematically showcasing the progress and potential optimization strategies for MSC-EV tracking. This review aspires to promote the standardization of MSC-EVs to evolve with the times, supporting the translation of related research from bench to bedside. Nonetheless, the fruition of the objectives is beset with obstacles. In the ensuing sections, we will discuss the quandaries confronting MSC-EVs research and provide potential innovative tracing methods for the tracing.

8.1. Quantify Tracing to Establish a Methodological Scoring System

Quantification of tracing efficacy stands as a critical metric for evaluating the appropriateness of a given methodology. For MSC-EVs, prevalent quantification techniques primarily encompass the assessment of optical intensity, magnetic signal, or radioactivity of labeled EVs. The sensitivity of the selected tracing approach directly influences the required dosage of labeling agents, which consequently directly correlates with its biosafety profile.[315] Increased labeling may enhance signal strength and prolong the observation window; however, it escalates the risk of toxicity and adverse physiological outcomes. For instance, Gd-based contrast agents for MRI have been implicated in inducing nephrogenic systemic fibrosis in patients with renal dysfunction.[316,317] Thus, the deployment in MSC-EVs tracing for renal damage therapy necessitates caution. Alternative administration routes other than intravenous injection should be considered to bypass renal clearance processes, minimizing uptake. Accordingly, a comprehensive assessment of a tracing strategy for MSC-EVs in disease-specific applications demands a careful balance of multiple factors, including tracing efficiency, sensitivity, labeling dosage, administration route, and biosafety. Developing a scoring system that integrates these aspects will have the potential to advance clinical translation. Assisted data analysis techniques such as machine learning are expected to provide solutions to this goal.

8.2. Simultaneous Visualization of Mechanisms of Action

The concurrent visualization of the recognition, internalization, intracellular trafficking, and release of MSC-EVs by recipient cells represents an advancing aspect of tracing. Recent studies indicate the significant role of key structural attributes—such as the glycocalyx,[318] surface charge distribution,[319] and protein corona[320] of MSC-EVs in modulating these processes, potentially influencing the biodistribution. The development of molecular probes, tailored to these specific surface characteristics, particularly probes capable of structural

https://doi.org/10.1021/cbmi.4c00085
Chem. Biomed. Imaging 2025, 3, 137−168

Table 2. Comparison of Advantages and Disadvantages of MSC-EVs from Different Sources

source type	advantages	disadvantages
BMSC-EVs	well-studied and mature techniques	invasive collection process with low patient acceptance
	rich in pro-angiogenic and anti-inflammatory factors, beneficial for bone repair and immune regulation	limited MSC quantity, often requiring *in vitro*expansion
	significantly promotes tissue regeneration	biological properties vary due to donor heterogeneity
ADSC-EVs	easy to collect and abundant source	the quality of adipose tissue from different donors may affect MSC-EV performance
	possess anti-inflammatory and immune regulatory properties	variability in bioactive molecule expression complicates standardization
	excels in skin damage repair and soft tissue regeneration	
UC-MSC-EVs	noninvasive collection and abundant source	relies on maternal donations, raising ethical concerns
	high biological activity, carrying miRNAs and growth factors	
	low immunogenicity, suitable for allogeneic transplantation	biological properties require further study
	widely applied in antiaging and anticancer therapies	
DPMSC-EVs	obtained from dental pulp tissue, relatively accessible	limited tissue availability, with high expansion costs
	rich in neurotrophic factors and growth factors, aiding in neural repair and bone regeneration	less studied compared to other sources, with mechanisms still unclear
amniotic MSC-EVs	abundant and noninvasive source	limited clinical research, with applications requiring further validation
	low immunogenicity, suitable for allogeneic therapies	performance of amniotic MSCs may vary between donors
	potential in tissue regeneration such as skin and corneal repair	

variation, coupled with the application of dynamic imaging techniques such as total internal reflection microscopy, is instrumental in delineating the mechanisms of MSC-EVs during optical tracing.[321−323] Furthermore, the colocalization of MSC-EVs and the cargoes offers a potential solution for achieving this objective.

8.3. Lack of Standardized Separation and Purification Procedures

The attainment of high-purity isolation and enrichment for MSC-EVs poses a persistent challenge. The application of lipophilic tracing labels introduces interference from contaminants like lipoproteins, engendering false-positive signals.[324] Moreover, distinct EV subpopulations, including exosomes, microvesicles, and apoptotic bodies, exhibit different functions in physiological and pathological states, amplifying the importance of discerning and analyzing the activities of specific MSC-EV subpopulations.[325−327] Nevertheless, the task of isolating the subpopulations, predicated on their physical properties or biochemical composition, confronts obstacles, pressing the need for novel and effective isolation strategies.[328]

8.4. Simultaneous Monitoring of Disease States

MSC-EVs have demonstrated significant therapeutic potential across various disease areas, including tissue repair,[18,64,329,330] inflammation mitigation,[331,332] and fibrosis attenuation.[65] The therapeutic efficacy is primarily attributed to the modulatory impacts on immune responses and regenerative processes within tissue microenvironments.[333−335] Concurrent tracking of MSC-EVs alongside real-time imaging of indicative markers, such as reactive oxygen species (ROS), which signify the disease status in tissue, enables monitoring of the therapeutic intervention.

8.5. Development of Labeling Strategies

Labeling techniques for tracing MSC-EVs encompass two primary categories: direct labeling, which involves marking the vesicles through membrane association or internalization, and indirect labeling, which relies on vesicle release from MSCs. An ideal tracer should preserve the biological functionality of MSC-EVs while maintaining stability and preventing dissociation throughout the tracking process.[155,315,336−338] Therefore, bioconjugation labeling based on click chemistry has attracted widespread attention.[21−23] Another aspect of probe design is the integration of targeting moieties, aimed at bolstering the retention of MSC-EVs within specific tissues, thereby enhancing the effectiveness of the labeling process.

8.6. Customized Clinical Tracing Protocols and Instruments

Due to limited tissue penetration depth and interference from endogenous background signals, optical tracing of MSC-EVs is confined to applications predominantly to preclinical studies involving cells, tissues, and small animal models. The potential for clinical application remains underexploited. Recent advancements in highly biocompatible probes operating within the NIR-II, coupled with optimized imaging platforms, have shown the potential to bridge the translational gap.[339] Clinical imaging modalities such as MRI, CT, SPECT, and PET provide a basis for implementing MSC-EV tracing in clinical settings. Nevertheless, the inherent sensitivity thresholds of the conventional modalities may compromise the efficacy of MSC-EV detection. There is a pressing need for the development of specialized tracing systems and instruments tailored explicitly for MSC-EV visualization.

8.7. Evaluating the Therapeutic Potential of MSC-EVs from Different Sources Using Tracing Techniques

MSC-EVs derived from various sources, such as BMSC-EVs and ADSC-EVs, exhibit distinct functionalities,[340] each with specific advantages and limitations for clinical applications, as summarized in Table 2. For example, while BMSC-EVs have been extensively studied, their collection requires invasive procedures, which may hinder their practical use. On the other hand, ADSC-EVs are easier to collect, but their efficacy and heterogeneity remain challenging. Thus, a comprehensive evaluation of the therapeutic value of MSC-EVs from different sources across various diseases, considering parameters such as efficacy and accessibility, is important, in which tracing strategies provide promising tools for assessing pharmacokinetics, targeting efficiency, and biodistribution.

8.8. Design of Theranostic Tracing Agents

MSC-EVs are frequently employed in treating conditions such as tissue repair and tumor therapy. Certain tracing agents, including gold (Au) nanomaterials used in CT imaging, exhibit

https://doi.org/10.1021/cbmi.4c00085
Chem. Biomed. Imaging 2025, 3, 137−168

enzyme-like ROS regulatory activity and photothermal conversion capabilities. These agents can inhibit bacterial growth by generating ROS at the injury site or reduce inflammation by scavenging ROS, and they can also be applied in tumor photothermal therapy and chemodynamic therapy.[341] Thus, these agents function as tracers for MSC-EVs and provide synergistic therapeutic benefits. Additionally, some organic drug molecules can be engineered with conjugated structures to achieve NIR fluorescence emission for tracing. For instance, photosensitizers like verteporfin (VER) have demonstrated the ability to enable visualization while concurrently treating lung injury in combination with MSC-EVs.[155]

AUTHOR INFORMATION

Corresponding Author

Dingbin Liu − *State Key Laboratory of Medicinal Chemical Biology, Tianjin Key Laboratory of Molecular Recognition and Biosensing, Frontiers Science Centers for Cell Responses and New Organic Matter, College of Chemistry, Nankai University, Tianjin 300071, China;* orcid.org/0000-0003-4153-9822; Email: liudb@nankai.edu.cn

Authors

Jingqi Li − *State Key Laboratory of Medicinal Chemical Biology, Tianjin Key Laboratory of Molecular Recognition and Biosensing, Frontiers Science Centers for Cell Responses and New Organic Matter, College of Chemistry, Nankai University, Tianjin 300071, China*

Zhaoyu Wang − *State Key Laboratory of Medicinal Chemical Biology, Tianjin Key Laboratory of Molecular Recognition and Biosensing, Frontiers Science Centers for Cell Responses and New Organic Matter, College of Chemistry, Nankai University, Tianjin 300071, China*

Yongchun Wei − *State Key Laboratory of Medicinal Chemical Biology, Tianjin Key Laboratory of Molecular Recognition and Biosensing, Frontiers Science Centers for Cell Responses and New Organic Matter, College of Chemistry, Nankai University, Tianjin 300071, China*

Wenshuai Li − *State Key Laboratory for Crop Stress Resistance and High-Efficiency Production, Shaanxi Key Laboratory of Agricultural and Environmental Microbiology, College of Life Sciences, Northwest A&F University, Yangling, Shaanxi 712100, China*

Mingzhu He − *State Key Laboratory of Medicinal Chemical Biology, Tianjin Key Laboratory of Molecular Recognition and Biosensing, Frontiers Science Centers for Cell Responses and New Organic Matter, College of Chemistry, Nankai University, Tianjin 300071, China*

Jingjing Kang − *State Key Laboratory of Medicinal Chemical Biology, Tianjin Key Laboratory of Molecular Recognition and Biosensing, Frontiers Science Centers for Cell Responses and New Organic Matter, College of Chemistry, Nankai University, Tianjin 300071, China*

Jia Xu − *State Key Laboratory of Medicinal Chemical Biology, Tianjin Key Laboratory of Molecular Recognition and Biosensing, Frontiers Science Centers for Cell Responses and New Organic Matter, College of Chemistry, Nankai University, Tianjin 300071, China*

Complete contact information is available at: https://pubs.acs.org/10.1021/cbmi.4c00085

Notes

The authors declare no competing financial interest.

REFERENCES

(1) Lazarus, H.; Haynesworth, S.; Gerson, S.; Rosenthal, N.; Caplan, A. Ex vivo expansion and subsequent infusion of human bone marrow-derived stromal progenitor cells (mesenchymal progenitor cells): implications for therapeutic use. *Bone Marrow Transplant.* **1995**, *16*, 557−564.

(2) Pollock, K.; Dahlenburg, H.; Nelson, H.; Fink, K. D; Cary, W.; Hendrix, K.; Annett, G.; Torrest, A.; Deng, P.; Gutierrez, J.; Nacey, C.; Pepper, K.; Kalomoiris, S.; Anderson, J. D; McGee, J.; Gruenloh, W.; Fury, B.; Bauer, G.; Duffy, A.; Tempkin, T.; Wheelock, V.; Nolta, J. A Human mesenchymal stem cells genetically engineered to overexpress brain-derived neurotrophic factor improve outcomes in Huntington's disease mouse models. *Mol. Ther.* **2016**, *24*, 965−977.

(3) Galipeau, J.; Sensébé, L. Mesenchymal stromal cells: clinical challenges and therapeutic opportunities. *Cell stem cell* **2018**, *22*, 824−833.

(4) Matthay, M. A; Calfee, C. S; Zhuo, H.; Thompson, B T.; Wilson, J. G; Levitt, J. E; Rogers, A. J; Gotts, J. E; Wiener-Kronish, J. P; Bajwa, E. K; Donahoe, M. P; McVerry, B. J; Ortiz, L. A; Exline, M.; Christman, J. W; Abbott, J.; Delucchi, K. L; Caballero, L.; McMillan, M.; McKenna, D. H; Liu, K. D; et al. Treatment with allogeneic mesenchymal stromal cells for moderate to severe acute respiratory distress syndrome (START study): a randomised phase 2a safety trial. *Lancet Respir. Med.* **2019**, *7*, 154−162.

(5) Prockop, D. J.; Prockop, S. E.; Bertoncello, I. Are clinical trials with mesenchymal stem/progenitor cells too far ahead of the science? Lessons from experimental hematology. *Stem Cells* **2014**, *32*, 3055−3061.

(6) Allan, D.; Tieu, A.; Lalu, M.; Burger, D. Mesenchymal stromal cell-derived extracellular vesicles for regenerative therapy and immune modulation: Progress and challenges toward clinical application. *Stem Cells Transl. Med.* **2020**, *9*, 39−46.

(7) Gnecchi, M.; He, H.; Liang, O. D; Melo, L. G; Morello, F.; Mu, H.; Noiseux, N.; Zhang, L.; Pratt, R. E; Ingwall, J. S; Dzau, V. J Paracrine action accounts for marked protection of ischemic heart by Akt-modified mesenchymal stem cells. *Nat. Med.* **2005**, *11*, 367−368.

(8) Mathew, B.; Ravindran, S.; Liu, X.; Torres, L.; Chennakesavalu, M.; Huang, C.-C.; Feng, L.; Zelka, R.; Lopez, J.; Sharma, M.; Roth, S. Mesenchymal stem cell-derived extracellular vesicles and retinal ischemia-reperfusion. *Biomaterials* **2019**, *197*, 146−160.

(9) Chen, T. S.; Arslan, F.; Yin, Y.; Tan, S. S.; Lai, R. C.; Choo, A. B. H.; Padmanabhan, J.; Lee, C. N.; de Kleijn, D. P.; Lim, S. K. Enabling a robust scalable manufacturing process for therapeutic exosomes through oncogenic immortalization of human ESC-derived MSCs. *J. Transl. Med.* **2011**, *9*, 47.

(10) Wang, B.; Yao, K.; Huuskes, B. M.; Shen, H.-H.; Zhuang, J.; Godson, C.; Brennan, E. P.; Wilkinson-Berka, J. L.; Wise, A. F.; Ricardo, S. D. Mesenchymal stem cells deliver exogenous microRNA-let7c via exosomes to attenuate renal fibrosis. *Mol. Ther.* **2016**, *24*, 1290−1301.

(11) Anderson, J. D.; Johansson, H. J.; Graham, C. S.; Vesterlund, M.; Pham, M. T.; Bramlett, C. S.; Montgomery, E. N.; Mellema, M. S.; Bardini, R. L.; Contreras, Z.; Hoon, M.; Bauer, G.; Fink, K. D.; Fury, B.; Hendrix, K. J.; Chedin, F.; EL-Andaloussi, S.; Hwang, B.; Mulligan, M. S.; Lehtio, J.; Nolta, J. A. Comprehensive proteomic analysis of mesenchymal stem cell exosomes reveals modulation of angiogenesis via nuclear factor-kappaB signaling. *Stem Cells* **2016**, *34*, 601−613.

(12) Mendt, M.; Kamerkar, S.; Sugimoto, H.; McAndrews, K. M.; Wu, C.-C.; Gagea, M.; Yang, S.; Blanko, E. V. R.; Peng, Q.; Ma, X.; Marszalek, J. R.; Maitra, A.; Yee, C.; Rezvani, K.; Shpall, E.; LeBleu, V. S.; Kalluri, R. Generation and testing of clinical-grade exosomes for pancreatic cancer. *JCI Insight* **2018**, *3*, No. e99263.

(13) Norouzi-Barough, L.; Shirian, S.; Gorji, A.; Sadeghi, M. Therapeutic potential of mesenchymal stem cell-derived exosomes as

a cell-free therapy approach for the treatment of skin, bone, and cartilage defects. *Connect. Tissue Res.* **2022**, *63*, 83−96.
(14) Lee, K. S.; Lee, J.; Kim, H. K.; Yeom, S. H.; Woo, C. H.; Jung, Y. J.; Yun, Y. E.; Park, S. Y.; Han, J.; Kim, E.; Sul, J. H.; Jung, J. M.; Park, J. H.; Choi, J. S.; Cho, Y. W.; Jo, D.-G. Extracellular vesicles from adipose tissue-derived stem cells alleviate osteoporosis through osteoprotegerin and miR-21−5p. *J. Extracell. Vesicles* **2021**, *10*, No. e12152.
(15) Koo, S.; Sohn, H. S.; Kim, T. H.; Yang, S.; Jang, S. Y.; Ye, S.; Choi, B.; Kim, S. H.; Park, K. S.; Shin, H. M.; Park, O. K.; Kim, C.; Kang, M.; Soh, M.; Yoo, J.; Kim, D.; Lee, N.; Kim, B.-S.; Jung, Y.; Hyeon, T. Ceria-vesicle nanohybrid therapeutic for modulation of innate and adaptive immunity in a collagen-induced arthritis model. *Nat. Nanotechnol.* **2023**, *18*, 1502−1514.
(16) Zhang, Z.; Wu, W.; Li, M.; Du, L.; Li, J.; Yin, X.; Zhang, W. Mesenchymal stem cell-derived extracellular vesicles: A novel nanoimmunoregulatory tool in musculoskeletal diseases. *Nano Today* **2024**, *57*, 102343.
(17) Yang, E.; Jing, S.; Wang, Y.; Wang, H.; Rodriguez, R.; Wang, Z. The Role of Mesenchymal Stem Cells and Exosomes in Tumor Development and Targeted Antitumor Therapies. *Stem Cells Int.* **2023**, *2023*, 7059289.
(18) Fang, A.; Wang, Y.; Guan, N.; Zuo, Y.; Lin, L.; Guo, B.; Mo, A.; Wu, Y.; Lin, X.; Cai, W.; Chen, X.; Ye, J.; Abdelrahman, Z.; Li, X.; Zheng, H.; Wu, Z.; Jin, S.; Xu, K.; Huang, Y.; Gu, X.; Yu, B.; Wang, X. Porous microneedle patch with sustained delivery of extracellular vesicles mitigates severe spinal cord injury. *Nat. Commun.* **2023**, *14*, 4011.
(19) Nakano, M.; Fujimiya, M. Potential effects of mesenchymal stem cell derived extracellular vesicles and exosomal miRNAs in neurological disorders. *Neural. Regen. Res.* **2021**, *16*, 2359−2366.
(20) Verweij, F. J.; Balaj, L.; Boulanger, C. M.; Carter, D. R. F.; Compeer, E. B.; D'Angelo, G.; El Andaloussi, S.; Goetz, J. G.; Gross, J. C.; Hyenne, V.; Kramer-Albers, E.-M.; Lai, C. P.; Loyer, X.; Marki, A.; Momma, S.; Nolte-'t Hoen, E. N. M.; Pegtel, D. M.; Peinado, H.; Raposo, G.; Rilla, K.; Tahara, H.; Thery, C.; van Royen, M. E.; Vandenbroucke, R. E.; Wehman, A. M.; Witwer, K.; Wu, Z.; Wubbolts, R.; van Niel, G. The power of imaging to understand extracellular vesicle biology in vivo. *Nat. Methods* **2021**, *18*, 1013−1026.
(21) Zhang, P.; Dong, B.; Zeng, E.; Wang, F.; Jiang, Y.; Li, D.; Liu, D. In vivo tracking of multiple tumor exosomes labeled by phospholipid-based bioorthogonal conjugation. *Anal. Chem.* **2018**, *90*, 11273−11279.
(22) Jiang, Y.; Wang, L.; Zhang, P.; Liu, X.; Di, H.; Yang, J.; Liu, S.-L.; Pang, D.-W.; Liu, D. Chemoenzymatic Labeling of Extracellular Vesicles for Visualizing Their Cellular Internalization in Real Time. *Anal. Chem.* **2020**, *92*, 2103−2111.
(23) Di, H.; Zeng, E.; Zhang, P.; Liu, X.; Zhang, C.; Yang, J.; Liu, D. General Approach to Engineering Extracellular Vesicles for Biomedical Analysis. *Anal. Chem.* **2019**, *91*, 12752−12759.
(24) Salunkhe, S.; Dheeraj; Basak, M.; Chitkara, D.; Mittal, A. Surface functionalization of exosomes for target-specific delivery and in vivo imaging & tracking: Strategies and significance. *J. Controlled Release* **2020**, *326*, 599−614.
(25) Betzer, O.; Barnoy, E.; Sadan, T.; Elbaz, I.; Braverman, C.; Liu, Z.; Popovtzer, R. Advances in imaging strategies for in vivo tracking of exosomes. *Wiley Interdiscip. Rev. Nanomed. Nanobiotechnol.* **2020**, *12*, No. e1594.
(26) Arifin, D. R.; Witwer, K. W.; Bulte, J. W. Non-Invasive imaging of extracellular vesicles: Quo vaditis in vivo? *J. Extracell. Vesicles* **2022**, *11*, 12241.
(27) Di Rocco, G.; Baldari, S.; Toietta, G. Towards therapeutic delivery of extracellular vesicles: strategies for in vivo tracking and biodistribution analysis. *Stem Cells Int.* **2016**, *2016*, 5029619.
(28) Kim, D. H.; Kothandan, V. K.; Kim, H. W.; Kim, K. S.; Kim, J. Y.; Cho, H. J.; Lee, Y.-k.; Lee, D.-E.; Hwang, S. R. Noninvasive assessment of exosome pharmacokinetics in vivo: a review. *Pharmaceutics* **2019**, *11*, 649.
(29) Gangadaran, P.; Hong, C. M.; Ahn, B. C. An Update on in Vivo Imaging of Extracellular Vesicles as Drug Delivery Vehicles. *Front. Pharmacol.* **2018**, *9*, 169.
(30) Ma, N.; Wu, C.; Meng, Z. In vivo imaging and tracking of exosomes for theranostics. *J. Innov. Opt. Health Sci.* **2021**, *14*, 2130005.
(31) Kim, J. E.; Kalimuthu, S.; Ahn, B.-C. In vivo cell tracking with bioluminescence imaging. *Nucl. Med. Mol. Imaging* **2015**, *49*, 3−10.
(32) Shimomura, T.; Seino, R.; Umezaki, K.; Shimoda, A.; Ezoe, T.; Ishiyama, M.; Akiyoshi, K. New lipophilic fluorescent dyes for labeling extracellular vesicles: characterization and monitoring of cellular uptake. *Bioconjugate Chem.* **2021**, *32*, 680−684.
(33) Tonniges, J.; Hansen, M.; Duncan, J.; Bassett, M.; Fritzsch, B.; Gray, B.; Easwaran, A.; Nichols, M. G. Photo-and bio-physical characterization of novel violet and near-infrared lipophilic fluorophores for neuronal tracing. *J. Microsc.* **2010**, *239*, 117−134.
(34) Chen, Z.; Wang, H.; Xia, Y.; Yan, F.; Lu, Y. Therapeutic Potential of Mesenchymal Cell-Derived miRNA-150−5p-Expressing Exosomes in Rheumatoid Arthritis Mediated by the Modulation of MMP14 and VEGF. *J. Immunol.* **2018**, *201*, 2472−2482.
(35) Tao, S. C.; Yuan, T.; Zhang, Y. L.; Yin, W. J.; Guo, S. C.; Zhang, C. Q. Exosomes derived from miR-140−5p-overexpressing human synovial mesenchymal stem cells enhance cartilage tissue regeneration and prevent osteoarthritis of the knee in a rat model. *Theranostics* **2017**, *7*, 180−195.
(36) Chen, P.; Zheng, L.; Wang, Y.; Tao, M.; Xie, Z.; Xia, C.; Gu, C.; Chen, J.; Qiu, P.; Mei, S.; Ning, L.; Shi, Y.; Fang, C.; Fan, S.; Lin, X. Desktop-stereolithography 3D printing of a radially oriented extracellular matrix/mesenchymal stem cell exosome bioink for osteochondral defect regeneration. *Theranostics* **2019**, *9*, 2439−2459.
(37) Cao, J.; Wang, B.; Tang, T.; Lv, L.; Ding, Z.; Li, Z.; Hu, R.; Wei, Q.; Shen, A.; Fu, Y.; Liu, B. Three-dimensional culture of MSCs produces exosomes with improved yield and enhanced therapeutic efficacy for cisplatin-induced acute kidney injury. *Stem Cell Res. Ther.* **2020**, *11*, 206.
(38) Du, W.; Zhang, K.; Zhang, S.; Wang, R.; Nie, Y.; Tao, H.; Han, Z.; Liang, L.; Wang, D.; Liu, J.; Liu, N.; Han, Z.; Kong, D.; Zhao, Q.; Li, Z. Enhanced proangiogenic potential of mesenchymal stem cell-derived exosomes stimulated by a nitric oxide releasing polymer. *Biomaterials* **2017**, *133*, 70−81.
(39) Liang, X.; Zhang, L.; Wang, S.; Han, Q.; Zhao, R. C. Exosomes secreted by mesenchymal stem cells promote endothelial cell angiogenesis by transferring miR-125a. *J. Cell. Sci.* **2016**, *129*, 2182−9.
(40) Ma, T.; Chen, Y.; Chen, Y.; Meng, Q.; Sun, J.; Shao, L.; Yu, Y.; Huang, H.; Hu, Y.; Yang, Z.; Yang, J.; Shen, Z. MicroRNA-132, Delivered by Mesenchymal Stem Cell-Derived Exosomes, Promote Angiogenesis in Myocardial Infarction. *Stem Cells Int.* **2018**, *2018*, 3290372.
(41) Yuan, Q.; Wang, X.; Liu, L.; Cai, Y.; Zhao, X.; Ma, H.; Zhang, Y. Exosomes Derived from Human Placental Mesenchymal Stromal Cells Carrying AntagomiR-4450 Alleviate Intervertebral Disc Degeneration Through Upregulation of ZNF121. *Stem Cells Dev.* **2020**, *29*, 1038−1058.
(42) Zhang, Z.; Yang, J.; Yan, W.; Li, Y.; Shen, Z.; Asahara, T. Pretreatment of Cardiac Stem Cells With Exosomes Derived From Mesenchymal Stem Cells Enhances Myocardial Repair. *J. Am. Heart Assoc.* **2016**, *5*, No. e002856.
(43) Wang, X.; Liu, D.; Zhang, X.; Yang, L.; Xia, Z.; Zhang, Q. Exosomes from adipose-derived mesenchymal stem cells alleviate sepsis-induced lung injury in mice by inhibiting the secretion of IL-27 in macrophages. *Cell Death Discovery* **2022**, *8*, 18.
(44) Cui, G. H.; Guo, H. D.; Li, H.; Zhai, Y.; Gong, Z. B.; Wu, J.; Liu, J. S.; Dong, Y. R.; Hou, S. X.; Liu, J. R. RVG-modified exosomes derived from mesenchymal stem cells rescue memory deficits by regulating inflammatory responses in a mouse model of Alzheimer's disease. *Immun. Ageing.* **2019**, *16*, 10.

https://doi.org/10.1021/cbmi.4c00085
Chem. Biomed. Imaging 2025, 3, 137−168

(45) Yang, J.; Zhang, X.; Chen, X.; Wang, L.; Yang, G. Exosome Mediated Delivery of miR-124 Promotes Neurogenesis after Ischemia. *Mol. Ther. Nucleic Acids* **2017**, *7*, 278−287.
(46) Xu, C. M.; Sabe, S. A.; Brinck-Teixeira, R.; Sabra, M.; Sellke, F. W.; Abid, M. R. Visualization of cardiac uptake of bone marrow mesenchymal stem cell-derived extracellular vesicles after intramyocardial or intravenous injection in murine myocardial infarction. *Physiol. Rep.* **2023**, *11*, No. e15568.
(47) Gangadaran, P.; Rajendran, R. L.; Lee, H. W.; Kalimuthu, S.; Hong, C. M.; Jeong, S. Y.; Lee, S. W.; Lee, J.; Ahn, B. C. Extracellular vesicles from mesenchymal stem cells activates VEGF receptors and accelerates recovery of hindlimb ischemia. *J. Controlled Release* **2017**, *264*, 112−126.
(48) Wen, S.; Dooner, M.; Papa, E.; Del Tatto, M.; Pereira, M.; Borgovan, T.; Cheng, Y.; Goldberg, L.; Liang, O.; Camussi, G.; Quesenberry, P. Biodistribution of Mesenchymal Stem Cell-Derived Extracellular Vesicles in a Radiation Injury Bone Marrow Murine Model. *Int. J. Mol. Sci.* **2019**, *20*, 5468.
(49) Hao, D.; Lu, L.; Song, H.; Duan, Y.; Chen, J.; Carney, R.; Li, J. J.; Zhou, P.; Nolta, J.; Lam, K. S.; Leach, J. K.; Farmer, D. L.; Panitch, A.; Wang, A. Engineered extracellular vesicles with high collagen-binding affinity present superior in situ retention and therapeutic efficacy in tissue repair. *Theranostics* **2022**, *12*, 6021−6037.
(50) Bruno, S.; Grange, C.; Deregibus, M. C.; Calogero, R. A.; Saviozzi, S.; Collino, F.; Morando, L.; Busca, A.; Falda, M.; Bussolati, B.; Tetta, C.; Camussi, G. Mesenchymal stem cell-derived microvesicles protect against acute tubular injury. *J. Am. Soc. Nephrol.* **2009**, *20*, 1053.
(51) Bruno, S.; Grange, C.; Collino, F.; Deregibus, M. C.; Cantaluppi, V.; Biancone, L.; Tetta, C.; Camussi, G. Microvesicles derived from mesenchymal stem cells enhance survival in a lethal model of acute kidney injury. *PLoS One* **2012**, *7*, No. e33115.
(52) Gatti, S.; Bruno, S.; Deregibus, M. C.; Sordi, A.; Cantaluppi, V.; Tetta, C.; Camussi, G. Microvesicles derived from human adult mesenchymal stem cells protect against ischaemia-reperfusion-induced acute and chronic kidney injury. *Nephrol. Dial. Transplant.* **2011**, *26*, 1474−1483.
(53) Grange, C.; Tapparo, M.; Bruno, S.; Chatterjee, D.; Quesenberry, P. J.; Tetta, C.; Camussi, G. Biodistribution of mesenchymal stem cell-derived extracellular vesicles in a model of acute kidney injury monitored by optical imaging. *Int. J. Mol. Med.* **2014**, *33*, 1055−63.
(54) Hu, J.; Jiang, Y.; Wu, X.; Wu, Z.; Qin, J.; Zhao, Z.; Li, B.; Xu, Z.; Lu, X.; Wang, X.; Liu, X. Exosomal miR-17−5p from adipose-derived mesenchymal stem cells inhibits abdominal aortic aneurysm by suppressing TXNIP-NLRP3 inflammasome. *Stem Cell Res. Ther.* **2022**, *13*, 349.
(55) Hu, L.; Wang, J.; Zhou, X.; Xiong, Z.; Zhao, J.; Yu, R.; Huang, F.; Zhang, H.; Chen, L. Exosomes derived from human adipose mensenchymal stem cells accelerates cutaneous wound healing via optimizing the characteristics of fibroblasts. *Sci. Rep.* **2016**, *6*, 32993.
(56) Li, M.; Wang, J.; Guo, P.; Jin, L.; Tan, X.; Zhang, Z.; Zhanghuang, C.; Mi, T.; Liu, J.; Wang, Z.; Wu, X.; Wei, G.; He, D. Exosome mimetics derived from bone marrow mesenchymal stem cells ablate neuroblastoma tumor in vitro and in vivo. *Biomater. Adv.* **2022**, *142*, 213161.
(57) Mendt, M.; Kamerkar, S.; Sugimoto, H.; McAndrews, K. M.; Wu, C. C.; Gagea, M.; Yang, S.; Blanko, E. V. R.; Peng, Q.; Ma, X.; Marszalek, J. R.; Maitra, A.; Yee, C.; Rezvani, K.; Shpall, E.; LeBleu, V. S.; Kalluri, R. Generation and testing of clinical-grade exosomes for pancreatic cancer. *JCI Insight* **2018**, *3*, No. e99263.
(58) Rajendran, R. L.; Gangadaran, P.; Bak, S. S.; Oh, J. M.; Kalimuthu, S.; Lee, H. W.; Baek, S. H.; Zhu, L.; Sung, Y. K.; Jeong, S. Y.; Lee, S. W.; Lee, J.; Ahn, B. C. Extracellular vesicles derived from MSCs activates dermal papilla cell in vitro and promotes hair follicle conversion from telogen to anagen in mice. *Sci. Rep.* **2017**, *7*, 15560.
(59) Wang, J.; Hendrix, A.; Hernot, S.; Lemaire, M.; De Bruyne, E.; Van Valckenborgh, E.; Lahoutte, T.; De Wever, O.; Vanderkerken, K.; Menu, E. Bone marrow stromal cell-derived exosomes as communicators in drug resistance in multiple myeloma cells. *Blood* **2014**, *124*, 555−66.
(60) Wu, X. D.; Kang, L.; Tian, J.; Wu, Y.; Huang, Y.; Liu, J.; Wang, H.; Qiu, G.; Wu, Z. Exosomes derived from magnetically actuated bone mesenchymal stem cells promote tendon-bone healing through the miR-21−5p/SMAD7 pathway. *Mater.Today Bio.* **2022**, *15*, 100319.
(61) Xu, C.; Zhao, J.; Li, Q.; Hou, L.; Wang, Y.; Li, S.; Jiang, F.; Zhu, Z.; Tian, L. Exosomes derived from three-dimensional cultured human umbilical cord mesenchymal stem cells ameliorate pulmonary fibrosis in a mouse silicosis model. *Stem Cell Res. Ther.* **2020**, *11*, 503.
(62) Zheng, J.; Lu, T.; Zhou, C.; Cai, J.; Zhang, X.; Liang, J.; Sui, X.; Chen, X.; Chen, L.; Sun, Y.; Zhang, J.; Chen, W.; Zhang, Y.; Yao, J.; Chen, G.; Yang, Y. Extracellular Vesicles Derived from Human Umbilical Cord Mesenchymal Stem Cells Protect Liver Ischemia/Reperfusion Injury by Reducing CD154 Expression on $CD4^+$ T Cells via CCT2. *Adv. Sci.* **2020**, *7*, 1903746.
(63) Deng, D.; Li, X.; Zhang, J.-J.; Yin, Y.; Tian, Y.; Gan, D.; Wu, R.; Wang, J.; Tian, B.-M.; Chen, F.-M.; He, X.-T. Biotin-avidin system-based delivery enhances the therapeutic performance of MSC-derived exosomes. *ACS Nano* **2023**, *17*, 8530−8550.
(64) Lai, J.; Pan, Q.; Chen, G.; Liu, Y.; Chen, C.; Pan, Y.; Liu, L.; Zeng, B.; Yu, L.; Xu, Y.; Tang, J.; Yang, Y.; Rao, L. Triple Hybrid Cellular Nanovesicles Promote Cardiac Repair after Ischemic Reperfusion. *ACS Nano* **2024**, *18*, 4443−4455.
(65) Long, Y.; Yang, B.; Lei, Q.; Gao, F.; Chen, L.; Chen, W.; Chen, S.; Ren, W.; Cao, Y.; Xu, L.; Wu, D.; Qu, J.; Li, H.; Yu, Y.; Zhang, A.; Wang, S.; Chen, W.; Wang, H.; Chen, T.; Chen, Z.; Li, Q. Targeting Senescent Alveolar Epithelial Cells Using Engineered Mesenchymal Stem Cell-Derived Extracellular Vesicles To Treat Pulmonary Fibrosis. *ACS Nano* **2024**, *18*, 7046−7063.
(66) Xu, R.; Bai, Y.; Min, S.; Xu, X.; Tang, T.; Ju, S. In vivo Monitoring and Assessment of Exogenous Mesenchymal Stem Cell-Derived Exosomes in Mice with Ischemic Stroke by Molecular Imaging. *Int. J. Nanomedicine* **2020**, *15*, 9011−9023.
(67) Tolomeo, A. M.; Zuccolotto, G.; Malvicini, R.; De Lazzari, G.; Penna, A.; Franco, C.; Caicci, F.; Magarotto, F.; Quarta, S.; Pozzobon, M.; Rosato, A.; Muraca, M.; Collino, F. Biodistribution of Intratracheal, Intranasal, and Intravenous Injections of Human Mesenchymal Stromal Cell-Derived Extracellular Vesicles in a Mouse Model for Drug Delivery Studies. *Pharmaceutics* **2023**, *15*, 548.
(68) Türker, S.; Onur, E.; Ozer, Y. Nasal route and drug delivery systems. *Pharm. World Sci.* **2004**, *26*, 137−42.
(69) Wang, J.; Tu, C.; Zhang, H.; Zhang, J.; Feng, Y.; Deng, Y.; Huo, Y.; Xie, M.; Yang, B.; Zhou, M.; Liu, J. Loading of metal isotope-containing intercalators for mass cytometry-based high-throughput quantitation of exosome uptake at the single-cell level. *Biomaterials* **2020**, *255*, 120152.
(70) Poon, R. Y. M.; Ohlsson-Wilhelm, B. M.; Bagwell, C. B.; Muirhead, K. A. Use of PKH Membrane Intercalating Dyes to Monitor Cell Trafficking and Function. In *In Living Color: Protocols in Flow Cytometry and Cell Sorting*; Diamond, R. A., Demaggio, S., Eds.; Springer: Berlin, Heidelberg, 2000; pp 302−352.
(71) Nakamura, Y.; Kita, S.; Tanaka, Y.; Fukuda, S.; Obata, Y.; Okita, T.; Nishida, H.; Takahashi, Y.; Kawachi, Y.; Tsugawa-Shimizu, Y.; Fujishima, Y.; Nishizawa, H.; Takakura, Y.; Miyagawa, S.; Sawa, Y.; Maeda, N.; Shimomura, I. Adiponectin Stimulates Exosome Release to Enhance Mesenchymal Stem-Cell-Driven Therapy of Heart Failure in Mice. *Mol. Ther.* **2020**, *28*, 2203−2219.
(72) Li, C.; Qin, T.; Zhao, J.; He, R.; Wen, H.; Duan, C.; Lu, H.; Cao, Y.; Hu, J. Bone Marrow Mesenchymal Stem Cell-Derived Exosome-Educated Macrophages Promote Functional Healing After Spinal Cord Injury. *Front. Cell. Neurosci.* **2021**, *15*, 725573.
(73) Yang, H.; Chen, J. Bone marrow mesenchymal stem cell-derived exosomes carrying long noncoding RNA ZFAS1 alleviate oxidative stress and inflammation in ischemic stroke by inhibiting microRNA-15a-5p. *Metab. Brain Dis.* **2022**, *37*, 2545−2557.
(74) Saccu, G.; Menchise, V.; Gai, C.; Bertolin, M.; Ferrari, S.; Giordano, C.; Manco, M.; Dastru, W.; Tolosano, E.; Bussolati, B.;

Calautti, E.; Camussi, G.; Altruda, F.; Fagoonee, S. Bone Marrow Mesenchymal Stromal/Stem Cell-Derived Extracellular Vesicles Promote Corneal Wound Repair by Regulating Inflammation and Angiogenesis. *Cells* **2022**, *11*, 3892.
(75) Zhang, Z.; Mi, T.; Jin, L.; Li, M.; Zhanghuang, C.; Wang, J.; Tan, X.; Lu, H.; Shen, L.; Long, C.; Wei, G.; He, D. Comprehensive proteomic analysis of exosome mimetic vesicles and exosomes derived from human umbilical cord mesenchymal stem cells. *Stem Cell Res. Ther.* **2022**, *13*, 312.
(76) Zhou, Y.; Wen, L. L.; Li, Y. F.; Wu, K. M.; Duan, R. R.; Yao, Y. B.; Jing, L. J.; Gong, Z.; Teng, J. F.; Jia, Y. J. Exosomes derived from bone marrow mesenchymal stem cells protect the injured spinal cord by inhibiting pericyte pyroptosis. *Neural Regen. Res.* **2022**, *17*, 194−202.
(77) Li, X.; Zhang, Y.; Wang, Y.; Zhao, D.; Sun, C.; Zhou, S.; Xu, D.; Zhao, J. Exosomes Derived from CXCR4-Overexpressing BMSC Promoted Activation of Microvascular Endothelial Cells in Cerebral Ischemia/Reperfusion Injury. *Neural. Plast.* **2020**, *2020*, 8814239.
(78) Li, Y.; Zhang, J.; Shi, J.; Liu, K.; Wang, X.; Jia, Y.; He, T.; Shen, K.; Wang, Y.; Liu, J.; Zhang, W.; Wang, H.; Zheng, Z.; Hu, D. Exosomes derived from human adipose mesenchymal stem cells attenuate hypertrophic scar fibrosis by miR-192−5p/IL-17RA/Smad axis. *Stem Cell Res. Ther.* **2021**, *12*, 221.
(79) Yi, X.; Wei, X.; Lv, H.; An, Y.; Li, L.; Lu, P.; Yang, Y.; Zhang, Q.; Yi, H.; Chen, G. Exosomes derived from microRNA-30b-3p-overexpressing mesenchymal stem cells protect against lipopolysaccharide-induced acute lung injury by inhibiting SAA3. *Exp. Cell Res.* **2019**, *383*, 111454.
(80) Thomi, G.; Surbek, D.; Haesler, V.; Joerger-Messerli, M.; Schoeberlein, A. Exosomes derived from umbilical cord mesenchymal stem cells reduce microglia-mediated neuroinflammation in perinatal brain injury. *Stem Cell Res. Ther.* **2019**, *10*, 105.
(81) Tamura, R.; Uemoto, S.; Tabata, Y. Immunosuppressive effect of mesenchymal stem cell-derived exosomes on a concanavalin A-induced liver injury model. *Inflamm. Regen.* **2016**, *36*, 26.
(82) Jia, Z.; Lv, Y.; Zhang, W.; Zhang, X.; Li, F.; Lu, X.; Zhao, S. Mesenchymal stem cell derived exosomes-based immunological signature in a rat model of corneal allograft rejection therapy. *Front. Biosci.* **2022**, *27*, 86.
(83) Shabbir, A.; Cox, A.; Rodriguez-Menocal, L.; Salgado, M.; Van Badiavas, E. Mesenchymal Stem Cell Exosomes Induce Proliferation and Migration of Normal and Chronic Wound Fibroblasts, and Enhance Angiogenesis In Vitro. *Stem Cells Dev.* **2015**, *24*, 1635−47.
(84) Chen, Y. A.; Lu, C. H.; Ke, C. C.; Chiu, S. J.; Jeng, F. S.; Chang, C. W.; Yang, B. H.; Liu, R. S. Mesenchymal Stem Cell-Derived Exosomes Ameliorate Alzheimer's Disease Pathology and Improve Cognitive Deficits. *Biomedicines* **2021**, *9*, 594.
(85) Eirin, A.; Zhu, X. Y.; Puranik, A. S.; Tang, H.; McGurren, K. A.; van Wijnen, A. J.; Lerman, A.; Lerman, L. O. Mesenchymal stem cell-derived extracellular vesicles attenuate kidney inflammation. *Kidney Int.* **2017**, *92*, 114−124.
(86) Xie, L.; Chen, Z.; Liu, M.; Huang, W.; Zou, F.; Ma, X.; Tao, J.; Guo, J.; Xia, X.; Lyu, F.; Wang, H.; Zheng, C.; Jiang, J. MSC-Derived Exosomes Protect Vertebral Endplate Chondrocytes against Apoptosis and Calcification via the miR-31−5p/ATF6 Axis. *Mol. Ther. Nucleic Acids* **2020**, *22*, 601−614.
(87) Zhang, Y.; Xie, Y.; Hao, Z.; Zhou, P.; Wang, P.; Fang, S.; Li, L.; Xu, S.; Xia, Y. Umbilical Mesenchymal Stem Cell-Derived Exosome-Encapsulated Hydrogels Accelerate Bone Repair by Enhancing Angiogenesis. *ACS Appl. Mater. Interfaces* **2021**, *13*, 18472−18487.
(88) Tamura, R.; Uemoto, S.; Tabata, Y. Augmented liver targeting of exosomes by surface modification with cationized pullulan. *Acta Biomater.* **2017**, *57*, 274−284.
(89) Tabata, Y.; Ikada, Y. Effect of the size and surface charge of polymer microspheres on their phagocytosis by macrophage. *Biomaterials* **1988**, *9*, 356−362.
(90) Takahashi, Y.; Nishikawa, M.; Shinotsuka, H.; Matsui, Y.; Ohara, S.; Imai, T.; Takakura, Y. Visualization and in vivo tracking of the exosomes of murine melanoma B16-BL6 cells in mice after intravenous injection. *J. Biotechnol.* **2013**, *165*, 77−84.
(91) Dehghani, M.; Gulvin, S. M.; Flax, J.; Gaborski, T. R. Systematic evaluation of PKH labelling on extracellular vesicle size by nanoparticle tracking analysis. *Sci. Rep.* **2020**, *10*, 9533.
(92) Eddy, J.; Maizels, N. Gene function correlates with potential for G4 DNA formation in the human genome. *Nucleic Acids Res.* **2006**, *34*, 3887−3896.
(93) Panigrahi, M.; Dash, S.; Patel, S.; Mishra, B. K. Syntheses of cyanines: a review. *Tetrahedron* **2012**, *68*, 781−805.
(94) Lee, H.; Berezin, M. Y.; Henary, M.; Strekowski, L.; Achilefu, S. Fluorescence lifetime properties of near-infrared cyanine dyes in relation to their structures. *J. Photochem. Photobiol., A* **2008**, *200*, 438−444.
(95) Zhang, C.; Shao, W.; Yuan, H.; Xiao, R.; Zhang, Y.; Wei, C.; Ni, X.; He, N.; Chen, G.; Gui, S.; Cheng, Z.; Wang, Q. Engineered Extracellular Vesicle-Based Nanoformulations That Coordinate Neuroinflammation and Immune Homeostasis, Enhancing Parkinson's Disease Therapy. *ACS Nano* **2024**, *18*, 23014−23031.
(96) Chang, C. Y.; Chen, K. Y.; Shih, H. J.; Chiang, M.; Huang, I. T.; Huang, Y. H.; Huang, C. J. Let-7i-5p Mediates the Therapeutic Effects of Exosomes from Human Placenta Choriodecidual Membrane-Derived Mesenchymal Stem Cells on Mitigating Endotoxin-Induced Mortality and Liver Injury in High-Fat Diet-Induced Obese Mice. *Pharmaceuticals (Basel)* **2022**, *15*, 36.
(97) He, Q.; Wang, L.; Zhao, R.; Yan, F.; Sha, S.; Cui, C.; Song, J.; Hu, H.; Guo, X.; Yang, M.; Cui, Y.; Sun, Y.; Sun, Z.; Liu, F.; Dong, M.; Hou, X.; Chen, L. Mesenchymal stem cell-derived exosomes exert ameliorative effects in type 2 diabetes by improving hepatic glucose and lipid metabolism via enhancing autophagy. *Stem Cell Res. Ther.* **2020**, *11*, 223.
(98) Shindy, H. A. Fundamentals in the chemistry of cyanine dyes: A review. *Dyes Pigm.* **2017**, *145*, 505−513.
(99) Neupane, Y. R.; Handral, H. K.; Alkaff, S. A.; Chng, W. H.; Venkatesan, G.; Huang, C.; Lee, C. K.; Wang, J.-W.; Sriram, G.; Dienzo, R. A.; Lu, W. F.; Ali, Y.; Czarny, B.; Pastorin, G. Cell-derived nanovesicles from mesenchymal stem cells as extracellular vesicle-mimetics in wound healing. *Acta Pharm. Sin. B* **2023**, *13*, 1887−1902.
(100) Qi, X.; Zhang, J.; Yuan, H.; Xu, Z.; Li, Q.; Niu, X.; Hu, B.; Wang, Y.; Li, X. Exosomes secreted by human-induced pluripotent stem cell-derived mesenchymal stem cells repair critical-sized bone defects through enhanced angiogenesis and osteogenesis in osteoporotic rats. *Int. J. Biol. Sci.* **2016**, *12*, 836.
(101) Wang, Y.; Yao, J.; Cai, L.; Liu, T.; Wang, X.; Zhang, Y.; Zhou, Z.; Li, T.; Liu, M.; Lai, R.; Liu, X. Bone-Targeted Extracellular Vesicles from Mesenchymal Stem Cells for Osteoporosis Therapy. *Int. J. Nanomedicine* **2020**, *15*, 7967−7977.
(102) Li, P.; Kaslan, M.; Lee, S. H.; Yao, J.; Gao, Z. Progress in exosome isolation techniques. *Theranostics* **2017**, *7*, 789.
(103) Collot, M.; Ashokkumar, P.; Anton, H.; Boutant, E.; Faklaris, O.; Galli, T.; Mély, Y.; Danglot, L.; Klymchenko, A. S. MemBright: a family of fluorescent membrane probes for advanced cellular imaging and neuroscience. *Cell Chem. Biol.* **2019**, *26*, 600−614 e7.
(104) Zhou, C.; Cox-Vázquez, S. J.; Chia, G. W.; Vázquez, R. J.; Lai, H. Y.; Chan, S. J.; Limwongyut, J.; Bazan, G. C. Water-soluble extracellular vesicle probes based on conjugated oligoelectrolytes. *Sci. Adv.* **2023**, *9*, No. eade2996.
(105) Luo, J.; Xie, Z.; Lam, J. W. Y.; Cheng, L.; Tang, B. Z.; Chen, H.; Qiu, C.; Kwok, H. S.; Zhan, X.; Liu, Y.; Zhu, D. Aggregation-induced emission of 1-methyl-1, 2, 3, 4, 5-pentaphenylsilole. *Chem. Commun.* **2001**, 1740−1741.
(106) Mei, J.; Hong, Y.; Lam, J. W.; Qin, A.; Tang, Y.; Tang, B. Z. Aggregation-induced emission: the whole is more brilliant than the parts. *Adv. Mater.* **2014**, *26*, 5429−5479.
(107) Mei, J.; Leung, N. L.; Kwok, R. T.; Lam, J. W.; Tang, B. Z. Aggregation-induced emission: together we shine, united we soar! *Chem. Rev.* **2015**, *115*, 11718−11940.

https://doi.org/10.1021/cbmi.4c00085
Chem. Biomed. Imaging 2025, 3, 137−168

(108) Cai, X.; Liu, B. Aggregation-induced emission: recent advances in materials and biomedical applications. *Angew. Chem., Int. Ed.* **2020**, *59*, 9868−9886.
(109) Würthner, F. Aggregation-induced emission (AIE): a historical perspective. *Angew. Chem., Int. Ed.* **2020**, *59*, 14192−14196.
(110) Wang, K.; Gao, H.; Zhang, Y.; Yan, H.; Si, J.; Mi, X.; Xia, S.; Feng, X.; Liu, D.; Kong, D.; Wang, T.; Ding, D. Highly bright AIE nanoparticles by regulating the substituent of rhodanine for precise early detection of atherosclerosis and drug screening. *Adv. Mater.* **2022**, *34*, 2106994.
(111) El Andaloussi, S.; Mäger, I.; Breakefield, X. O.; Wood, M. J. Extracellular vesicles: biology and emerging therapeutic opportunities. *Nat. Rev. Drug Discovery* **2013**, *12*, 347−357.
(112) Akishiba, M.; Takeuchi, T.; Kawaguchi, Y.; Sakamoto, K.; Yu, H.-H.; Nakase, I.; Takatani-Nakase, T.; Madani, F.; Gräslund, A.; Futaki, S. Cytosolic antibody delivery by lipid-sensitive endosomolytic peptide. *Nat. Chem.* **2017**, *9*, 751−761.
(113) Cao, H.; Yue, Z.; Gao, H.; Chen, C.; Cui, K.; Zhang, K.; Cheng, Y.; Shao, G.; Kong, D.; Li, Z.; Ding, D.; Wang, Y. In Vivo Real-Time Imaging of Extracellular Vesicles in Liver Regeneration via Aggregation-Induced Emission Luminogens. *ACS Nano* **2019**, *13*, 3522−3533.
(114) Cao, H.; Cheng, Y.; Gao, H.; Zhuang, J.; Zhang, W.; Bian, Q.; Wang, F.; Du, Y.; Li, Z.; Kong, D.; Ding, D.; Wang, Y. In Vivo Tracking of Mesenchymal Stem Cell-Derived Extracellular Vesicles Improving Mitochondrial Function in Renal Ischemia-Reperfusion Injury. *ACS Nano* **2020**, *14*, 4014−4026.
(115) Zhang, J.; He, B.; Hu, Y.; Alam, P.; Zhang, H.; Lam, J. W. Y.; Tang, B. Z. Stimuli-Responsive AIEgens. *Adv. Mater.* **2021**, *33*, 2008071.
(116) Ouyang, J.; Sun, L.; Zeng, F.; Wu, S. Biomarker-activatable probes based on smart AIEgens for fluorescence and optoacoustic imaging. *Coord. Chem. Rev.* **2022**, *458*, 214438.
(117) Chalfie, M.; Tu, Y.; Euskirchen, G.; Ward, W. W.; Prasher, D. C. Green fluorescent protein as a marker for gene expression. *Science* **1994**, *263*, 802−805.
(118) Tsien, R. Y. The green fluorescent protein. *Annu. Rev. Biochem.* **1998**, *67*, 509−544.
(119) Heim, R.; Tsien, R. Y. Engineering green fluorescent protein for improved brightness, longer wavelengths and fluorescence resonance energy transfer. *Curr. Biol.* **1996**, *6*, 178−182.
(120) Gorabi, A. M.; Kiaie, N.; Barreto, G. E.; Read, M. I.; Tafti, H. A.; Sahebkar, A. The therapeutic potential of mesenchymal stem cell-derived exosomes in treatment of neurodegenerative diseases. *Mol. Neurobiol.* **2019**, *56*, 8157−8167.
(121) Zhang, Z. G.; Buller, B.; Chopp, M. Exosomes—beyond stem cells for restorative therapy in stroke and neurological injury. *Nat. Rev. Neurol.* **2019**, *15*, 193−203.
(122) Giunti, D.; Marini, C.; Parodi, B.; Usai, C.; Milanese, M.; Bonanno, G.; Kerlero de Rosbo, N.; Uccelli, A. Role of miRNAs shuttled by mesenchymal stem cell-derived small extracellular vesicles in modulating neuroinflammation. *Sci. Rep.* **2021**, *11*, 1740.
(123) Zhang, J.; Buller, B. A.; Zhang, Z. G.; Zhang, Y.; Lu, M.; Rosene, D. L.; Medalla, M.; Moore, T. L.; Chopp, M. Exosomes derived from bone marrow mesenchymal stromal cells promote remyelination and reduce neuroinflammation in the demyelinating central nervous system. *Exp. Neurol.* **2022**, *347*, 113895.
(124) Yan, J.; Zhang, L.; Li, L.; He, W.; Liu, W. Developmentally engineered bio-assemblies releasing neurotrophic exosomes guide in situ neuroplasticity following spinal cord injury. *Mater. Today Bio.* **2022**, *16*, 100406.
(125) Gonzalez-King, H.; Garcia, N. A.; Ontoria-Oviedo, I.; Ciria, M.; Montero, J. A.; Sepulveda, P. Hypoxia Inducible Factor-1alpha Potentiates Jagged 1-Mediated Angiogenesis by Mesenchymal Stem Cell-Derived Exosomes. *Stem Cells* **2017**, *35*, 1747−1759.
(126) Phinney, D. G.; Di Giuseppe, M.; Njah, J.; Sala, E.; Shiva, S.; St Croix, C. M.; Stolz, D. B.; Watkins, S. C.; Di, Y. P.; Leikauf, G. D.; Kolls, J.; Riches, D. W.; Deiuliis, G.; Kaminski, N.; Boregowda, S. V.; McKenna, D. H.; Ortiz, L. A. Mesenchymal stem cells use extracellular vesicles to outsource mitophagy and shuttle microRNAs. *Nat. Commun.* **2015**, *6*, 8472.
(127) Li, J.; Lv, Y.; Zhu, D.; Mei, X.; Huang, K.; Wang, X.; Li, Z.; Zhang, S.; Hu, S.; D. Popowski, K.; Cheng, K.; Wang, J. Intrapericardial hydrogel injection generates high cell retention and augments therapeutic effects of mesenchymal stem cells in myocardial infarction. *Chem. Eng. J.* **2022**, *427*, 131581.
(128) Karasev, M.; Stepanenko, O.; Rumyantsev, K.; Turoverov, K.; Verkhusha, V. Near-infrared fluorescent proteins and their applications. *Biochemistry (Moscow)* **2019**, *84*, 32−50.
(129) Lenzini, S.; Bargi, R.; Chung, G.; Shin, J. W. Matrix mechanics and water permeation regulate extracellular vesicle transport. *Nat. Nanotechnol.* **2020**, *15*, 217−223.
(130) Luker, K.E.; Pata, P.; Shemiakina, I.I.; Pereverzeva, A.; Stacer, A.C.; Shcherbo, D.S.; Pletnev, V.Z.; Skolnaja, M.; Lukyanov, K.A.; Luker, G.D.; Pata, I.; Chudakov, D.M. Comparative study reveals better far-red fluorescent protein for whole body imaging. *Sci. Rep.* **2015**, *5*, 10332.
(131) Feilmeier, B. J.; Iseminger, G.; Schroeder, D.; Webber, H.; Phillips, G. J. Green fluorescent protein functions as a reporter for protein localization in Escherichia coli. *J. Bacteriol.* **2000**, *182*, 4068−4076.
(132) Röllen, K.; Granzin, J.; Remeeva, A.; Davari, M. D.; Gensch, T.; Nazarenko, V. V.; Kovalev, K.; Bogorodskiy, A.; Borshchevskiy, V.; Hemmer, S. Structural and mechanistic insight into spectral tuning in flavin-binding fluorescent proteins. *BioRxiv* **2021**, 2021.01.08.425906.
(133) Chia, H. E.; Marsh, E. N. G.; Biteen, J. S. Extending fluorescence microscopy into anaerobic environments. *Curr. Opin. Chem. Biol.* **2019**, *51*, 98−104.
(134) Sakamoto, S.; Kiyonaka, S.; Hamachi, I. Construction of ligand assay systems by protein-based semisynthetic biosensors. *Curr. Opin. Chem. Biol.* **2019**, *50*, 10−18.
(135) van Niel, G.; Carter, D. R.; Clayton, A.; Lambert, D. W.; Raposo, G.; Vader, P. Challenges and directions in studying cell-cell communication by extracellular vesicles. *Nat. Rev. Mol. Cell Biol.* **2022**, *23*, 369−382.
(136) Mead, B.; Tomarev, S. Bone Marrow-Derived Mesenchymal Stem Cells-Derived Exosomes Promote Survival of Retinal Ganglion Cells Through miRNA-Dependent Mechanisms. *Stem Cells Transl. Med.* **2017**, *6*, 1273−1285.
(137) Wen, Z.; Mai, Z.; Zhu, X.; Wu, T.; Chen, Y.; Geng, D.; Wang, J. Mesenchymal stem cell-derived exosomes ameliorate cardiomyocyte apoptosis in hypoxic conditions through microRNA144 by targeting the PTEN/AKT pathway. *Stem Cell Res. Ther.* **2020**, *11*, 36.
(138) Mathew, B.; Ravindran, S.; Liu, X.; Torres, L.; Chennakesavalu, M.; Huang, C. C.; Feng, L.; Zelka, R.; Lopez, J.; Sharma, M.; Roth, S. Mesenchymal stem cell-derived extracellular vesicles and retinal ischemia-reperfusion. *Biomaterials* **2019**, *197*, 146−160.
(139) Kim, Y. J.; Yoo, S. M.; Park, H. H.; Lim, H. J.; Kim, Y. L.; Lee, S.; Seo, K. W.; Kang, K. S. Exosomes derived from human umbilical cord blood mesenchymal stem cells stimulates rejuvenation of human skin. *Biochem. Biophys. Res. Commun.* **2017**, *493*, 1102−1108.
(140) Hao, D.; Swindell, H. S.; Ramasubramanian, L.; Liu, R.; Lam, K. S.; Farmer, D. L.; Wang, A. Extracellular Matrix Mimicking Nanofibrous Scaffolds Modified With Mesenchymal Stem Cell-Derived Extracellular Vesicles for Improved Vascularization. *Front. Bioeng. Biotechnol.* **2020**, *8*, 633.
(141) Kalluri, R.; McAndrews, K. M. Review The role of extracellular vesicles in cancer. *Cell* **2023**, *186*, 1610−1626.
(142) Diener, C.; Keller, A.; Meese, E. Emerging concepts of miRNA therapeutics: from cells to clinic. *Trends Genet.* **2022**, *38*, 613−626.
(143) Kanasty, R.; Dorkin, J. R.; Vegas, A.; Anderson, D. Delivery materials for siRNA therapeutics. *Nat. Mater.* **2013**, *12*, 967−977.
(144) Yu, H.; Cheng, J.; Shi, W.; Ren, B.; Zhao, F.; Shi, Y.; Yang, P.; Duan, X.; Zhang, J.; Fu, X.; Hu, X.; Ao, Y. Bone marrow mesenchymal stem cell-derived exosomes promote tendon regeneration by

https://doi.org/10.1021/cbmi.4c00085
Chem. Biomed. Imaging 2025, 3, 137−168

facilitating the proliferation and migration of endogenous tendon stem/progenitor cells. *Acta Biomater.* **2020**, *106*, 328−341.
(145) Narayanan, R.; Huang, C. C.; Ravindran, S. Hijacking the Cellular Mail: Exosome Mediated Differentiation of Mesenchymal Stem Cells. *Stem Cells Int.* **2016**, *2016*, 3808674.
(146) Bakhtyar, N.; Jeschke, M. G.; Herer, E.; Sheikholeslam, M.; Amini-Nik, S. Exosomes from acellular Wharton's jelly of the human umbilical cord promotes skin wound healing. *Stem Cell Res. Ther.* **2018**, *9*, 193.
(147) Huleihel, L.; Hussey, G. S.; Naranjo, J. D.; Zhang, L.; Dziki, J. L.; Turner, N. J.; Stolz, D. B.; Badylak, S. F. Matrix-bound nanovesicles within ECM bioscaffolds. *Sci. Adv.* **2016**, *2*, No. e1600502.
(148) Wang, B.; Yao, K.; Huuskes, B. M.; Shen, H. H.; Zhuang, J.; Godson, C.; Brennan, E. P.; Wilkinson-Berka, J. L.; Wise, A. F.; Ricardo, S. D. Mesenchymal Stem Cells Deliver Exogenous MicroRNA-let7c via Exosomes to Attenuate Renal Fibrosis. *Mol. Ther.* **2016**, *24*, 1290−301.
(149) Lehrbach, N. J.; Miska, E. A. Regulation of pre-miRNA Processing. *Adv. Exp. Med. Biol.* **2010**, *700*, 67−75.
(150) Kubota, M.; Nainar, S.; Parker, S. M.; England, W.; Furche, F.; Spitale, R. C. Expanding the scope of RNA metabolic labeling with vinyl nucleosides and inverse electron-demand Diels-Alder chemistry. *ACS Chem. Biol.* **2019**, *14*, 1698−1707.
(151) Klöcker, N.; Weissenboeck, F. P.; Rentmeister, A. Covalent labeling of nucleic acids. *Chem. Soc. Rev.* **2020**, *49*, 8749−8773.
(152) Samaeekia, R.; Rabiee, B.; Putra, I.; Shen, X.; Park, Y. J.; Hematti, P.; Eslani, M.; Djalilian, A. R. Effect of Human Corneal Mesenchymal Stromal Cell-derived Exosomes on Corneal Epithelial Wound Healing. *Investig. Ophthalmol. Vis. Sci.* **2018**, *59*, 5194−5200.
(153) Singh, A.; Raghav, A.; Shiekh, P. A.; Kumar, A. Transplantation of engineered exosomes derived from bone marrow mesenchymal stromal cells ameliorate diabetic peripheral neuropathy under electrical stimulation. *Bioact. Mater.* **2021**, *6*, 2231−2249.
(154) Gao, L.; Mei, S.; Zhang, S.; Qin, Q.; Li, H.; Liao, Y.; Fan, H.; Liu, Z.; Zhu, H. Cardio-renal exosomes in myocardial infarction serum regulate proangiogenic paracrine signaling in adipose mesenchymal stem cells. *Theranostics* **2020**, *10*, 1060.
(155) Liang, L.; Peng, W.; Qin, A.; Zhang, J.; Chen, R.; Zhou, D.; Zhang, X.; Zhou, N.; Yu, X.-Y.; Zhang, L. Intracellularly Synthesized Artificial Exosome Treats Acute Lung Injury. *ACS Nano* **2024**, *18*, 21009−21023.
(156) Lin, L.; Liu, A.-A.; Zhao, W.; Yang, Y.; Zhu, D.-L.; Dong, B.-R.; Ding, F.; Ning, D.; Zhu, X.; Liu, D.; Pang, D.-W. Multihierarchical Regulation To Achieve Quantum Dot Nanospheres with a Photoluminescence Quantum Yield Close to 100%. *J. Am. Chem. Soc.* **2024**, *146*, 21348−21356.
(157) Ma, H.; Zhang, X.; Liu, L.; Huang, Y.; Sun, S.; Chen, K.; Xin, Q.; Liu, P.; Yan, Y.; Wang, Y.; Li, Y.; Liu, H.; Zhao, R.; Tan, K.; Chen, X.; Yuan, X.; Li, Y.; Liu, Y.; Dai, H.; Liu, C.; Wang, H.; Zhang, X.-D. Bioactive NIR-II gold clusters for three-dimensional imaging and acute inflammation inhibition. *Sci. Adv.* **2023**, *9*, No. eadh7828.
(158) Khosravi, N.; Pishavar, E.; Baradaran, B.; Oroojalian, F.; Mokhtarzadeh, A. Stem cell membrane, stem cell-derived exosomes and hybrid stem cell camouflaged nanoparticles: A promising biomimetic nanoplatforms for cancer theranostics. *J. Control.Release* **2022**, *348*, 706−722.
(159) Lipták, N.; Bösze, Z.; Hiripi, L. GFP transgenic animals in biomedical research: a review of potential disadvantages. *Physiol. Res.* **2019**, *68*, 525−530.
(160) Scholz, O.; Thiel, A.; Hillen, W.; Niederweis, M. Quantitative analysis of gene expression with an improved green fluorescent protein. *Eur. J. Biochem.* **2000**, *267*, 1565−1570.
(161) Contag, C. H.; Bachmann, M. H. Advances in in vivo bioluminescence imaging of gene expression. *Annu. Rev. Biomed. Eng.* **2002**, *4*, 235−260.
(162) Badr, C. E.; Tannous, B. A. Bioluminescence imaging: progress and applications. *Trends Biotechnol.* **2011**, *29*, 624−633.
(163) Zambito, G.; Chawda, C.; Mezzanotte, L. Emerging tools for bioluminescence imaging. *Curr. Opin. Chem. Biol.* **2021**, *63*, 86−94.
(164) Kalimuthu, S.; Gangadaran, P.; Li, X. J.; Oh, J. M.; Lee, H. W.; Jeong, S. Y.; Lee, S. W.; Lee, J.; Ahn, B. C. In Vivo therapeutic potential of mesenchymal stem cell-derived extracellular vesicles with optical imaging reporter in tumor mice model. *Sci. Rep.* **2016**, *6*, 30418.
(165) Zhang, K.; Zhao, X.; Chen, X.; Wei, Y.; Du, W.; Wang, Y.; Liu, L.; Zhao, W.; Han, Z.; Kong, D.; Zhao, Q.; Guo, Z.; Han, Z.; Liu, N.; Ma, F.; Li, Z. Enhanced Therapeutic Effects of Mesenchymal Stem Cell-Derived Exosomes with an Injectable Hydrogel for Hindlimb Ischemia Treatment. *ACS Appl. Mater. Interfaces* **2018**, *10*, 30081−30091.
(166) Deng, Z.; Xu, X.; Iordachita, I.; Dehghani, H.; Zhang, B.; Wong, J. W.; Wang, K. K.-H. Mobile bioluminescence tomography-guided system for pre-clinical radiotherapy research. *Biomed. Opt. Express* **2022**, *13*, 4970−4989.
(167) Akter, F.; Simon, B.; de Boer, N. L.; Redjal, N.; Wakimoto, H.; Shah, K. Pre-clinical tumor models of primary brain tumors: Challenges and opportunities. *Biochim. Biophys. Acta* **2021**, *1875*, 188458.
(168) Gangadaran, P.; Ahn, B. C. Molecular Imaging: A Useful Tool for the Development of Natural Killer Cell-Based Immunotherapies. *Front. Immunol.* **2017**, *8*, 1090.
(169) Klose, A. D.; Paragas, N. Automated quantification of bioluminescence images. *Nat. Commun.* **2018**, *9*, 4262.
(170) Derfus, A. M.; Chan, W. C.; Bhatia, S. N. Probing the cytotoxicity of semiconductor quantum dots. *Nano Lett.* **2004**, *4*, 11−18.
(171) So, M.-K.; Xu, C.; Loening, A. M.; Gambhir, S. S.; Rao, J. Self-illuminating quantum dot conjugates for in vivo imaging. *Nat. Biotechnol.* **2006**, *24*, 339−343.
(172) Bellini, M.; Riva, B.; Tinelli, V.; Rizzuto, M. A.; Salvioni, L.; Colombo, M.; Mingozzi, F.; Visioli, A.; Marongiu, L.; Frascotti, G.; Christodoulou, M. S.; Passarella, D.; Prosperi, D.; Fiandra, L. Engineered ferritin nanoparticles for the bioluminescence tracking of nanodrug delivery in cancer. *Small* **2020**, *16*, 2001450.
(173) Schwinn, M. K.; Machleidt, T.; Zimmerman, K.; Eggers, C. T.; Dixon, A. S.; Hurst, R.; Hall, M. P.; Encell, L. P.; Binkowski, B. F.; Wood, K. V. CRISPR-mediated tagging of endogenous proteins with a luminescent peptide. *ACS Chem. Biol.* **2018**, *13*, 467−474.
(174) Ahn, B.-C. Requisites for successful theranostics with radionuclide-based reporter gene imaging. *J. Drug Target.* **2014**, *22*, 295−303.
(175) Chakravarty, R.; Goel, S.; Dash, A.; Cai, W. Radiolabeled inorganic nanoparticles for positron emission tomography imaging of cancer: an overview. *Q. J. Nucl. Med. Mol. Im.* **2017**, *61*, 181−204.
(176) Shukla, A. K.; Kumar, U. Positron emission tomography: An overview. *Med. Phys.* **2006**, *31*, 13−21.
(177) Treglia, G.; Muoio, B.; Giovanella, L.; Salvatori, M. The role of positron emission tomography and positron emission tomography/computed tomography in thyroid tumours: an overview. *Eur. Arch. Oto.-Rhino.-L.* **2013**, *270*, 1783−1787.
(178) Rahmim, A.; Zaidi, H. PET versus SPECT: strengths, limitations and challenges. *Nucl. Med. Commun.* **2008**, *29*, 193−207.
(179) James, M. L.; Gambhir, S. S. A molecular imaging primer: modalities, imaging agents, and applications. *Physiol. Rev.* **2012**, *92*, 897−965.
(180) Rosenkrans, Z. T.; Thickens, A. S.; Kink, J. A.; Aluicio-Sarduy, E.; Engle, J. W.; Hematti, P.; Hernandez, R. Investigating the in vivo biodistribution of extracellular vesicles isolated from various human cell sources using positron emission tomography. *Mol. Pharmaceutics* **2024**, *21*, 4324−4335.
(181) Sharma, S. K.; Chow, A.; Monette, S.; Vivier, D.; Pourat, J.; Edwards, K. J.; Dilling, T. R.; Abdel-Atti, D.; Zeglis, B. M.; Poirier, J. T.; Lewis, J. S. Fc-Mediated Anomalous Biodistribution of Therapeutic Antibodies in Immunodeficient Mouse ModelsThe Influence of Host Immunobiology on Antibody Biodistribution. *Cancer Res.* **2018**, *78*, 1820−1832.

https://doi.org/10.1021/cbmi.4c00085
Chem. Biomed. Imaging 2025, 3, 137−168

(182) Martins, Á. M.; Ramos, C. C.; Freitas, D.; Reis, C. A. Glycosylation of cancer extracellular vesicles: capture strategies, functional roles and potential clinical applications. *Cells* **2021**, *10*, 109.
(183) Williams, C.; Royo, F.; Aizpurua-Olaizola, O.; Pazos, R.; Boons, G.-J.; Reichardt, N.-C.; Falcon-Perez, J. M. Glycosylation of extracellular vesicles: current knowledge, tools and clinical perspectives. *J. Extracell. Vesicles* **2018**, *7*, 1442985.
(184) Nagaishi, K.; Mizue, Y.; Chikenji, T.; Otani, M.; Nakano, M.; Saijo, Y.; Tsuchida, H.; Ishioka, S.; Nishikawa, A.; Saito, T.; Fujimiya, M. Umbilical cord extracts improve diabetic abnormalities in bone marrow-derived mesenchymal stem cells and increase their therapeutic effects on diabetic nephropathy. *Sci. Rep.* **2017**, *7*, 8484.
(185) Sun, Y.; Shi, H.; Yin, S.; Ji, C.; Zhang, X.; Zhang, B.; Wu, P.; Shi, Y.; Mao, F.; Yan, Y.; Xu, W.; Qian, H. Human Mesenchymal Stem Cell Derived Exosomes Alleviate Type 2 Diabetes Mellitus by Reversing Peripheral Insulin Resistance and Relieving beta-Cell Destruction. *ACS Nano* **2018**, *12*, 7613−7628.
(186) Yaghoubi, Y.; Movassaghpour, A.; Zamani, M.; Talebi, M.; Mehdizadeh, A.; Yousefi, M. Human umbilical cord mesenchymal stem cells derived-exosomes in diseases treatment. *Life Sci.* **2019**, *233*, 116733.
(187) Grange, C.; Tapparo, M.; Bruno, S.; Chatterjee, D.; Quesenberry, P. J.; Tetta, C.; Camussi, G. Biodistribution of mesenchymal stem cell-derived extracellular vesicles in a model of acute kidney injury monitored by optical imaging. *Int. J. Mol. Med.* **2014**, *33*, 1055−1063.
(188) Wen, S.; Dooner, M.; Papa, E.; Del Tatto, M.; Pereira, M.; Borgovan, T.; Cheng, Y.; Goldberg, L.; Liang, O.; Camussi, G.; Quesenberry, P. Biodistribution of mesenchymal stem cell-derived extracellular vesicles in a radiation injury bone marrow murine model. *Int. J. Mol. Sci.* **2019**, *20*, 5468.
(189) Li, J.; Komatsu, H.; Poku, E. K.; Olafsen, T.; Huang, K. X.; Huang, L. A.; Chea, J.; Bowles, N.; Chang, B.; Rawson, J.; Peng, J.; Wu, A. M.; Shively, J. E.; Kandeel, F. R. Biodistribution of Intra-Arterial and Intravenous Delivery of Human Umbilical Cord Mesenchymal Stem Cell-Derived Extracellular Vesicles in a Rat Model to Guide Delivery Strategies for Diabetes Therapies. *Pharmaceuticals (Basel)* **2022**, *15*, 595.
(190) Slomka, P. J.; Miller, R. J. H.; Hu, L.-H.; Germano, G.; Berman, D. S. Solid-State Detector SPECT Myocardial Perfusion Imaging. *J. Nucl. Med.* **2019**, *60*, 1194−1204.
(191) Zeraatkar, N.; Kalluri, K. S.; Auer, B.; Konik, A.; Fromme, T. J.; Furenlid, L. R.; Kuo, P. H.; King, M. A. Investigation of Axial and Angular Sampling in Multi-Detector Pinhole-SPECT Brain Imaging. *IEEE Trans. Med. Imaging* **2020**, *39*, 4209−4224.
(192) Cherry, S. R.; Sorenson, J. A.; Phelps, M. E. The Gamma Camera: Basic Principles. *Monte Carlo Calculations in Nuclear Medicine: Applications in Diagnostic Imaging*; Taylor & Francis, 2012; Vol. 3.
(193) Brouwer, O. R.; Buckle, T.; Vermeeren, L.; Klop, W. M. C.; Balm, A. J.M.; van der Poel, H. G.; van Rhijn, B. W.; Horenblas, S.; Nieweg, O. E.; van Leeuwen, F. W.B.; Valdes Olmos, R. A. Comparing the Hybrid Fluorescent-Radioactive Tracer Indocyanine Green-Tc-99m-Nanocolloid with Tc-99m-Nanocolloid for Sentinel Node Identification: A Validation Study Using Lymphoscintigraphy and SPECT/CT. *J. Nucl. Med.* **2012**, *53*, 1034−1040.
(194) Gibbons, R. J.; Miller, T. D.; Christian, T. F. Infarct size measured by single photon emission computed tomographic imaging with Tc-99m-sestamibi - A measure of the efficacy of therapy in acute myocardial infarction. *Circulation* **2000**, *101*, 101−108.
(195) Morishita, M.; Takahashi, Y.; Nishikawa, M.; Sano, K.; Kato, K.; Yamashita, T.; Imai, T.; Saji, H.; Takakura, Y. Quantitative analysis of tissue distribution of the B16BL6-derived exosomes using a streptavidin-lactadherin fusion protein and iodine-125-labeled biotin derivative after intravenous injection in mice. *J. Pharm. Sci.* **2015**, *104*, 705−713.
(196) Faruqu, F. N.; Wang, J. T.-W.; Xu, L.; McNickle, L.; Chong, E. M.-Y.; Walters, A.; Gurney, M.; Clayton, A.; Smyth, L. A.; Hider, R.; Sosabowski, J.; Al-Jamal, K. T. Membrane radiolabelling of exosomes for comparative biodistribution analysis in immunocompetent and immunodeficient mice-a novel and universal approach. *Theranostics* **2019**, *9*, 1666.
(197) Shi, S.; Li, T.; Wen, X.; Wu, S. Y.; Xiong, C.; Zhao, J.; Lincha, V. R.; Chow, D. S.; Liu, Y.; Sood, A. K.; Li, C. Copper-64 labeled PEGylated exosomes for in vivo positron emission tomography and enhanced tumor retention. *Bioconjugate Chem.* **2019**, *30*, 2675−2683.
(198) Lu, C. H.; Chen, Y. A.; Ke, C. C.; Chiu, S. J.; Chen, C. C.; Hsieh, Y. J.; Yang, B. H.; Liu, R. S. Preclinical Characterization and In Vivo Imaging of (111) In-Labeled Mesenchymal Stem Cell-Derived Extracellular Vesicles. *Mol. Imaging Biol.* **2021**, *23*, 361−371.
(199) Gholamrezanezhad, A.; Mirpour, S.; Bagheri, M.; Mohamadnejad, M.; Alimoghaddam, K.; Abdolahzadeh, L.; Saghari, M.; Malekzadeh, R. In vivo tracking of 111In-oxine labeled mesenchymal stem cells following infusion in patients with advanced cirrhosis. *Nucl. Med. Biol.* **2011**, *38*, 961−967.
(200) Gildehaus, F. J.; Haasters, F.; Drosse, I.; Wagner, E.; Zach, C.; Mutschler, W.; Cumming, P.; Bartenstein, P.; Schieker, M. Impact of Indium-111 Oxine Labelling on Viability of Human Mesenchymal Stem Cells In Vitro, and 3D Cell-Tracking Using SPECT/CT In Vivo. *Mol. Imaging Biol.* **2011**, *13*, 1204−1214.
(201) Ruter, R.; O'Connor, M.; Peller, P. ACR Accreditation of SPECT systems using In-111 radiopharmaceuticals. *J. Nucl. Med.* **2011**, *52*, 2331.
(202) Zhao, C. L.; Shuke, N.; Okizaki, A.; Yamamoto, W.; Sato, J.; Iwata, K.; Kanno, T.; Hasebe, N.; Kikuchi, K.; Aburano, T. Naturally formed coronary arterial thrombus detected by In-111 oxine platelet imaging. *Clin. Med. Res.* **2005**, *30*, 492−495.
(203) Webb, R. L.; Kaiser, E. E.; Scoville, S. L.; Thompson, T. A.; Fatima, S.; Pandya, C.; Sriram, K.; Swetenburg, R. L.; Vaibhav, K.; Arbab, A. S.; Baban, B.; Dhandapani, K. M.; Hess, D. C.; Hoda, M. N.; Stice, S. L. Human Neural Stem Cell Extracellular Vesicles Improve Tissue and Functional Recovery in the Murine Thromboembolic Stroke Model. *Transl. Stroke Res.* **2018**, *9*, 530−539.
(204) Wadas, T. J.; Wong, E. H.; Weisman, G. R.; Anderson, C. J. Coordinating radiometals of copper, gallium, indium, yttrium, and zirconium for PET and SPECT imaging of disease. *Chem. Rev.* **2010**, *110*, 2858−2902.
(205) Yoo, M. H.; Lee, A. R.; Moon, K.-S. Characteristics of Extracellular Vesicles and Preclinical Testing Considerations Prior to Clinical Applications. *Biomedicines* **2022**, *10*, 869.
(206) Cowan, A. J.; Green, D. J.; Kwok, M.; Lee, S.; Coffey, D. G.; Holmberg, L. A.; Tuazon, S.; Gopal, A. K.; Libby, E. N. Diagnosis and Management of Multiple Myeloma A Review. *JAMA-J. Am. Med. Assoc.* **2022**, *327*, 464−477.
(207) Halpin, D. M. G.; Criner, G. J.; Papi, A.; Singh, D.; Anzueto, A.; Martinez, F. J.; Agusti, A. A.; Vogelmeier, C. F. Global Initiative for the Diagnosis, Management, and Prevention of Chronic Obstructive Lung Disease The 2020 GOLD Science Committee Report on COVID-19 and Chronic Obstructive Pulmonary Disease. *Am. J. Respir. Crit. Care Med.* **2021**, *203*, 24−36.
(208) Shi, F.; Wang, J.; Shi, J.; Wu, Z.; Wang, Q.; Tang, Z.; He, K.; Shi, Y.; Shen, D. Review of Artificial Intelligence Techniques in Imaging Data Acquisition, Segmentation, and Diagnosis for COVID-19. *IEEE Rev. Biomed. Eng.* **2021**, *14*, 4−15.
(209) Wang, J.-L.; Ding, B.-Z.; Xia, F.-F. Preoperative computed tomography-guided localization for multiple lung nodules: a Meta-analysis. *Minim. Invasive Ther. Allied. Technol.* **2022**, *31*, 1123−1130.
(210) Caldemeyer, K. S.; Buckwalter, K. A. The basic principles of computed tomography and magnetic resonance imaging. *J. Am. Acad. Dermatol.* **1999**, *41*, 768−771.
(211) Hathcock, J. T.; Stickle, R. L. Principles and concepts of computed tomography. *Vet. Clin. North Am. Small Anim. Pract.* **1993**, *23*, 399−415.
(212) Kamalian, S.; Lev, M. H.; Gupta, R. Computed tomography imaging and angiography - principles. *Handb. Clin. Neurol.* **2016**, *135*, 3−20.
(213) Willemink, M. J.; de Jong, P. A.; Leiner, T.; de Heer, L. M.; Nievelstein, R. A. J.; Budde, R. P. J.; Schilham, A. M. R. Iterative

https://doi.org/10.1021/cbmi.4c00085
Chem. Biomed. Imaging 2025, 3, 137−168

reconstruction techniques for computed tomography Part 1: Technical principles. *Eur. Radiol.* **2013**, *23*, 1623−1631.
(214) Song, G.; Cheng, L.; Chao, Y.; Yang, K.; Liu, Z. Emerging nanotechnology and advanced materials for cancer radiation therapy. *Adv. Mater.* **2017**, *29*, 1700996.
(215) Zheng, L.; Zhu, R.; Chen, L.; Fu, Q.; Li, J.; Chen, C.; Song, J.; Yang, H. X-ray sensitive high-Z metal nanocrystals for cancer imaging and therapy. *Nano Res.* **2021**, *14*, 3744−3755.
(216) Betzer, O.; Chemla, Y.; Markus, A.; Motiei, M.; Sadan, T.; Liu, Z.; Mandel, Y.; Popovtzer, R. Multimodal High-Resolution Imaging of Photoreceptor Precursor Cells Using Gold Nanoparticles. *Symposium on Nanoscale Imaging, Sensing, and Actuation for Biomedical Applications*; SPIE BiOS Conference, San Francisco, CA, 2020.
(217) Betzer, O.; Gao, Y.; Shamul, A.; Motiei, M.; Sadan, T.; Yehuda, R.; Atkins, A.; Cohen, C. J.; Shen, M.; Shi, X.; Popovtzer, R. Multifunctional nanoprobe for real-time in vivo monitoring of T cell activation. *Nanomedicine* **2022**, *46*, 102596.
(218) Betzer, O.; Shwartz, A.; Motiei, M.; Kazimirsky, G.; Gispan, I.; Damti, E.; Brodie, C.; Yadid, G.; Popovtzer, R. Nanoparticle-Based CT Imaging Technique for Longitudinal and Quantitative Stem Cell Tracking within the Brain: Application in Neuropsychiatric Disorders. *ACS Nano* **2014**, *8*, 9274−9285.
(219) Chen, M.; Betzer, O.; Fan, Y.; Gao, Y.; Shen, M.; Sadan, T.; Popovtzer, R.; Shi, X. Multifunctional Dendrimer-Entrapped Gold Nanoparticles for Labeling and Tracking T Cells Via Dual-Modal Computed Tomography and Fluorescence Imaging. *Biomacromolecules* **2020**, *21*, 1587−1595.
(220) Meir, R.; Betzer, O.; Motiei, M.; Kronfeld, N.; Brodie, C.; Popovtzer, R. Design principles for noninvasive, longitudinal and quantitative cell tracking with nanoparticle-based CT imaging. *Nanomedicine* **2017**, *13*, 421−429.
(221) Zhuang, X.; Xiang, X.; Grizzle, W.; Sun, D.; Zhang, S.; Axtell, R. C; Ju, S.; Mu, J.; Zhang, L.; Steinman, L.; Miller, D.; Zhang, H.-G. Treatment of brain inflammatory diseases by delivering exosome encapsulated anti-inflammatory drugs from the nasal region to the brain. *Mol. Ther.* **2011**, *19*, 1769−1779.
(222) Yang, T.; Martin, P.; Fogarty, B.; Brown, A.; Schurman, K.; Phipps, R.; Yin, V. P.; Lockman, P.; Bai, S. Exosome delivered anticancer drugs across the blood-brain barrier for brain cancer therapy in Danio rerio. *Pharm. Res.* **2015**, *32*, 2003−2014.
(223) Ha, D.; Yang, N.; Nadithe, V. Exosomes as therapeutic drug carriers and delivery vehicles across biological membranes: current perspectives and future challenges. *Acta Pharm. Sin. B* **2016**, *6*, 287−296.
(224) Sun, D.; Zhuang, X.; Xiang, X.; Liu, Y.; Zhang, S.; Liu, C.; Barnes, S.; Grizzle, W.; Miller, D.; Zhang, H.-G. A novel nanoparticle drug delivery system: the anti-inflammatory activity of curcumin is enhanced when encapsulated in exosomes. *Mol. Ther.* **2010**, *18*, 1606−1614.
(225) Shwartz, A.; Betzer, O.; Kronfeld, N.; Kazimirsky, G.; Cazacu, S.; Finniss, S.; Lee, H. K.; Motiei, M.; Dagan, S. Y.; Popovtzer, R.; Brodie, C.; Yadid, G. Therapeutic effect of astroglia-like mesenchymal stem cells expressing glutamate transporter in a genetic rat model of depression. *Theranostics* **2017**, *7*, 2690.
(226) Betzer, O.; Meir, R.; Motiei, M.; Yadid, G.; Popovtzer, R. Gold Nanoparticle-Cell Labeling Methodology for Tracking Stem Cells within the Brain. *Nanoscale Imaging, Sensing, and Actuation for Biomedical Applications XIV*; SPIE: 2017; pp 189−197.
(227) Arvizo, R.; Bhattacharya, R.; Mukherjee, P. Gold nanoparticles: opportunities and challenges in nanomedicine. *Expert Opin. Drug Delivery* **2010**, *7*, 753−763.
(228) Betzer, O.; Perets, N.; Angel, A.; Motiei, M.; Sadan, T.; Yadid, G.; Offen, D.; Popovtzer, R. In Vivo Neuroimaging of Exosomes Using Gold Nanoparticles. *ACS Nano* **2017**, *11*, 10883−10893.
(229) Haney, M. J.; Klyachko, N. L.; Zhao, Y.; Gupta, R.; Plotnikova, E. G.; He, Z.; Patel, T.; Piroyan, A.; Sokolsky, M.; Kabanov, A. V.; Batrakova, E. V. Exosomes as drug delivery vehicles for Parkinson's disease therapy. *J. Controlled Release* **2015**, *207*, 18−30.
(230) Perets, N.; Betzer, O.; Shapira, R.; Brenstein, S.; Angel, A.; Sadan, T.; Ashery, U.; Popovtzer, R.; Offen, D. Golden Exosomes Selectively Target Brain Pathologies in Neurodegenerative and Neurodevelopmental Disorders. *Nano Lett.* **2019**, *19*, 3422−3431.
(231) Rogers, J.; Mastroeni, D.; Leonard, B.; Joyce, J.; Grover, A. Neuroinflammation in Alzheimer's disease and Parkinson's disease: are microglia pathogenic in either disorder? *Int. Rev. Neurobiol.* **2007**, *82*, 235−246.
(232) Li, D.-D.; Zheng, C.-Q.; Zhang, F.; Shi, J.-S. Potential neuroprotection by Dendrobium nobile Lindl alkaloid in Alzheimer's disease models. *Neural Regen. Res.* **2022**, *17*, 972−977.
(233) Teleanu, D. M.; Niculescu, A.-G.; Lungu, I. I.; Radu, C. I.; Vladacenco, O.; Roza, E.; Costachescu, B.; Grumezescu, A. M.; Teleanu, R. I. An Overview of Oxidative Stress, Neuroinflammation, and Neurodegenerative Diseases. *Int. J. Mol. Sci.* **2022**, *23*, 5938.
(234) Long, Q.; Upadhya, D.; Hattiangady, B.; Kim, D.-K.; An, S. Y.; Shuai, B.; Prockop, D. J.; Shetty, A. K. Intranasal MSC-derived A1-exosomes ease inflammation, and prevent abnormal neurogenesis and memory dysfunction after status epilepticus. *Proc. Natl. Acad. Sci. U.S.A.* **2017**, *114*, No. E3536-E3545.
(235) Yang, Y.; Ye, Y.; Su, X.; He, J.; Bai, W.; He, X. MSCs-derived exosomes and neuroinflammation, neurogenesis and therapy of traumatic brain injury. *Front. Cell. Neurosci.* **2017**, *11*, 55.
(236) Guo, S.; Perets, N.; Betzer, O.; Ben-Shaul, S.; Sheinin, A.; Michaelevski, I.; Popovtzer, R.; Offen, D.; Levenberg, S. Intranasal Delivery of Mesenchymal Stem Cell Derived Exosomes Loaded with Phosphatase and Tensin Homolog siRNA Repairs Complete Spinal Cord Injury. *ACS Nano* **2019**, *13*, 10015−10028.
(237) Fan, B.; Wei, Z.; Feng, S. Progression in translational research on spinal cord injury based on microenvironment imbalance. *Bone Res.* **2022**, *10*, 35.
(238) Fan, L.; Liu, C.; Chen, X.; Zheng, L.; Zou, Y.; Wen, H.; Guan, P.; Lu, F.; Luo, Y.; Tan, G.; Yu, P.; Chen, D.; Deng, C.; Sun, Y.; Zhou, L.; Ning, C. Exosomes-Loaded Electroconductive Hydrogel Synergistically Promotes Tissue Repair after Spinal Cord Injury via Immunoregulation and Enhancement of Myelinated Axon Growth. *Adv. Sci.* **2022**, *9*, 2105586.
(239) Flack, J. A.; Sharma, K. D.; Xie, J. Y. Delving into the recent advancements of spinal cord injury treatment: a review of recent progress. *Neural. Regen. Res.* **2022**, *17*, 283−291.
(240) Mahar, M.; Cavalli, V. Intrinsic mechanisms of neuronal axon regeneration. *Nat. Rev. Neurosci.* **2018**, *19*, 323−337.
(241) Faden, A. I.; Wu, J.; Stoica, B. A.; Loane, D. J. Progressive inflammation-mediated neurodegeneration after traumatic brain or spinal cord injury. *Br. J. Pharmacol.* **2016**, *173*, 681−691.
(242) Bradbury, E. J.; Moon, L. D.; Popat, R. J.; King, V. R.; Bennett, G. S.; Patel, P. N.; Fawcett, J. W.; McMahon, S. B. Chondroitinase ABC promotes functional recovery after spinal cord injury. *Nature* **2002**, *416*, 636−640.
(243) Lachyankar, M. B.; Sultana, N.; Schonhoff, C. M.; Mitra, P.; Poluha, W.; Lambert, S.; Quesenberry, P. J.; Litofsky, N. S.; Recht, L. D.; Nabi, R.; Miller, S. J.; Ohta, S.; Neel, B. G.; Ross, A. H. A role for nuclear PTEN in neuronal differentiation. *J. Neurosci.* **2000**, *20*, 1404−1413.
(244) Liu, K.; Lu, Y.; Lee, J. K; Samara, R.; Willenberg, R.; Sears-Kraxberger, I.; Tedeschi, A.; Park, K. K.; Jin, D.; Cai, B.; Xu, B.; Connolly, L.; Steward, O.; Zheng, B.; He, Z. PTEN deletion enhances the regenerative ability of adult corticospinal neurons. *Nat. Neurosci.* **2010**, *13*, 1075−1081.
(245) Christie, K. J.; Webber, C. A.; Martinez, J. A.; Singh, B.; Zochodne, D. W. PTEN inhibition to facilitate intrinsic regenerative outgrowth of adult peripheral axons. *J. Neurosci.* **2010**, *30*, 9306−9315.
(246) Terenzio, M.; Koley, S.; Samra, N.; Rishal, I.; Zhao, Q.; Sahoo, P. K.; Urisman, A.; Marvaldi, L.; Oses-Prieto, J. A.; Forester, C.; Gomes, C.; Kalinski, A. L.; Di Pizio, A.; Doron-Mandel, E.; Perry, R. B.-T.; Koppel, I.; Twiss, J. L.; Burlingame, A. L.; Fainzilber, M. Locally translated mTOR controls axonal local translation in nerve injury. *Science* **2018**, *359*, 1416−1421.

https://doi.org/10.1021/cbmi.4c00085
Chem. Biomed. Imaging 2025, 3, 137−168

(247) Hwang, D. W.; Choi, H.; Jang, S. C.; Yoo, M. Y.; Park, J. Y.; Choi, N. E.; Oh, H. J.; Ha, S.; Lee, Y.-S.; Jeong, J. M.; Gho, Y. S.; Lee, D. S. Noninvasive imaging of radiolabeled exosome-mimetic nanovesicle using ^{99m}Tc-HMPAO. *Sci. Rep.* **2015**, *5*, 1−10.
(248) Zhang, S. J.; Wu, J. C. Comparison of imaging techniques for tracking cardiac stem cell therapy. *J. Nucl. Med.* **2007**, *48*, 1916−1919.
(249) Cohen, O.; Betzer, O.; Elmaliach-Pnini, N.; Motiei, M.; Sadan, T.; Cohen-Berkman, M.; Dagan, O.; Popovtzer, A.; Yosepovich, A.; Barhom, H.; Michaeli, S.; Popovtzer, R. 'Golden' exosomes as delivery vehicles to target tumors and overcome intratumoral barriers: in vivo tracking in a model for head and neck cancer. *Biomater. Sci.* **2021**, *9*, 2103−2114.
(250) Chung, N. N.; Ting, L. L.; Hsu, W. C.; Lui, L. T.; Wang, P. M. Impact of magnetic resonance imaging versus CT on nasopharyngeal carcinoma: Primary tumor target delineation for radiotherapy. *Head Neck-J. Sci. Spec.* **2004**, *26*, 241−246.
(251) Antwi-Baah, R.; Wang, Y.; Chen, X.; Yu, K. Metal-Based Nanoparticle Magnetic Resonance Imaging Contrast Agents: Classifications, Issues, and Countermeasures toward their Clinical Translation. *Adv. Mater. Interfaces* **2022**, *9*, 2101710.
(252) Lu, Z.-R.; Laney, V.; Li, Y. Targeted Contrast Agents for Magnetic Resonance Molecular Imaging of Cancer. *Acc. Chem. Res.* **2022**, *55*, 2833−2847.
(253) Qin, R.; Li, S.; Qiu, Y.; Feng, Y.; Liu, Y.; Ding, D.; Xu, L.; Ma, X.; Sun, W.; Chen, H. Carbonized paramagnetic complexes of Mn (II) as contrast agents for precise magnetic resonance imaging of submillimeter-sized orthotopic tumors. *Nat. Commun.* **2022**, *13*, 1938.
(254) Maumus, M.; Jorgensen, C.; Noël, D. Mesenchymal stem cells in regenerative medicine applied to rheumatic diseases: role of secretome and exosomes. *Biochimie* **2013**, *95*, 2229−2234.
(255) Bruno, S.; Grange, C.; Deregibus, M. C.; Calogero, R. A.; Saviozzi, S.; Collino, F.; Morando, L.; Busca, A.; Falda, M.; Bussolati, B.; Tetta, C.; Camussi, G. Mesenchymal stem cell-derived microvesicles protect against acute tubular injury. *J. Am. Soc. Nephrol.* **2009**, *20*, 1053−1067.
(256) Kourembanas, S. Exosomes: vehicles of intercellular signaling, biomarkers, and vectors of cell therapy. *Annu. Rev. Physiol.* **2015**, *77*, 13−27.
(257) Hu, L.; Wickline, S. A.; Hood, J. L. Magnetic resonance imaging of melanoma exosomes in lymph nodes. *Magn. Reson. Med.* **2015**, *74*, 266−271.
(258) Johnsen, K. B.; Gudbergsson, J. M.; Skov, M. N.; Christiansen, G.; Gurevich, L.; Moos, T.; Duroux, M. Evaluation of electroporation-induced adverse effects on adipose-derived stem cell exosomes. *Cytotechnology* **2016**, *68*, 2125−2138.
(259) Silva, A. K.; Wilhelm, C.; Kolosnjaj-Tabi, J.; Luciani, N.; Gazeau, F. Cellular transfer of magnetic nanoparticles via cell microvesicles: impact on cell tracking by magnetic resonance imaging. *Pharm. Res.* **2012**, *29*, 1392−403.
(260) Busato, A.; Bonafede, R.; Bontempi, P.; Scambi, I.; Schiaffino, L.; Benati, D.; Malatesta, M.; Sbarbati, A.; Marzola, P.; Mariotti, R. Magnetic resonance imaging of ultrasmall superparamagnetic iron oxide-labeled exosomes from stem cells: a new method to obtain labeled exosomes. *Int. J. Nanomedicine* **2016**, *11*, 2481−90.
(261) Dabrowska, S.; Del Fattore, A.; Karnas, E.; Frontczak-Baniewicz, M.; Kozlowska, H.; Muraca, M.; Janowski, M.; Lukomska, B. Imaging of extracellular vesicles derived from human bone marrow mesenchymal stem cells using fluorescent and magnetic labels. *Int. J. Nanomedicine* **2018**, *13*, 1653−1664.
(262) Liu, T.; Zhu, Y.; Zhao, R.; Wei, X.; Xin, X. Visualization of exosomes from mesenchymal stem cells in vivo by magnetic resonance imaging. *Magn. Reson. Imaging* **2020**, *68*, 75−82.
(263) Gilad, A. A.; Winnard, P. T., Jr; van Zijl, P. C.; Bulte, J. W. Developing MR reporter genes: promises and pitfalls. *NMR Biomed.* **2007**, *20*, 275−290.
(264) Gilad, A. A.; Ziv, K.; McMahon, M. T.; Van Zijl, P. C.; Neeman, M.; Bulte, J. W. MRI reporter genes. *J. Nucl. Med.* **2008**, *49*, 1905−1908.
(265) Patrick, P. S.; Hammersley, J.; Loizou, L.; Kettunen, M. I.; Rodrigues, T. B.; Hu, D.-E.; Tee, S.-S.; Hesketh, R.; Lyons, S. K.; Soloviev, D.; Lewis, D. Y.; Aime, S.; Fulton, S. M.; Brindle, K. M. Dual-modality gene reporter for in vivo imaging. *Proc. Natl. Acad. Sci. U.S.A.* **2014**, *111*, 415−420.
(266) Louie, A. Y.; Hüber, M. M.; Ahrens, E. T.; Rothbächer, U.; Moats, R.; Jacobs, R. E.; Fraser, S. E.; Meade, T. J. In vivo visualization of gene expression using magnetic resonance imaging. *Nat. Biotechnol.* **2000**, *18*, 321−325.
(267) Bartelle, B. B.; Szulc, K. U.; Suero-Abreu, G. A.; Rodriguez, J. J.; Turnbull, D. H. Divalent metal transporter, DMT1: a novel MRI reporter protein. *Magn. Reson. Med.* **2013**, *70*, 842−850.
(268) Withers, P. J.; Bouman, C.; Carmignato, S.; Cnudde, V.; Grimaldi, D.; Hagen, C. K.; Maire, E.; Manley, M.; Du Plessis, A.; Stock, S. R. X-ray computed tomography. *Nat. Rev. Methods Primers* **2021**, *1*, 18.
(269) Li, L.; Zhu, L.; Ma, C.; Lin, L.; Yao, J.; Wang, L.; Maslov, K.; Zhang, R.; Chen, W.; Shi, J.; Wang, L. V. Single-impulse panoramic photoacoustic computed tomography of small-animal whole-body dynamics at high spatiotemporal resolution. *Nat. Biomed. Eng.* **2017**, *1*, 0071.
(270) Ning, Y.; Zhou, I. Y.; Caravan, P. Quantitative in Vivo Molecular MRI. *Adv. Mater.* **2024**, *36*, 2407262.
(271) Koopmans, P. J.; Yacoub, E. Strategies and prospects for cortical depth dependent T2 and T2* weighted BOLD fMRI studies. *NeuroImage* **2019**, *197*, 668−676.
(272) Kalra, S.; Müller, H.-P.; Ishaque, A.; Zinman, L.; Korngut, L.; Genge, A.; Beaulieu, C.; Frayne, R.; Graham, S. J.; Kassubek, J. A prospective harmonized multicenter DTI study of cerebral white matter degeneration in ALS. *Neurology* **2020**, *95*, No. e943-e952.
(273) Nguyen, H. V. T.; Chen, Q.; Paletta, J. T.; Harvey, P.; Jiang, Y.; Zhang, H.; Boska, M. D.; Ottaviani, M. F.; Jasanoff, A.; Rajca, A.; Johnson, J. A. Nitroxide-Based Macromolecular Contrast Agents with Unprecedented Transverse Relaxivity and Stability for Magnetic Resonance Imaging of Tumors. *ACS Cent. Sci.* **2017**, *3*, 800−811.
(274) Garmendia, S.; Mantione, D.; Alonso-de Castro, S.; Jehanno, C.; Lezama, L.; Hedrick, J. L.; Mecerreyes, D.; Salassa, L.; Sardon, H. Polyurethane based organic macromolecular contrast agents (PU-ORCAs) for magnetic resonance imaging. *Polym. Chem.* **2017**, *8*, 2693−2701.
(275) Wang, X.; Pang, Y.; Ku, G.; Xie, X.; Stoica, G.; Wang, L. V. Noninvasive laser-induced photoacoustic tomography for structural and functional in vivo imaging of the brain. *Nat. Biotechnol.* **2003**, *21*, 803−806.
(276) Chen, Q.; Liang, C.; Sun, X.; Chen, J.; Yang, Z.; Zhao, H.; Feng, L.; Liu, Z. H_2O_2-responsive liposomal nanoprobe for photoacoustic inflammation imaging and tumor theranostics via in vivo chromogenic assay. *Proc. Natl. Acad. Sci. U.S.A.* **2017**, *114*, 5343−5348.
(277) Ding, H.; Cai, Y.; Gao, L.; Liang, M.; Miao, B.; Wu, H.; Liu, Y.; Xie, N.; Tang, A.; Fan, K.; Yan, X.; Nie, G. Exosome-like Nanozyme Vesicles for H_2O_2-Responsive Catalytic Photoacoustic Imaging of Xenograft Nasopharyngeal Carcinoma. *Nano Lett.* **2019**, *19*, 203−209.
(278) Jang, Y.; Kim, H.; Yoon, S.; Lee, H.; Hwang, J.; Jung, J.; Chang, J. H.; Choi, J.; Kim, H. Exosome-based photoacoustic imaging guided photodynamic and immunotherapy for the treatment of pancreatic cancer. *J. Controlled Release* **2021**, *330*, 293−304.
(279) Bell, A. G. On the production and reproduction of sound by light. *Am. J. Sci.* **1880**, *s3-20*, 305−324.
(280) Lin, L.; Wang, L. V. The emerging role of photoacoustic imaging in clinical oncology. *Nat. Rev. Clin. Oncol.* **2022**, *19*, 365−384.
(281) Liu, Y.; Teng, L.; Yin, B.; Meng, H.; Yin, X.; Huan, S.; Song, G.; Zhang, X.-B. Chemical Design of Activatable Photoacoustic Probes for Precise Biomedical Applications. *Chem. Rev.* **2022**, *122*, 6850−6918.
(282) Zhang, Y.; Fang, J.; Ye, S.; Zhao, Y.; Wang, A.; Mao, Q.; Cui, C.; Feng, Y.; Li, J.; Li, S.; Zhang, M.; Shi, H. A hydrogen sulphide-

responsive and depleting nanoplatform for cancer photodynamic therapy. *Nat. Commun.* **2022**, *13*, 1685.
(283) Berninger, M. T.; Mohajerani, P.; Wildgruber, M.; Beziere, N.; Kimm, M. A.; Ma, X.; Haller, B.; Fleming, M. J.; Vogt, S.; Anton, M.; Imhoff, A. B.; Ntziachristos, V.; Meier, R.; Henning, T. D. Detection of intramyocardially injected DiR-labeled mesenchymal stem cells by optical and optoacoustic tomography. *Photoacoustics* **2017**, *6*, 37−47.
(284) Huang, X.; Shen, A.; Peng, R.; Chen, S.; Lin, S.; Ding, S.; Li, H.; Zhou, D. A Novel Biomimetic Nanoprobe as a Photoacoustic Contrast Agent. *Front. Chem.* **2021**, *9*, 721799.
(285) Li, Y.; Lin, J.; Ma, J.; Song, L.; Lin, H.; Tang, B.; Chen, D.; Su, G.; Ye, S.; Zhu, X.; Luo, F.; Hou, Z. Methotrexate-Camptothecin Prodrug Nanoassemblies as a Versatile Nanoplatform for Biomodal Imaging-Guided Self-Active Targeted and Synergistic Chemotherapy. *ACS Appl. Mater. Interfaces* **2017**, *9*, 34650−34665.
(286) Li, Y.; Wu, Y.; Chen, J.; Wan, J.; Xiao, C.; Guan, J.; Song, X.; Li, S.; Zhang, M.; Cui, H.; Li, T.; Yang, X.; Li, Z.; Yang, X. A Simple Glutathione-Responsive Turn-On Theranostic Nanoparticle for Dual-Modal Imaging and Chemo-Photothermal Combination Therapy. *Nano Lett.* **2019**, *19*, 5806−5817.
(287) Zhang, N.; Song, Y.; Huang, Z.; Chen, J.; Tan, H.; Yang, H.; Fan, M.; Li, Q.; Wang, Q.; Gao, J.; Pang, Z.; Qian, J.; Ge, J. Monocyte mimics improve mesenchymal stem cell-derived extracellular vesicle homing in a mouse MI/RI model. *Biomaterials* **2020**, *255*, 120168.
(288) Zheng, P.; Ding, B.; Shi, R.; Jiang, Z.; Xu, W.; Li, G.; Ding, J.; Chen, X. A Multichannel Ca^{2+} Nanomodulator for Multilevel Mitochondrial Destruction-Mediated Cancer Therapy. *Adv. Mater.* **2021**, *33*, 2007426.
(289) Lu, Z.; Acter, S.; Teo, B. M.; Bishop, A. I.; Tabor, R. F.; Vidallon, M. L. P. Mesoporous, anisotropic nanostructures from bioinspired polymeric catecholamine neurotransmitters and their potential application as photoacoustic imaging agents. *J. Mater. Chem. B* **2022**, *10*, 9662−9670.
(290) Vidallon, M. L. P.; Salimova, E.; Crawford, S. A.; Teo, B. M.; Tabor, R. F.; Bishop, A. I. Enhanced photoacoustic imaging in tissue-mimicking phantoms using polydopamine-shelled perfluorocarbon emulsion droplets. *Ultrason. Sonochem.* **2022**, *86*, 106041.
(291) Liang, L.; Shen, Y.; Dong, Z.; Gu, X. Photoacoustic image-guided corpus cavernosum intratunical injection of adipose stem cell-derived exosomes loaded polydopamine thermosensitive hydrogel for erectile dysfunction treatment. *Bioact. Mater.* **2022**, *9*, 147−156.
(292) Zhang, X.-D.; Wang, H.; Antaris, A. L.; Li, L.; Diao, S.; Ma, R.; Nguyen, A.; Hong, G.; Ma, Z.; Wang, J.; Zhu, S.; Castellano, J. M.; Wyss-Coray, T.; Liang, Y.; Luo, J.; Dai, H. Traumatic brain injury imaging in the second near-infrared window with a molecular fluorophore. *Adv. Mater.* **2016**, *28*, 6872−6879.
(293) Yan, T.; Su, M.; Wang, Z.; Zhang, J. Second Near-Infrared Plasmonic Nanomaterials for Photoacoustic Imaging and Photothermal Therapy. *Small* **2023**, *19*, 2300539.
(294) Zheng, S.; Gao, D.; Wu, Y.; Hu, D.; Li, Z.; Wang, Y.; Zheng, H.; Li, Y.; Sheng, Z. X-Ray Activatable Au/Ag Nanorods for Tumor Radioimmunotherapy Sensitization and Monitoring of the Therapeutic Response Using NIR-II Photoacoustic Imaging. *Adv. Sci.* **2023**, *10*, 2206979.
(295) Jathoul, A. P.; Laufer, J.; Ogunlade, O.; Treeby, B.; Cox, B.; Zhang, E.; Johnson, P.; Pizzey, A. R.; Philip, B.; Marafioti, T.; Lythgoe, M. F.; Pedley, R. B.; Pule, M. A.; Beard, P. Deep in vivo photoacoustic imaging of mammalian tissues using a tyrosinase-based genetic reporter. *Nat. Photonics* **2015**, *9*, 239−246.
(296) He, Y.; Wan, H.; Jiang, X.; Peng, C. Piezoelectric Micromachined Ultrasound Transducer Technology: Recent Advances and Applications. *Biosensors-Basel* **2023**, *13*, 55.
(297) Ren, D.; Yin, Y.; Li, C.; Chen, R.; Shi, J. Recent Advances in Flexible Ultrasonic Transducers: From Materials Optimization to Imaging Applications. *Micromachines* **2023**, *14*, 126.
(298) Zhao, Y.; Wang, L. V. Single-shot photoacoustic imaging with single-element transducer through a spatiotemporal encoder. *J. Biomed. Opt.* **2023**, *28*, 046004.
(299) Knoepp, F.; Bettmer, J.; Fronius, M. Gadolinium released by the linear gadolinium-based contrast-agent Gd-DTPA decreases the activity of human epithelial Na+ channels (ENaCs). *Biochim Biophys Acta Biomembr* **2017**, *1859*, 1040−1048.
(300) Abello, J.; Nguyen, T. D. T.; Marasini, R.; Aryal, S.; Weiss, M. L. Biodistribution of gadolinium- and near infrared-labeled human umbilical cord mesenchymal stromal cell-derived exosomes in tumor bearing mice. *Theranostics* **2019**, *9*, 2325−2345.
(301) Mathivanan, S.; Ji, H.; Simpson, R. J. Exosomes: extracellular organelles important in intercellular communication. *J. Proteomics* **2010**, *73*, 1907−1920.
(302) Jing, B.; Gai, Y.; Qian, R.; Liu, Z.; Zhu, Z.; Gao, Y.; Lan, X.; An, R. Hydrophobic insertion-based engineering of tumor cell-derived exosomes for SPECT/NIRF imaging of colon cancer. *J. Nanobiotechnology* **2021**, *19*, 7.
(303) Jing, B.; Qian, R.; Jiang, D.; Gai, Y.; Liu, Z.; Guo, F.; Ren, S.; Gao, Y.; Lan, X.; An, R. Extracellular vesicles-based pre-targeting strategy enables multi-modal imaging of orthotopic colon cancer and image-guided surgery. *J. Nanobiotechnology* **2021**, *19*, 151.
(304) Chen, Y.; Zhang, S.; Lu, J.; Li, D.; Wu, H.; Zhang, L.; Li, X.; Gao, X.; Xu, Y.; Zeng, Z.; Zeng, L.; Ding, X.; Li, X.; Ding, S. DNA-Guided Extracellular-Vesicle Metallization with High Catalytic Activity for Accurate Diagnosis of Pulmonary Nodules. *Small* **2023**, *19*, 2208142.
(305) Zhang, X.; Wu, Y.; Chen, L.; Song, J.; Yang, H. Optical and Photoacoustic Imaging In Vivo: Opportunities and Challenges. *CBMI* **2023**, *1*, 99−109.
(306) Zhang, Y.; Wang, G.; Yang, L.; Wang, F.; Liu, A. Recent advances in gold nanostructures based biosensing and bioimaging. *Coord. Chem. Rev.* **2018**, *370*, 1−21.
(307) Tsang, M.-K.; Wong, Y.-T.; Hao, J. Cutting-Edge Nanomaterials for Advanced Multimodal Bioimaging Applications. *Small Methods* **2018**, *2*, 1700265.
(308) Sedlmeier, A.; Gorris, H. H. Surface modification and characterization of photon-upconverting nanoparticles for bioanalytical applications. *Chem. Soc. Rev.* **2015**, *44*, 1526−1560.
(309) Bai, G.; Tsang, M. K.; Hao, J. Luminescent ions in advanced composite materials for multifunctional applications. *Adv. Funct. Mater.* **2016**, *26*, 6330−6350.
(310) Zhang, C.; Cui, X.; Yang, J.; Shao, X.; Zhang, Y.; Liu, D. Stimulus-responsive surface-enhanced Raman scattering: a "Trojan horse" strategy for precision molecular diagnosis of cancer. *Chem. Sci.* **2020**, *11*, 6111−6120.
(311) Zhang, C.; Liu, X.; Xu, Z.; Liu, D. Multichannel stimulus-responsive nanoprobes for H_2O_2 sensing in diverse biological milieus. *Anal. Chem.* **2020**, *92*, 12639−12646.
(312) Matoba, O.; Quan, X.; Xia, P.; Awatsuji, Y.; Nomura, T. Multimodal imaging based on digital holography. *Proc. IEEE Inst. Electr. Electron. Eng.* **2017**, *105*, 906−923.
(313) Rosen, J.; Brooker, G. Non-scanning motionless fluorescence three-dimensional holographic microscopy. *Nat. Photonics* **2008**, *2*, 190−195.
(314) Zhang, X.; Lu, Y.; Wu, S.; Zhang, S.; Li, S.; Tan, J. An overview of current research on mesenchymal stem cell-derived extracellular vesicles: a bibliometric analysis from 2009 to 2021. *Front. Bioeng. Biotechnol.* **2022**, *10*, 910812.
(315) Wiklander, O. P. B.; Nordin, J. Z.; O'Loughlin, A.; Gustafsson, Y.; Corso, G.; Mager, I.; Vader, P.; Lee, Y.; Sork, H.; Seow, Y.; Heldring, N.; Alvarez-Erviti, L.; Smith, C. E.; Le Blanc, K.; Macchiarini, P.; Jungebluth, P.; Wood, M. J. A.; Andaloussi, S. E. Extracellular vesicle in vivo biodistribution is determined by cell source, route of administration and targeting. *J. Extracell. Vesicles* **2015**, *4*, 26316.
(316) Todd, D. J.; Kay, J. Gadolinium-induced fibrosis. *Annu. Rev. Med.* **2016**, *67*, 273−291.
(317) Li, J.; Wu, C.; Hou, P.; Zhang, M.; Xu, K. One-pot preparation of hydrophilic manganese oxide nanoparticles as T1 nano-contrast agent for molecular magnetic resonance imaging of renal carcinoma in vitro and in vivo. *Biosens. Bioelectron.* **2018**, *102*, 1−8.

https://doi.org/10.1021/cbmi.4c00085
Chem. Biomed. Imaging 2025, 3, 137−168

(318) Zheng, W.; He, R.; Liang, X.; Roudi, S.; Bost, J.; Coly, P.-M.; van Niel, G.; Andaloussi, S. E. L. Cell-specific targeting of extracellular vesicles through engineering the glycocalyx. *J. Extracell. Vesicles* **2022**, *11*, No. e12290.
(319) Feng, K.; Xie, X.; Yuan, J.; Gong, L.; Zhu, Z.; Zhang, J.; Li, H.; Yang, Y.; Wang, Y. Reversing the surface charge of MSC-derived small extracellular vesicles by εPL-PEG-DSPE for enhanced osteoarthritis treatment. *J. Extracell. Vesicles* **2021**, *10*, No. e12160.
(320) Liam-Or, R.; Faruqu, F. N.; Walters, A.; Han, S.; Xu, L.; Wang, J. T.-W.; Oberlaender, J.; Sanchez-Fueyo, A.; Lombardi, G.; Dazzi, F.; Mailaender, V.; Al-Jamal, K. T. Cellular uptake and in vivo distribution of mesenchymal-stem-cell-derived extracellular vesicles are protein corona dependent. *Nat. Nanotechnol.* **2024**, *19*, 846−855.
(321) Wong, J. J.; Chen, Z.; Chung, J. K.; Groves, J. T.; Jardetzky, T. S. EphrinB2 clustering by Nipah virus G is required to activate and trap F intermediates at supported lipid bilayer-cell interfaces. *Sci. Adv.* **2021**, *7*, No. eabe1235.
(322) An, S. J.; Grabner, C. P.; Zenisek, D. Real-time visualization of complexin during single exocytic events. *Nat. Neurosci.* **2010**, *13*, 577−583.
(323) Dyett, B. P.; Yu, H.; Strachan, J.; Drummond, C. J.; Conn, C. E. Fusion dynamics of cubosome nanocarriers with model cell membranes. *Nat. Commun.* **2019**, *10*, 4492.
(324) Simonsen, J. B. Pitfalls associated with lipophilic fluorophore staining of extracellular vesicles for uptake studies. *J. Extracell. Vesicles* **2019**, *8*, 1582237.
(325) Schöne, N.; Kemper, M.; Menck, K.; Evers, G.; Krekeler, C.; Schulze, A. B.; Lenz, G.; Wardelmann, E.; Binder, C.; Bleckmann, A. PD-L1 on large extracellular vesicles is a predictive biomarker for therapy response in tissue PD-L1-low and -negative patients with non-small cell lung cancer. *J. Extracell. Vesicles* **2024**, *13*, No. e12418.
(326) Zhang, H.; Freitas, D.; Kim, H. S.; Fabijanic, K.; Li, Z.; Chen, H.; Mark, M. T.; Molina, H.; Martin, A. B.; Bojmar, L.; Fang, J.; Rampersaud, S.; Hoshino, A.; Matei, I.; Kenific, C. M.; Nakajima, M.; Mutvei, A. P.; Sansone, P.; Buehring, W.; Wang, H.; Jimenez, J. P.; Cohen-Gould, L.; Paknejad, N.; Brendel, M.; Manova-Todorova, K.; Magalhães, A.; Ferreira, J. A.; Osório, H.; Silva, A. M.; Massey, A.; Cubillos-Ruiz, J. R.; Galletti, G.; Giannakakou, P.; Cuervo, A. M.; Blenis, J.; Schwartz, R.; Brady, M. S.; Peinado, H.; Bromberg, J.; Matsui, H.; Reis, C. A.; Lyden, D. Identification of distinct nanoparticles and subsets of extracellular vesicles by asymmetric flow field-flow fractionation. *Nat. Cell Biol.* **2018**, *20*, 332−343.
(327) van de Wakker, S. I.; Bauzá-Martinez, J.; Ríos Arceo, C.; Manjikian, H.; Snijders Blok, C. J. B.; Roefs, M. T.; Willms, E.; Maas, R. G. C.; Pronker, M. F.; de Jong, O. G.; Wu, W.; Görgens, A.; El Andaloussi, S.; Sluijter, J. P. G.; Vader, P. Size matters: Functional differences of small extracellular vesicle subpopulations in cardiac repair responses. *J. Extracell. Vesicles* **2024**, *13*, 12396.
(328) Yang, D.; Zhang, W.; Zhang, H.; Zhang, F.; Chen, L.; Ma, L.; Larcher, L. M.; Chen, S.; Liu, N.; Zhao, Q.; Tran, P. H.L.; Chen, C.; Veedu, R. N; Wang, T. Progress, opportunity, and perspective on exosome isolation-efforts for efficient exosome-based theranostics. *Theranostics* **2020**, *10*, 3684.
(329) Liu, H.; Zhang, X.; Zhang, M.; Zhang, S.; Li, J.; Zhang, Y.; Wang, Q.; Cai, J. P.; Cheng, K.; Wang, S. Mesenchymal Stem Cell Derived Exosomes Repair Uterine Injury by Targeting Transforming Growth Factor-β Signaling. *ACS Nano* **2024**, *18*, 3509−3519.
(330) Fan, X.; Shi, L.; Yang, Z.; Li, Y.; Zhang, C.; Bai, B.; Chen, L.; Yilihamu, E. E.-Y.; Qi, Z.; Li, W.; Xiao, P.; Liu, M.; Qiu, J.; Yang, F.; Ran, N.; Shang, Y.; Liu, J.; Zhang, T.; Kong, X.; Liu, H.; Zhou, H.; Feng, S. Targeted Repair of Spinal Cord Injury Based on miRNA-124−3p-Loaded Mesoporous Silica Camouflaged by Stem Cell Membrane Modified with Rabies Virus Glycoprotein. *Adv. Sci.* **2024**, *11*, 2309305.
(331) Nie, M.; Huang, D.; Chen, G.; Zhao, Y.; Sun, L. Bioadhesive Microcarriers Encapsulated with IL-27 High Expressive MSC Extracellular Vesicles for Inflammatory Bowel Disease Treatment. *Adv. Sci.* **2023**, *10*, 2303349.
(332) Cao, H.; Chen, M.; Cui, X.; Liu, Y.; Liu, Y.; Deng, S.; Yuan, T.; Fan, Y.; Wang, Q.; Zhang, X. Cell-Free Osteoarthritis Treatment with Sustained-Release of Chondrocyte-Targeting Exosomes from Umbilical Cord-Derived Mesenchymal Stem Cells to Rejuvenate Aging Chondrocytes. *ACS Nano* **2023**, *17*, 13358−13376.
(333) Xu, F.; Fei, Z.; Dai, H.; Xu, J.; Fan, Q.; Shen, S.; Zhang, Y.; Ma, Q.; Chu, J.; Peng, F.; Zhou, F.; Liu, Z.; Wang, C. Mesenchymal Stem Cell-Derived Extracellular Vesicles with High PD-L1 Expression for Autoimmune Diseases Treatment. *Adv. Mater.* **2022**, *34*, 2106265.
(334) Tong, B.; Liao, Z.; Liu, H.; Ke, W.; Lei, C.; Zhang, W.; Liang, H.; Wang, H.; He, Y.; Lei, J.; Yang, K.; Zhang, X.; Li, G.; Ma, L.; Song, Y.; Hua, W.; Feng, X.; Wang, K.; Wu, X.; Tan, L.; Gao, Y.; Yang, C. Augmenting Intracellular Cargo Delivery of Extracellular Vesicles in Hypoxic Tissues through Inhibiting Hypoxia-Induced Endocytic Recycling. *ACS Nano* **2023**, *17*, 2537−2553.
(335) Chetty, V. K.; Ghanam, J.; Lichá, K.; Brenzel, A.; Reinhardt, D.; Thakur, B. K. Y-box binding protein 1 in small extracellular vesicles reduces mesenchymal stem cell differentiation to osteoblasts—implications for acute myeloid leukaemia. *J. Extracell. Vesicles* **2024**, *13*, No. e12417.
(336) Wang, D.; Du, S.; Cazenave-Gassiot, A.; Ge, J.; Lee, J.-S.; Wenk, M. R.; Yao, S. Q. Global Mapping of Protein-Lipid Interactions by Using Modified Choline-Containing Phospholipids Metabolically Synthesized in Live Cells. *Angew. Chem., Int. Ed.* **2017**, *56*, 5829−5833.
(337) Lassailly, F.; Griessinger, E.; Bonnet, D. Microenvironmental contaminations" induced by fluorescent lipophilic dyes used for noninvasive in vitro and in vivo cell tracking. *Blood* **2010**, *115*, 5347−5354.
(338) Li, P.; Zhang, R.; Sun, H.; Chen, L.; Liu, F.; Yao, C.; Du, M.; Jiang, X. PKH26 can transfer to host cells in vitro and vivo. *Stem Cells Dev.* **2013**, *22*, 340−344.
(339) Wang, F.; Zhong, Y.; Bruns, O.; Liang, Y.; Dai, H. In vivo NIR-II fluorescence imaging for biology and medicine. *Nat. Photonics* **2024**, *18*, 535−547.
(340) Wang, Z.-g.; He, Z.-y.; Liang, S.; Yang, Q.; Cheng, P.; Chen, A.-m. Comprehensive proteomic analysis of exosomes derived from human bone marrow, adipose tissue, and umbilical cord mesenchymal stem cells. *Stem Cell Res. Ther.* **2020**, *11*, 511.
(341) Lou-Franco, J.; Das, B.; Elliott, C.; Cao, C. Gold Nanozymes: From Concept to Biomedical Applications. *Nano-Micro Letters* **2021**, *13*, 10.

https://doi.org/10.1021/cbmi.4c00085
Chem. Biomed. Imaging 2025, 3, 137−168